Republic of Iraq
Ministry of Higher Education
And Scientific Research
University of Babylon
College of Materials Engineering
Department of Metallurgical Engineering

Different Surface Modification Techniques of 316L Stainless Steel for Surgical Tools

A Thesis
Submitted to the Department of Metallurgical Engineering at College of Materials Engineering / University of Babylon in Partial Fulfillment of the Requirements for the degree of Master in Engineering Materials / Metallurgical

By
Nada Talib Jaber Taeimuh
(B.SC. in material Engineering /2012)
(Higher Diploma in Materials Engineering / Metallurgical /2019)

Supervised by
Prof. Dr Ali Hubi Haleem
Asst. Prof. Dr Nabaa Sattar Radhi

2023 **1444**

بِسْمِ اللَّهِ الرَّحْمَنِ الرَّحِيمِ

إِنَّا فَتَحْنَا لَكَ فَتْحًا مُبِينًا

صدق الله العلي العظيم

سورة الفتح (آية ١)

<u>Supervisor Certificates</u>

We certify that this thesis, entitled **(Different Surface Modification Techniques of 316L Stainless Steel for Surgical Tools)** was prepared by **(Nada Talib Jaber)** under our supervision at the Department of Metallurgy Engineering / College of Materials Engineering / University of Babylon in Partial Fulfilment of the requirements for the degree of Master in Metallurgy Engineering.

Signature:

Name: Prof. Dr. Ali Hobi Haleem
(supervisor)
Date: / / 2023

Signature:

Name: Asst. Prof. Dr Nabaa Sattar Radhi
(supervisor)
Date: / / 2023

Signature:

Prof. Dr. Hayder H. Jaber

Head of the Department of Metallurgy Engineering:

Date: / /2023

Certification

We certify that have read this thesis **(Different Surface Modification Techniques of 316L Stainless Steel for Surgical Tools)** and examining committee, we have examined the student **(Nada Talib Jaber)** in the contents and that in our opinion it meets the standard of a thesis for the degree of Master in Materials Engineering / Metallurgical.

Signature:

Prof. Dr. Zuheir Talib Khulief

Committee Chairman

Date: / /2023

Signature:
Asst. Prof.Dr. Mohsin Talib Mohammed

Committee Member

Date: / /2023

Signature:
Asst. Prof.Dr. Zaineb Fadhil Kadhim

Committee Member

Date: / /2023

Signature:
Prof.Dr. Ali Hobi Haleem
Committee Member& Supervisor

Date: / /2023

Signature:
Asst. Prof.Dr. Nabaa Sattar Radhi
Committee Member& Supervisor

Date: / /2023

Approval of the Department of

Metallurgical Engineering

Head of Metallurgical Engineering

Department

Signature:

Prof. Dr. Hayder H. Jaber
Date: / /2023

Approval of the College of

Material Engineering

Dean of collage of Materials

Material Engineerin

Signature:

Prof. Dr. Abdulraheem Kadhim AbidAli
Date: / /2023

Dedication

"It always seems impossible until it's done."
Nelson Mandela

To my family, either here or in the sky

Nada Talib

2023

Acknowledgment

In the name of Allah, the most gracious, the most merciful. First of all, great thanks be to (ALLAH His MAJESTY) for enabling me to finish this study.

I would like to thank my family for their love and support throughout my entire academic career. Their constant encouragement and dedication to my success have made this effort possible.

I would like to express my sincere thanks to my research advisor, **Dr. Ali Hubi Haleem** & **Dr Nabaa Sattar Radhi**, for their guidance throughout my time at the University of Babylon. I am indebted to them for their support, which has helped shape me on both a professional and personal level.

I would like to thank my great colleagues, **Karar**, **Nawar**, **Noor**, **Nuha**, and the staff of the Metallurgical Lab for their many valuable discussions and their help with my research.

Special thanks are to **my brothers** for encouraging and helping me through the time of the study.

Nada Talib

2023

Abstract

Most medical instruments are made out of metal, from the grade of γ-stainless steel and titanium alloy, having high corrosion resistance, acceptable mechanical characteristics, with a high degree of biocompatibility. Due to improper maintenance by medical staff during decontamination and sterilizing procedures, the lifespan of medical instruments is often limited, or the use of substandard water or unsuitable chemical reagents in the cleansing procedure.

To bypass these limitations, various surface modifications were performed on the 316L SS alloy in this thesis. The effect of the type of surface modification and its parameters were examined for ways to improve their properties as mechanical strengths, surface properties, and anti-bacterial activity. As well as knowing the adhesion strength, and corrosion resistance of the surface coating formed as a result of these surface modifications and determining the preferable values for those parameters.

Two surface modification treatments for 316L stainless steel alloy were used with different conditions for each treatment. Anodization technique at a voltage of (6, 8, 10) v and a distance of (2, 4, 6) cm with times of (5,10) min; after that, the preferable sample $A_{8,5,4}$ coated by silver with physical vapor deposition. DC sputtering plasma technique at a voltage of (1400V) and a current of (20) mA with times of (2) hrs.

The tests were used to examine the generated surface layer Vickers micro-hardness, (FESEM), (AFM), (EDS), (XRD), antibacterial inhibition zone E.Coli, and adhesion test. Finally, the behavior of surface-modified samples in the fluid simulating the human body (Tyrode's solution) was

studied using open circuit potential, Potentiodynamic and cyclic polarization tests.

The obtained results indicated the optimum factors of anodic such as voltages, times, and distances effect on anodic oxide scale A34 (8-volt, 5min, and 4cm)

The results showed the high hardness value for the anodized sample was (475) HV. The results of (XRD) and (FE-SEM) revealed the formation of new phases in the surface layer (Cr_2O_3), which indicates that the surface modification conditions were very good. In contrast, the results of (AFM) displayed a development in the roughness of the surface values of the surface-modified samples with the increase in the treatment time.

The results of the antibacterial activity test with E.Coli strains showed that the formed layer from surface modifications has a strong antibacterial effect to prevent bacterial growth. As for the results of the adhesion resistance test, it was shown that the modified layer for all types of surface treatments used had an acceptable adhesion strength.

The results of the polarization curves showed a rise in the corrosion resistance of the surface-modified samples related to the untreated samples. The results revealed that the best condition for anodization was at the time (5) min, (8)v, and (4) cm where has a higher improvement (75%) in Tyrode's solution, while for the deposition of silver using DC sputtering plasma technique at the time (2) hrs, where the percentage of improvement was 81%

The treatments and surface modifications that were used to develop 316L SS in mechanical and surface properties and corrosion resistance meet the future requirements of applying the alloy as a strong and alternative competitor for biomedical applications as surgical tools.

List of Content

Chapter One (Introduction)

Chapter Two (Theoretical Part and Literature Review)

Chapter Three (Experimental Work)

Chapter four (Results and Discussion)

Chapter five (Conclusion & Future Work)

References

List of Tables

List of Figures

List of Abbreviations

Abbreviation	Express
DC	Direct current
SS	Stainless Steel
ASTM	American Society for Testing Materials
AISI	American Iron and Steel Institute
FDA	Food and Drug Administration
PVD	Physical Evaporation Deposition
Cr_2O_3	Chromium oxide
LOM	Light Optical Microscope
SCE	saturated calomel electrode
HV	Micro Hardness
CR	corrosion rate
XRD	X-Ray Diffraction
AFM	Atomic Force Microscopy
FESEM	Field emission Scanning Electron Microscope
H_2SO_4	Sulfuric acid
HNO_3	Nitric acid
C_3H_6O	Acetone
H_2O	distilled water
Ag	Silver
SBF	simulated body fluid
OCP	open circuit potential
E.Coli	Escherichia Coli

List of Symbols

symbol	Express
γ	Austenite Phase
ρ	Density
Wt.%	Weight Percentage
α	Ferrite Phase
λ	The Wavelength of Cu Kα
θ	The Diffraction Angle

Chapter One

Introduction

Introduction

1.1. General Introduction

Metals and alloys, including stainless steel, titanium, and its alloys and cobalt alloys, have been widely used clinically due to their high strength, good wear resistance, good corrosion resistance, high fatigue properties, and good biocompatibility, such as dental implants, hip and knee replacements, bone plates and screws. It was reported that up to 2.5 million dollars inmedical devices were made of metals and alloys [1].

The bacterial infection or inflammation that seriously threatens human health has already become a worldwide complaint issue [2]. So, research on antibacterial technologies [3], including mechanical clearance, surface modification [4], and antibacterial materials is urgently necessary.

In practical applications, the surface of a material is subjected to the influence of various external stimuli. Often a surface-related property of the material renders it a poor performer. Corrosion, oxidation, wear, and fatigue are a few such material degradation phenomena, which initiate at the surface. Thus, it has been a constant endeavor by engineers and scientists to improve the surface-related properties of biomaterials. Surface engineering seems to offer solutions for improved functionality and biocompatibility [5].

Stainless steel (SS) is the first metallic material used for medical applications due to its lower cost, easy accessibility, strong corrosion resistance, approved biocompatibility, and high strength compared to other metallic implants [6].

Although 316L SS has excellent bulk mechanical and physical properties, its low resistance to localized corrosion has restricted its use as a biomedical implant. The surface modification of 316L SS was carried out to obtain attractive properties of the surface while retaining the important properties of bulk material [7].

Surface modification is the physical alteration of the surface topography or attachment of various ligands or molecules to bring forth distinct physical, chemical, or biological properties. Surface modification can be achieved by modifying surface atoms/molecules via physical/chemical route or depositing a layer over the surface [8].

Surface treatments or modifications, can be classified into four categories: mechanical, physical, chemical, and biochemical surface modifications. Machining, grinding, polishing, and blasting are mechanical surface modifications. Physical surface treatments include thermal spraying, physical vapor deposition, ion implantation, and deposition, and glow discharge plasma treatment. Chemical surface modifications include chemical treatment (acid, hydrogen peroxide, alkaline), anodic oxidation, the sol–gel process, and chemical vapor deposition [9].

Electrochemical anodic oxidation surface modification is an oxidation–reduction reaction that occurs through the cathode and anode of an electrochemical set. By applying a potential that is proportional to the electrolyte used, the desired oxide layer will be formed on the surface; indeed, the ability and tendency of the metal to tailor a self-protective oxide layer are used [10].

Sputter deposition is a non-thermal vaporization process where physical sputtering is used to vaporize particles from a surface and subsequently get deposited on a substrate [11]. During sputter deposition processes a target that consists of the desired coating material is bombarded by energetic gaseous ions which are created in a low-pressure plasma. The impulse of these ions is transferred to the target atoms which as a result are physically ejected from the surface of the target. These vaporized particles are transported to the substrate and condensate on the surface, where finally the growth of the film occurs. On the way from the vaporization source to the substrate, the sputtered atoms can collide with gas atoms. Due to these collisions, the sputtered atoms lose energy. To reduce the number of collisions and thus create a long mean free path these sputtering processes are performed in a low-pressure atmosphere, typically below $1*10^{-2}$ bar [12].

1.2 Main Issue

316L stainless steel is still not resistant to localized forms of corrosion such as pitting, crevice, and stress corrosion cracking when used as implants. It has been reported that 316L corrodes in the body environment and releases iron, chromium, and nickel. Moreover, it contains 12.0–15.0% of nickel, which can be toxic to the human body if released. There is evidence that high levels of nickel ions in tissues are the cause of genotoxic and mutagenic activities or in contact with the skin causing the most widespread contact allergy and cancer [13].

Stainless steel has been the standard material for non-precision scalpels and is used to produce cheap disposable blades for ophthalmologic surgery. Due to the grain size limitations of steel and the economic manufacturing processes used. The low hardness and strength values of typical stainless steel also cause the edge to degrade significantly over several incisions due to plastic deformation of the cutting edge [14]. poor antimicrobial property is one of the major limitations of Stainless Steel 316 L (SS 316 L) that is primarily utilized in manufacturing surgical instruments due to its characteristics such as ease of fabrication, good mechanical strength, reasonable corrosion resistance, biocompatible and low-cost [13].

These problems are sometimes severe in metallic instruments. So, to overcome these problems, 316L stainless steel is modified in two ways anodic oxidation and DC sputtering plasma which is close as possible to practical conditions. This research is sought to cover the limited area of research about this problem.

1.3 Objectives of the Present Study

This research aims to modify the 316L SS by anodic oxidation to enhance their surface properties, especially corrosion resistance for biomedical applications and DC sputtering plasma to close the porosity. The objectives of the research are to the application of anodic technique under different parameters (voltage, time, and distance) to form a stable and compact oxide layer that can rebuild itself, it can be described as bioinert since this surface can prevent the transmission of undesirable ions and study the response to plasma technique to deposit suitable coatings layers of silver on a medical grade 316L stainless steels to enhance their surface properties for biomedical applications. The present study aims to accomplish the following goals:

1- Evaluation of oxide bioactive layers using different parameters that control anodic technique, especially applied voltage and deposition time.
2- Studying the surface morphology (homogeneity and porosity) and surface roughness for all oxide layers.
3- Studying the corrosion resistance of samples after immersing them in Tyrode's solution using the linear potentiodynamic polarization technique and cyclic polarization.
4- Study the antibacterial activity of oxide layers.
5- Getting multi-properties surface layers gathering high mechanical properties and biocompatibility.

1.4 Thesis Outline

The thesis consists of five chapters, which can be briefly described as follows:

- **Chapter one:** deals with the general introduction related to the surface modification of 316L and the objectives of the present study.
- **Chapter two:** gives an explanation of stainless steel and the alloying elements, anodizing technique, and its parameters. Also, it includes the theoretical principle of the DC sputtering plasma of silver, in addition to some articles related to this thesis's main objective with a brief abstract defining the major idea.
- **Chapter three:** describes the experimental setup, which includes 316L alloy preparation and modification by anodizing with various voltage, distances, and times to estimate the characterization of XRD, FESEM, and AFM. Also, to estimate the corrosion rate, antibacterial, hardness, and coating thickness.
- **Chapter four:** all the experimental results of the work have been obtained and discussed in detail.
- **Chapter five:** gives the main conclusions obtained from this investigation with recommendations for possible future works.

Chapter Two

Theoretical Part and Literature Review

Chapter Two

Theoretical Part and Literature Review

2.1. Introduction

This chapter shows a brief interview about medical devices, stainless steel and its alloys, their classifications, and modification of 316l alloy, using of the anodic process to enhance corrosion resistance and using DC sputtering plasma for closing the porous, and a literature review of studies close to the present work.

2.2 Medical Devices in General

Most medical devices are made of metal, which will suffer from corrosion, wear, and human body rejection service. The most commonly used material today is stainless steel, titanium alloys, polymers, etc. There are two important parameters used for the selection of these materials. First, physical and mechanical properties such as strength and deformation, surface finish, surface texture, fatigue and creep, friction and wear resistance, flow resistance, etc. Second, biocompatibility and hemocompatibility [15].

Hemocompatibility and biocompatibility of biomaterials mainly depend on their surface properties. Therefore, surface treatment of devices and implants fabricated using synthetic biomaterials is necessary to avoid complications like thrombus formation, inflammation, infections, etc. [16].

However, a single material is unable to deliver all the properties and hence modifications are made so as to fulfill the requirements. The coating material of desired functionality on the surface, conversion of existing surfaces into more desirable morphologies, and removal of material from the existing surface are some of the ways in which this can be achieved [17].

Coatings can improve the surface properties of the devices and extend their life. Generally, medical devices can be grouped into two categories: surgical devices, and interventional medical devices [18].

2.2.1 Surgical Instruments

stainless steel is widely used for the manufacture of surgical instruments, and other metals such as titanium, copper, aluminum, chromium, vanadium, molybdenum, and even a certain amount of silver and gold are also used [19]. Figure (2.1) refer to the medical instruments used in clinical operations. These instruments are tools designed for specific actions in specific types of surgery and can have long lifespans. They can also become contaminated, however, due to the adherence of bacteria to the material, especially if there are corroded or worn areas where the adherence of deposits is facilitated by inadequate or imperfect cleaning of surgical instruments. Such contamination can have a tremendous impact on patient health. In addition, one must consider that hospitals and clinics are enabling environments for contamination and consequent host infection [20].

Figure (2.1): Surgical instruments [20]

2.2.2 Origin and History of Surgical Instruments

Humans first learned to treat injuries by using the mouth to suck out stings, hands to stop bleeding, and teeth to finish amputation [21]. Before long, they realized that appropriate tools could dramatically improve the treatment efficiency and outcome. Natural materials such as animal teeth and bamboo were then used to provide a cleaner cut. With the discovery of copper, bronze, and iron, surgical tools were manufactured with great functionality, better precision, and durability [22].

Although not evidenced, it is reasonably suspected that some surgical instruments were initially invented to mimic human actions, such as grasping, compressing, and cutting. Table (2.1) illustrates some modern instruments possibly derived from such actions [21].

Table 2.1: Possible Links between Natural Actions and Instruments [21]

	Mouth	Teeth			Thumb	Nail	
Action	Suck	Bite	Grind	Clench	Compress	Cut	Scrape
Instrument	Aspirator	Rongeurs	Saw	Clamp	Tourniquet	Scalpel	Rasp
	Finger					Fist	
Action	Hook	Probe	Retract	Dilate	Pinch	Grasp	Hammer
Instrument	Hook	Probe	Retractor	Speculum	Spring Forceps	Clamp	Mallet

surgical instruments and implants which are in direct contact with tissue and could cause transmission of disease. These items must be both high-level disinfected and sterilized between each use. Liquid chemical disinfectant is used in compliance with instructions for concentration, contact time, and temperature. All microorganisms including bacterial spores require to be destroyed for sterility [23].

2.2.3 Surgical Instrument Metallic Alloy

The most common types of modern metals used in the manufacture of surgical instruments in the 20th and 21st centuries include steel, copper, nickel, titanium, and silver [24].

The grades of stainless steel used to manufacture surgical and dental instruments. 17 types of stainless steel are listed, named from A to S. The chemical compositions of all steel types are listed with tolerances in Table (2.2.) [25].

Table 2.2: Chemical compositions of surgical grade stainless steels [25]

Grade	Type	C	Si	Mn	P	S	Cr	Mo	Ni
A	Martensitic	0.09 – 0.15	1 max	1 max	0.04 max	0.03 max	11.5 – 13.5	–	1 max
B	Martensitic	0.16 – 0.25	1 max	1 max	0.04 max	0.03 max	12.0 – 14.0	–	1 max
C	Martensitic	0.26 – 0.35	1 max	1 max	0.04 max	0.03 max	12.0 – 14.0	–	1 max
D	Martensitic	0.42 – 0.50	1 max	1 max	0.04 max	0.03 max	12.5 – 14.5	–	1 max
E	Martensitic	0.47 – 0.57	0.5 max	1 max	0.03 max	0.025 max	13.7 – 15.2	–	0.5 max
F	Martensitic	0.60 – 0.70	0.5 max	1 max	0.03 max	0.025 max	12.0 – 13.5	–	0.5 max
G	Martensitic	0.65 – 0.75	1 max	1 max	0.04 max	0.03 max	12.0 – 14.0	0.50 max	1 max

H	Martensitic	0.35 – 0.40	1 max	1 max	0.045 max	0.03 max	14.0 – 15.0	0.40 – 0.60	–
I	Martensitic	0.42 – 0.55	1 max	1 max	0.045 max	0.03 max	12.0 – 15.0	0.45 – 0.90	–
K	Martensitic	0.33 – 0.43	1 max	1 max	0.03 max	0.03 max	15.0 – 17.0	1.00 – 1.50	1 max
L	Ferritic	0.08 max	1 max	1.5 max	0.06 max	0.15 – 0.35	16.0 – 18.0	0.60 max	1 max
M	Austenitic	0.07 max	1 max	2 max	0.045 max	0.03 max	17.0 – 19.0	–	8.0 – 11.0
N	Austenitic	0.12 max	1 max	2 max	0.06 max	0.15 – 0.35	17.0 – 19.0	0.70 max	8.0 – 10.0
O	Austenitic	0.15 max	1 max	2 max	0.045 max	0.03 max	16.0 – 18.0	–	6.0 – 8.0
P	Austenitic	0.07 max	1 max	2 max	0.045 max	0.03 max	16.5 – 18.5	2.0 – 2.5	10.5 – 13.5
R	Martensitic	0.85 – 0.95	1 max	1 max	0.045 max	0.03 max	17.0 – 19.0	0.90 – 1.30	–
S	Martensitic	0.60 – 0.75	1 max	1 max	0.04 max	0.03 max	16.0 – 18.0	0.75 max	–

- **400 Series Stainless Steel**

Heat treating and passivation are processes used for the manufacture of instruments requiring a dissection or debulking edge to maintain the necessary sharpness to cut both soft and compact or bony tissues. Passivation is the terminal process of submerging instruments in a nitric acid bath, which removes any traces of foreign particles and creates a coating of chromium oxide to resist corrosion. Instruments made of this grade of steel do not readily bend or flex while in use. Other instruments that require this level of hardness are used for secure grasping and holding. Examples of instruments made of 400 series stainless steel include [24]:

● Scissors: Used to dissect fine and heavy soft tissues and suture materials.

●Chisels, osteotomes, and rongeurs: Used for debulking and dissecting bone or other compact tissue

● Curettes and rasps: Used to remove, shape, or smooth dense tissue

● Clamps and hemostats: Crushing and non crushing for mechanical hemostasis, occlusion of lumens, and stabilizing tissue

● Needle holders: Used for tissue approximation by grasping suture needles attached to strands of suture material to allow for passage through tissue layers

● Forceps: Used to grasp and hold various types of tissues

● Dilators: Used to sequentially expand a lumen or opening

- **300 Series Stainless Steel**

Instruments that require slight to moderate malleability are composed of 300-series stainless steel. This type of steel is also corrosion-resistant. Instruments that are made of 300 series stainless steel include [24]:

● Suction cannulas: Used for the removal of fluids and substances from the surgical field.

● Probes: Used for exploration of depth or direction of anatomic areas and blunt dissection or separation of tissue planes.

- Retractors: Malleable (bendable or shapeable) for displacement or repositioning of tissues to enhance visualization at the surgical site.
- Surgical wire: Used for stabilization of fractures.
- Surgical steel suture: Used for tissue approximation and wound closure.

2.2.4 Interventional Medical Devices

Interventional medical instruments are inserted into the human body or natural cavity by surgical means for short-time treatment or examination and then taken them out. Interventional medical devices include endovascular catheters (angiography catheter, balloon catheter, PTCA catheter, etc.), guide wires and sheaths (hard guide wire, soft head guide wire, micro guide wire, arterial sheath, venous sheath, etc.), embolization device (filter, spring plug, packer, etc.). The materials used in interventional medical devices are mainly polymer materials and metal materials. High-performance polymer materials are ideal for conveying tubes of interventional medical devices because of their high strength, corrosion, and wear resistance, low friction coefficient, and easy processing. Metal materials are more commonly used as stents and guide wires. In order to make the product more easily through the blood vessels and the natural cavity, and avoid possible puncture and friction damage, the coating prepared on catheter and guide wires requires a super-hydrophilic and super-lubricating effect [20].

2.2.5 Properties of Surgical Instrument Surface

The effect of surface finish on instrument drying and corrosion resistance is important as shown below [22].

- Surface Finish: Matt finish is applied to instruments to reduce reflection. The instrument may feel better to the touch or look more refined. At least one manufacturer matt finishes all their instruments as a matter of policy. Other, sometimes more traditional manufacturers maintain that polished finishes dry more readily and are therefore more corrosion resistant [22].

- Passivation: although it is well known that passivation can enhance the corrosion resistance of instruments, how it changes instruments behavior in disinfection [22].
- Steel Type: It is known that the mechanical characteristics of a material are governed by its bulk composition while how it interacts with the environment is dependent on the surface properties [26].

2.3. Stainless Steel

Stainless Steel (SS) is an alloy based on iron containing (11–30) percent wt. of chromium and also an unspecified quantity of nickel. In the 1920s, 316 L SS had become an applicant implant and had a wide range of applications, such as medical devices high resistance to corrosion, combined with good mechanical performance, was the primary reason for its widespread use in extremely severe environments, like saltwater, or the body of a human. Although the resistance to corrosion is high, small amounts of metal ions may be released from the SS surface in interaction with various fluids. SS has ductility higher than one α-Ti (with the structure of a hexagonal crystal) [27].

Stainless steel is a remarkable achievement of modern metallurgy and was discovered when the identification of chromium as an element began [28]. Stainless steel is an iron-based alloy with a minimum of 11 wt% chromium [29], which can also have several other alloying elements such as nickel, molybdenum, and manganese [30]. Due to the high corrosion resistance of stainless steel in combination with their good mechanical properties, they are used in a wide range of applications, e.g., food and beverage relevant applications, building and construction, biomedical applications, and jewelry [31].

The corrosion resistance of stainless steels is due to the presence of a very thin self-healing chromium-rich passive surface oxide, with 1 – 3 nm thickness [32]. This surface oxide schematically shown in Figure (2.2) is believed to contain two layers: i) an inner layer, predominantly containing iron and chromium oxides, and ii) an outermost layer containing chromium hydroxides and/or oxyhydroxides [33 -37] .

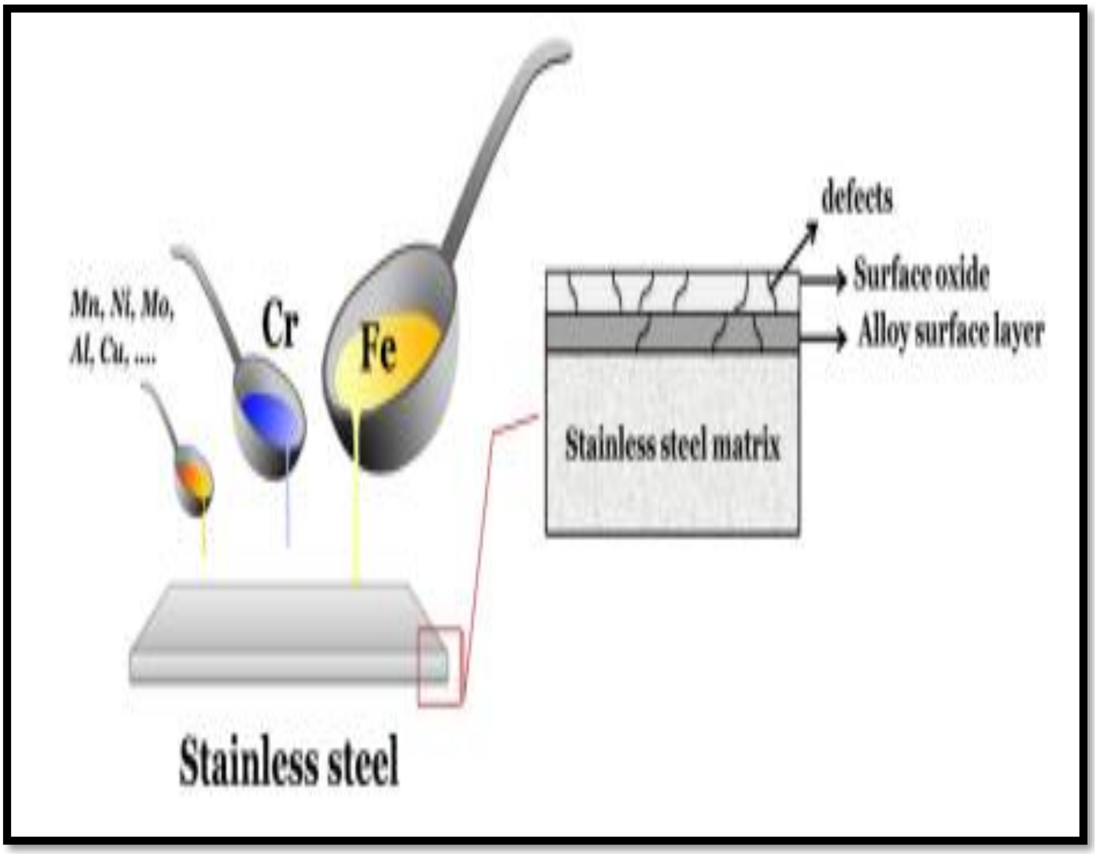

Figure (2.2): Schematic illustration of stainless steel and its outermost surface oxide, inspired by G. Herting [37]

2.4. Classification of Stainless Steels Alloys

Based on the alloying constituents and microstructure of stainless steels, they are graded into four categories by the AISI system Figure (2.3): ferritic, austenitic, duplex, and martensitic stainless steels [38], which are briefly discussed below.

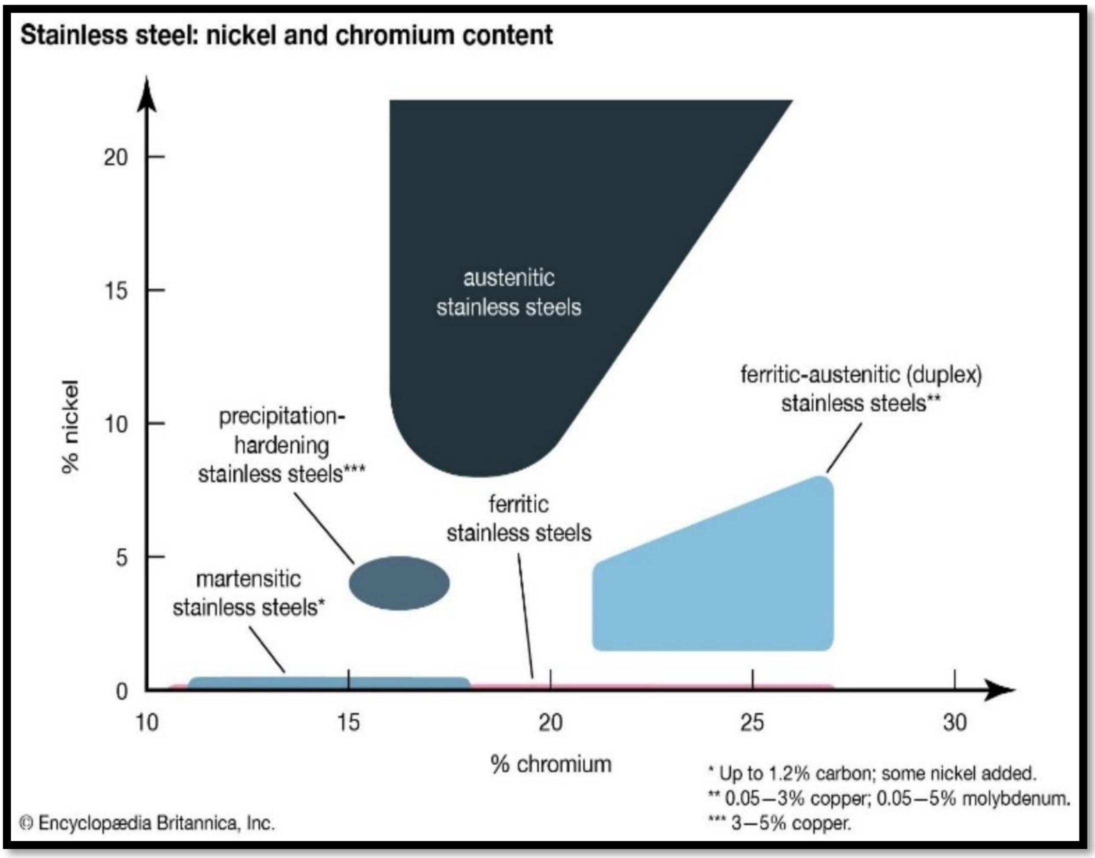

Figure (2.3): The nickel and chromium content of different types of stainless steel [38].

- **Ferritic Stainless Steel**

Ferritic stainless steels (designated as 400 series by AISI) are nickel-free materials with a 10.5 – 30 wt% chromium content and are typically used in domestic appliances, kitchenware, containers, building, and construction. The absence of nickel makes these grades a more attractive and cost-optimized option [39 - 40].

- **Austenitic Stainless Steel**

Austenitic stainless steels have a face-centered cubic lattice structure. They are the most common type of stainless steel used due to the fact that they are formable, wieldable, and have very high corrosion resistance, making them suitable for a wide-ranging application from high temperature to cryogenic temperature. The main alloying elements of stainless steels are Cr and Ni. The Cr is added to improve corrosion resistance although it stabilizes the ferrite phase (it is also known as a ferrite stabilizer). The Ni is added to improve ductility and toughness as well as to stabilize the austenite phase. Thus, Ni is also known as an austenite stabilizer. Other elements such as Mo, Cu ,Si, N, Nb, C, Ti, Al, S, and Mn can also be added. These elements can be classified as austenite or ferrite stabilizers depending on the effect on the crystallographic structure [41].

Generally, austenite stabilizers have an FCC phase structure and are more soluble in the austenite phase. Therefore, they restrict the formation of the ferrite phase because they are thermodynamically more stable in the austenite phase. The alloys are usually added to stabilize the microstructure and improve strength or corrosion properties. A brief overview of their effect is given below [41].

Chromium: All stainless steels have Cr content above 12-13 wt %. With increasing Cr content, the main effect of Cr is to improve corrosion resistance and stabilize the ferrite phase [41].

Nickel: Nickel is an austenite stabilizer that gives stainless steel strength, ductility, and toughness at high and low temperatures. It also improves the corrosion resistance of stainless steel in acidic environments [41].

Carbon: is an austenite stabilizer that improves mechanical strength; however, it is generally undesirable in austenitic stainless steels due to the fact that it has a high thermodynamic affinity for Cr. Because of the high affinity of chromium, carbon causes the formation of chromium carbides at grain boundaries when a supersaturation state in austenite is reached and diffusion is fast enough for the segregation of Cr and C to occur. This typically happens at temperatures between 1123 K to 723 K when the stainless steel is slowly cooled [42].

Molybdenum: Improves corrosion resistance of stainless steels to uniform and localized corrosion. It also stabilizes the ferrite microstructure and improves mechanical strength [41].

Copper: An austenite stabilizer that improves the corrosion resistance of stainless steels in certain acids. Also, added some grades to improve machinability by reducing work hardening [41].

Nitrogen: is an austenite stabilizer that increases mechanical strength and corrosion resistance. Typically added as an alternative to carbon to increase the yield strength and reduce the propensity of chromium carbides formation at grain boundaries [41].

Niobium: is a strong ferrite stabilizer that improves intergranular corrosion resistance by forming Niobium carbides at grain boundaries thereby helping to prevent the formation of grain boundary chromium carbides [41].

Silicon: enhances the formation of ferrite and is used as a deoxidizer in the manufacture of steels. Also improves oxidation resistance at high temperatures and in oxidizing solutions at low temperatures. Silicon forms aluminum silicates inclusion in stainless steels [41].

Titanium: Used in austenitic stainless steels with high carbon content to prevent the formation of chromium carbides. Also improves mechanical properties at high temperatures [41].

Aluminum: Improves oxidation resistance of stainless steel by forming an oxide protection layer on the steel [41].

Austenitic stainless-steel grades, with a minimum of 16 wt% chromium, are classified as 200 (Fe – Cr – Ni – Mn – N stainless steels with ≥ 2 wt% Mn) and 300 series (Fe – Cr – Ni stainless steels with ≤ 2 wt% Mn) by AISI. They are the most common grades of stainless steel and typically used in a wide range of applications such as cutleries, kitchen utensils, transport equipment, jewelries, surgical equipment and as implants [43 – 44]. The family tree of austenitic stainless steels is shown in Figure (2.4) [45].

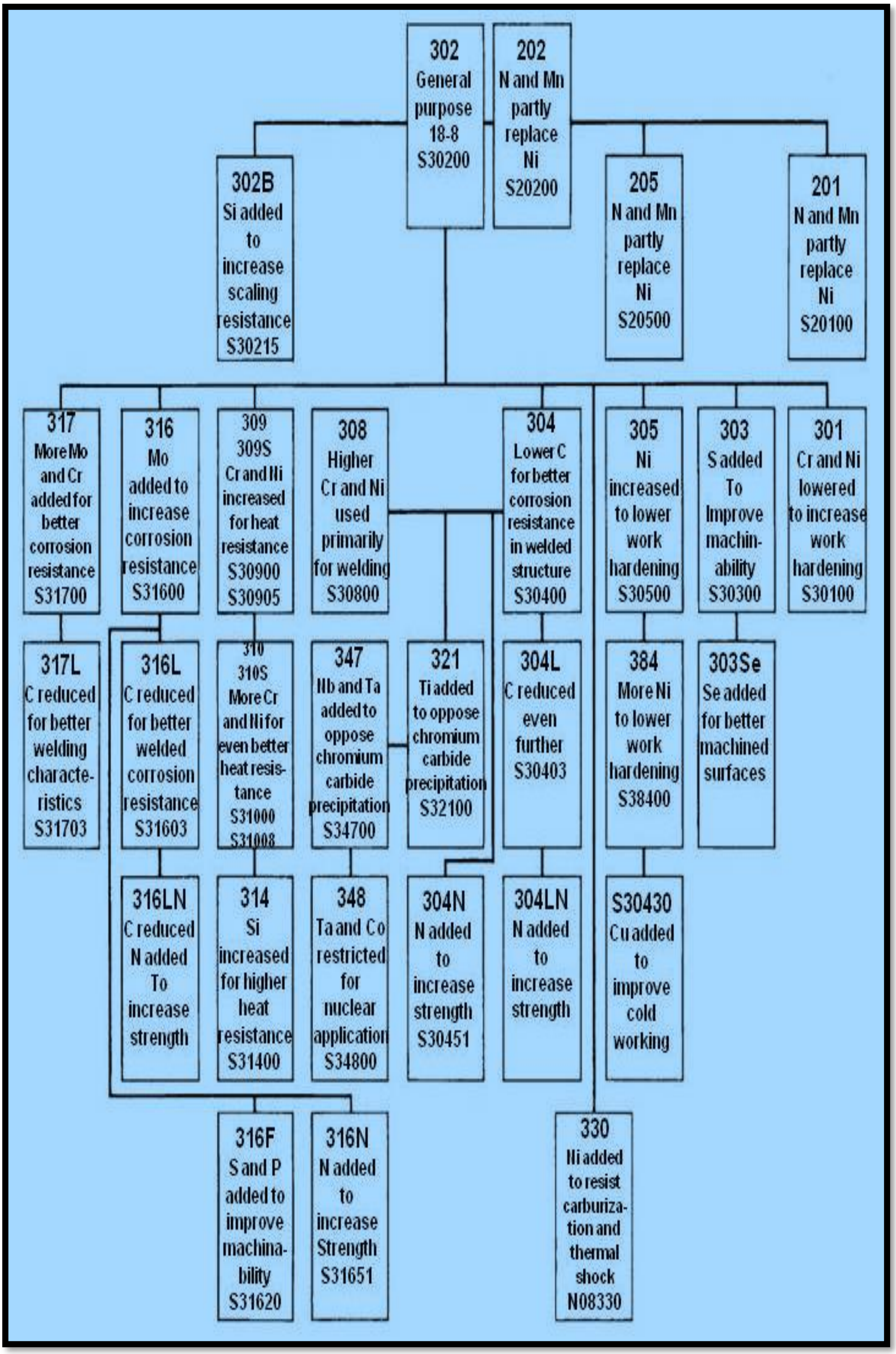

Figure (2.4): Family tree of austenitic stainless steels [45].

- **Duplex Stainless Steel**

Duplex stainless steels have a mixed structure of austenite and ferrite and typically contain chromium (20 – 25 wt%) and nickel (1.5 – 7 wt%) as the main alloying elements [46]. Depending on their application, other alloying elements such as molybdenum, and nitrogen may be added to obtain certain corrosion resistance characteristics. They are commonly used in e.g., bridges, storage tanks, and water heaters [47].

- **Martensitic Stainless Steel**

Martensitic stainless steels (designated as 400 series by AISI) are essentially alloys of chromium (10.5 – 18 wt%) and carbon (0.1 – 1.2 wt%) and are typically used in cutlery and knife applications due to their hardness [48]. These grades usually show lower corrosion resistance in comparison with other stainless-steel grades, particularly in oxidizing environments [46].

2.5. Type AISI 316L Stainless Steel

Type AISI 316L stainless steel (SS), a single-phase austenitic stainless steel is one of the most commonly used materials for biomedical implant applications due to its relatively low cost ,ease of fabrication, moderate strength, and reasonable corrosion resistance. The “L” in 316L designates low carbon content (<0.03%) in the alloy. A low level of carbon content in the alloy is necessary to prevent the formation of chromium carbides since these carbides can form preferentially along grain boundaries, leaving the adjacent areas with depleted chromium levels which are thus prone to intergranular corrosion [49]. Chromium is present in 316L SS passive oxide film primarily in the form of a Cr_2O_3 surface layer, which is crucial to its corrosion resistance. This surface layer is known as the passive oxide film, which is highly adhesive and promotes self-healing in the presence of oxygen. The minimum percentage of chromium in stainless steels is about 11 wt.%, which is known as the minimum amount required to prevent the formation of rust in an unpolluted atmosphere [49].

Further enhancement in corrosion resistance, as well as mechanical properties, is achieved by the presence of other alloying elements. The presence of nickel, molybdenum, and nitrogen in 316L SS stabilizes the formation of an austenite phase and also contributes to its increased corrosion resistance. Alloying elements such as chromium and nickel provide oxidation resistance while molybdenum and nitrogen enhance the localized corrosion resistance of 316L SS. Molybdenum is considered as one of the principal alloying elements in austenitic stainless steel which enhances the pitting corrosion resistance by molybdenum carbide formation, thereby reducing the amount of chromium carbide formation. Nickel is the main alloying element that stabilizes the formation of austenite in stainless steel and also contributes to increased corrosion resistance by the formation of protective oxide films [49].

316L SS is an excellent example of an alloy that exhibits corrosion resistance in a variety of environments as a result of surface passivation. Thus, 316L SS is extensively employed in various industrial applications such as architectural structures, automotive parts, and biomedical devices [49]. In biomedical applications, 316L SS comprises a substantial percentage of clinical use as it is currently used in orthopedic surgery as temporary fixation devices (nails, screws, plates, and wire) [50], cardiovascular surgery (e.g., electric terminal and stents) [51], and surgical instruments (e.g., bone drills, knives, needles, etc.) [49]. Despite these applications, the resistivity of 316L SS to pitting corrosion is still not satisfactory for long-term applications. Therefore, its current applications are mostly confined to short-term implant devices, medical surgery instruments, and implant manufacturing equipment; nevertheless, 316L SS is still the predominant material used for coronary stents, which are long-term implants [52].

2.6. Surface Modifications for Biomedical Materials

Surface engineering technology is a suitable method for coatings on metal surfaces or performing surface modification treatment, this can improve corrosion resistance and biocompatibility of metals [53].

Surface modification is a process that changes a material’s surface composition, structure, and morphology, leaving the bulk mechanical properties intact [54].

Surface modifications of biomaterials have led to improvements in device multi-functionality, tribological and mechanical properties, and the biocompatibility of artificial devices while avoiding the need for additional costs and time. It changes the physiochemical properties of the materials such as surface charge, surface energy and surface composition [55].

Surface modification can be accomplished by physically or chemically altering surface atoms/molecules or depositing a layer on top of the surface. A polymer layer, an organic layer, or a thin coating of another material might be used. Figure 2.5 depicts a variety of surface modification techniques. A specific approach can be used depending on the substrate's surface and the modification's requirements [56].

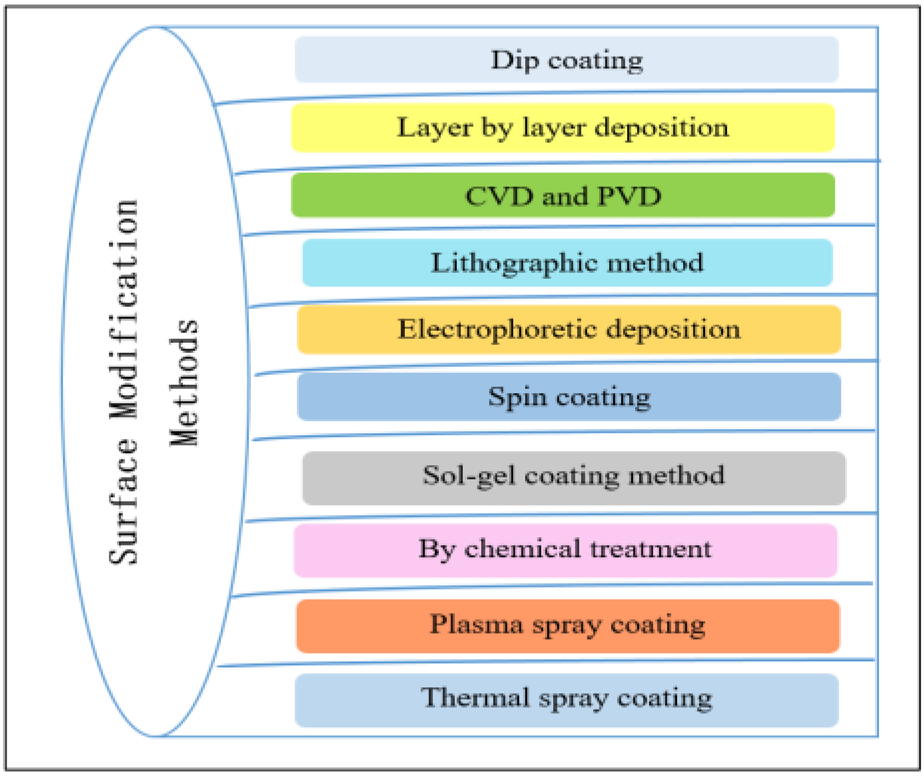

Figure (2.5): Schematic Diagram Showing Different Surface Modifications [56].

2.7. Anodization Process and its Principle

Anodization is an electrolytic process used to grow a passive layer on the metal surface at the anode. Metals, which can be anodized, are able to form a thin oxide film in oxygen-contented ambient. The dense and uniform layer of anodized oxide inhibits ionic conductivity; thus, they can be regarded as barrier oxides to effectively protect the metal from further corrosion [57]. On top of that, the anodized oxide film can improve the surface properties of metal, such as wearing, galling, adhesion, and dielectric layer. Transition metals are a common source of materials used in anodization, metals such as Al, Ti, Mg, Zn, Ta, and W are often used during anodization process. Interestingly, some anodized metal oxide films can also be applied as decorations since the colors of anodized films are variable, also called interference layer[58]

Figure (2-6) shows an anodization cell, the working metal is set as the anode to oxidize during the electrochemical process. The cathode can be any electronic conductor that would not react in the anodizing bath. The electrolytes are chosen by the insolubility with the anodized oxide, or a higher growth rate of oxide when compared to its dissolution rate. When the reaction is taking place, electrons are withdrawn from the metal at the positive terminal, allowing ions at the metal surface to react with the water in the electrolyte to form a dense oxide layer on the metal. The electrons later return back to the electrolyte where they react with hydrogen ions to generate hydrogen [59].

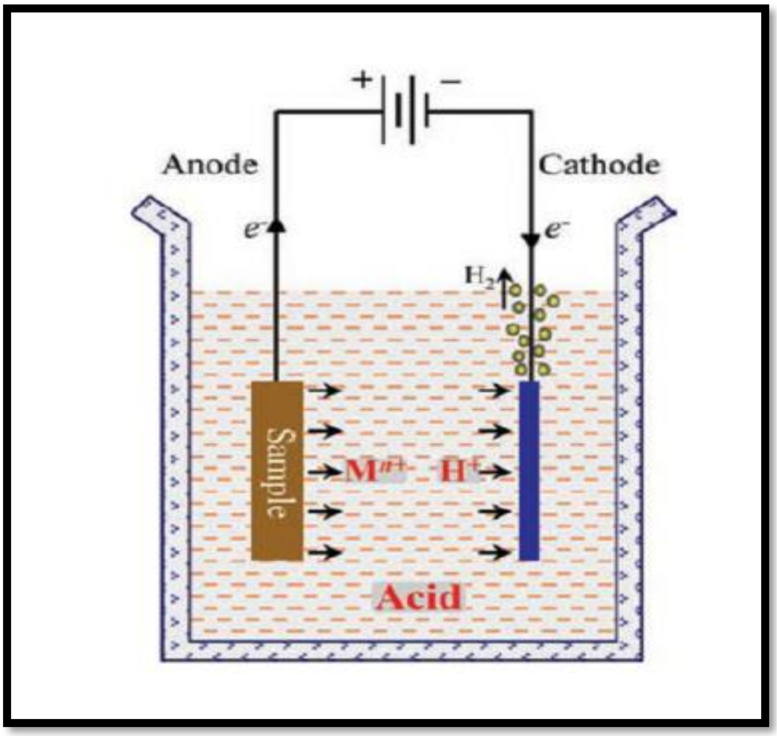

Figure (2.6): Schematic diagram of the anodizing cell [59].

2.7.1. Anodization Principle

In anodization, the metal is immersed into an acid electrolyte bath and current is passed through a circuit. As shown in Figure 2.10, the cathode electrode is placed inside the anodizing tank while the metal acts as an anode. The cathode enhances the release of oxygen atoms from the electrolyte solution, creating a layer of metal oxide on the anode. The anodized surface layer ranges from a few nm to as much as several m [60]. Anodizing improves corrosion and wear resistivity along with paint adhesion. This process also creates electrical insulation and facilitates dying for cosmetic and other purposes [61].

2.7.2 Anodization-Affecting Parameters

The following parameters affect the anodization process, depending on the type of material [62]:

- Concentration of acid (100–300 g/L for sulfuric acid)
- Temperature of bath (20-30 ^{0}C)
- Additives (dyes, electrodes)
- Current density (depending on metal and electrolyte solution)
- Reaction time
- Voltage (5 –100 DC)
- Efficient bath agitation and bath cooling

2.7.3 Benefits of Anodization

Anodization facilitates both science and nature by providing the following advantages:

- Enhancing biomaterials to be more biocompatible and corrosion resistive [63].
- Making the material highly abrasion-resistant and durable for corrosion prevention [64].
- Creating anodic coatings that do not peel, chip, or flake off, etc. [65].
- Creating anodic coatings that are translucent, resulting in a deep, rich metallic appearance [66].
- Creating anodic coatings that are not affected by sunlight and have outstanding finished areas [66].
- Making some metals colorful, even for decorative purpose [67].

2. 8. Physical Sputtering Processes

Sputtering is a term that describes a system in which energetic particles (specifically, the ion Ar^+ under high voltage acceleration) launch atoms from the surface. Initially, it was found in 1852 and developed as a thin film deposition process by Langmuir in 1920 [68]. When a solid surface is bombarded with energetic ions, the surface atoms scatter backward due to collisions between the surface atoms and the energetic particles as shown in Figure (2.7). When a thin film is bombarded with energetic particles, some of the scattered atoms transmit through the foil. A phenomenon known as "back-sputtering" or "simply-sputtering" occurs [69].

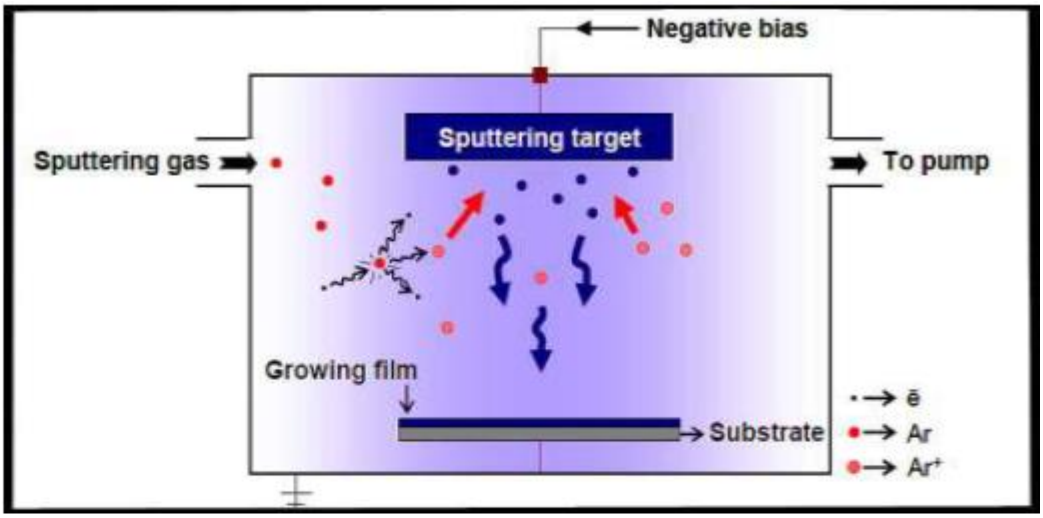

Figure (2.7): Schematic of a simple sputtering setup with Ar as sputtering gas [70].

There are many types of sputtering, including, DC Sputtering, and RF. Sputtering, Magnetron sputtering, etching plasma sputtering, and Ion beam sputtering [71]. Direct current sputtering (DC sputtering) is the simplest of these sputtering systems.

2. 8. 1 DC Sputtering Deposition

It is one of the Physical Vapor Deposition (PVD) techniques. The Sputtering system consists of two plates, a vacuum chamber, and a pair of planar electrodes; the material to be deposited in the cathode, and the anode is where the substrates are placed. The sputtering chamber is filled with a mixture of Ar and O_2 discharge gas [72]. Under the application of DC voltage between the electrodes, the glow discharge is maintained. The Ar+ ions produced by the glow discharge are accelerated at the cathode fall (sheath) and sputter the cathode target, resulting in thin films of the cathode target being deposited on the substrates [73]. Since the glow discharge (i.e., current flow) is maintained between the metallic electrodes in the DC sputtering system, the target is made of metal [74]. A gas discharge occurs when a sufficiently high potential difference is applied between two electrodes in a gas, causing the latter to break down into positive ions and electrons [75]. When a potential difference is applied, however, the electric field in front of the cathode accelerates the electrons, causing them to collide with the gas atoms [76]. Ionization collisions result in the formation of new electrons and ions. The electric field accelerates the ions toward the cathode, where ion induced secondary electron emission releases new electrons [77]. The glow discharge is formed by the processes of electron emission at the cathode and ionization in the plasma [78]. Figure (2.8) the mechanism of atomization in the plasma sputtering technique [79].

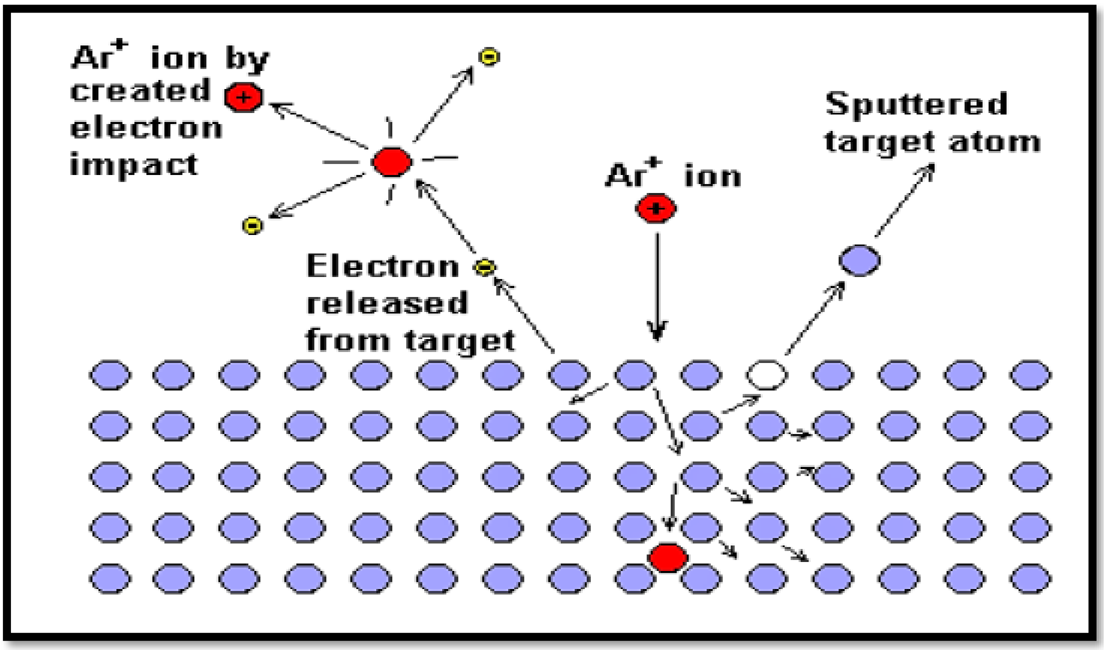

Figure (2.8): The mechanism of atomization in the plasma sputtering technique [79].

2.8.2 Benefits of DC Sputtering

DC Sputtering (Low - pressure) is the most basic and inexpensive type of sputtering for PVD metal deposition and electrically conductive target coating materials [80]. If you're undertaking metal deposition for coating, the DC process has two significant advantages : it's easy to control and it's a low-cost option, limited material choice (metal only) [81]. It produces nanomaterials selectively and of very good quality. It produces impurity-free, clean, thin films and Atomization gives homogeneous films over a large base area [82].

2.8.3 Applications of DC Plasma Technique

Low-pressure plasma technology has a wide range of applications in the microelectronics industry and the processing of materials surfaces [75]. The field of glow discharge plasma has recently seen a rise in interest, etching and semiconductor wafer processing, polymerization in optical fiber fabrication, fibrous material treatment, surface modification by deposition of diamond films and corrosion resistance coatings, plasma immersed ion implantation for plasma nitriding, flat plate displays, high-pressure arcs and jets for ceramic coating and plasma paralysis applications [83].

2.9. Silver

Silver is a transition metal with atomic number 47 and an atomic mass of 107.87. It has widely been used as an antibacterial agent for centuries because it is a non-selective toxic biocide [84]. Silver has a strong inhibitory and bactericidal effect on a range of bacteria, fungi, and viral pathogens. The antibacterial activity of silver was first demonstrated in the 19th century. Now, the use of various forms of silver as a topical agent is commonplace [85]. The excellent thermal and chemical stability of silver and its relatively low cost make it an ideal candidate for its incorporation in a wide variety of materials. In addition to these advantages, the discovery of the antibacterial properties of silver nanoparticles has further increased the interest in silver as key component in antimicrobial materials. [86]. Silver's antimicrobial properties are now being used on catheters, medical devices, wound dressings, clothing and everyday items such as grocery carts and door handles [87]. In the recent past, silver has been used in film coatings and on other types of surfaces [88].

The Food and Drug Administration (FDA) has already approved some silver-coated devices for clinical use. Silver has been used for centuries to keep the water clean and for other sanitary purposes, but recently it is receiving a lot of attention due to the rise in antibiotic-resistant bacteria. Silver is a counter to this because it works in many ways, making bacterial resistance very rare [89].

The exact mechanism by which silver exerts its antimicrobial activity still remains unclear today. Silver can be applied in different forms, namely as a metal, as a compound, or as the free-dissolved ion. The ancient users of silver had no idea what form of silver worked best, but they just observed the positive effects of silver and silver salts. They also realized that silver worked best when some moisture was present [90]. It was only relatively recently discovered that the silver ion (Ag+) was responsible for the antimicrobial activity of silver [91].

Silver can be incorporated into or coated on polymers or metals by e.g., lyophilization, dip coating, electrospinning, and additive manufacturing. These techniques provide great potential for the use of silver to enhance the antibacterial property of biomaterials [92- 96].

2.10. Literature Review

The literature review reported has been divided into subgroups. The first section deals with the anodization modification. The second section reviews the physical deposition of 316L alloy.

2.10.1. Studies Related to Anodization Modification

***In 2014, Ni S, Sun L, et al*. [97]:** In this study, 316L stainless steel with tunable nanometer pit sizes (0, 25, 50, and 60 nm) were fabricated by an anodization procedure in an ethylene glycol electrolyte solution containing 5 vol % perchloric acid. It was found that the nano-pit arrays on all of the 316L stainless steel samples were in a regular arrangement. The surface properties of the 316L stainless steel nano-pit surface showed improved wettability properties as compared with the untreated 316L stainless steel. The anodized 316L stainless steel surfaces with 50 nm and 60 nm diameter pits were also rougher at the nanoscale. According to MTT assays, compared with un anodized, the 50 and 60 nm diameter nano-pit surfaces dramatically enhanced initial human dermal fibroblast attachment and growth for up to 3 days in culture. Mechanistically, this study also provided the first evidence of greater select protein adsorption (specifically, vitronectin and fibronectin which have been shown to enhance fibroblast adhesion) on the anodized 316L stainless steel compared with un anodized stainless steel. Such nano-pit surfaces can be designed to support fibroblast growth and, thus, improve the use of 316L stainless steel for various implant applications (such as for enhanced skin healing for amputee devices and for percutaneous implants).

***In 2017, Nazly Hassan. et al*. [98]:** Focused on the surface treatment of 316L SS in different electrochemical baths. Then, the corrosion behavior and protective efficiency of the treated samples were studied. 316L SS samples were electropolished in several electropolishing baths of H_3PO_4 and H_2SO_4 at 2–6 applied volts and 50–110°C for different time intervals. The corrosion behavior then was studied by means of the potentiodynamic polarization technique and electrochemical impedance spectroscopy in SBF at 37°C. The results proved that the treated samples had better corrosion resistance than the non-polished ones. The highest corrosion resistance was observed for the treated sample at 5 V and 90°C in a 10:90 ratio of acidic electrolyte (H_3PO_4:H_2SO_4) for 15 min. Moreover, the corrosion resistances of anodically treated samples were found to be dependent greatly on applied volt, bath temperature, polishing time, and phosphoric to sulphuric acids ratio.

In 2020, Hsu HJ, Wu CY, et al. **[99]:** In this study, an electrochemical anodizing method was applied as surface modification of the 316L biomedical stainless steel (BSS). It was found that the oxide layer of dichromium trioxide (Cr_2O_3) was formed on the modified 316L BSS specimens after the different anodization modifications. Moreover, a dual porous (micro/nanoporous) topography can also be discovered on the surface of the modified 316L BSS specimens. The microstructure of the anodized oxide layer was composed of an amorphous austenite phase and nano-Cr_2O_3. Furthermore, in vitro cell culture assay also demonstrated that the osteoblast-like cells (MG-63) on the anodized 316L BSS specimens were completely adhered and covered as compared with the unmodified 316L BSS specimen. As a result, the anodized 316L BSS with a dual porous (micro/nanoporous) oxide layer has great potential to induce cell adhesion and promote bone formation.

In 2021, Cho YC, et al. **[100]:** The study aimed to analyze the recovery period of the anodized 316L biomedical stainless steel (BSS) mini-implant through its implantation on femur of rabbit model. An electrochemical anodization approach with different voltages was used to modify the 316L BSS mini-implant. It was found that the topography of the anodized mini-implant at 5 V for 5 min consisted of a dual (micro/nano) porous structure.

The oxide film of Cr_2O_3 was formed on the surface of the anodized mini-implant after anodizing with 5 V for 5 min. In vitro cell culture assay revealed that fibroblast cells (NIH-3T3) on the anodized samples were more firmly attached as compared with the control sample. Moreover, histological analysis demonstrated that the anodized mini-implant improved bone recovery at 4 weeks after implantation. Thus, this study suggests that the anodized 316L BSS mini-implant could be a potential choice as an anchorage device for effective and efficient orthodontic treatment.

In 2021, Turalıoğlu K, Taftalı M, et al. **[101]:** this study it was aimed to suggest a bimetallic implant material that has superior properties by including titanium alloy with anodizing for having higher wear resistance at the surface part, and also will be cost-effective by including stainless steel at the large part of it. Additionally, an oxide layer was formed on Ti6Al4V/316L layered substrates via anodic oxidation. According to the outcomes, the wear and corrosion resistance of the anodic oxidized specimens were higher compared to untreated 316L and layered Ti6Al4V/316L substrates, and the best results were obtained from the anodized specimen treated for 60 min.

2.10.2. Studies Related to DC Sputtering Coating.

In 2015, Allion-Maurer, Audrey, et al. **[102]:** A plasma-deposited coating, containing silver nanoparticles embedded in an organosilicon matrix, was synthesized, using AISI 316L stainless steel as the underlying substrate. The coating antibacterial property was evaluated on the Gram-negative Escherichia coli K12 MG1655 and the Gram-positive Staphylococcus aureus MW2 strains, by combining indirect (plate counting) and in situ (fluorescent bacteria labeling) methods. Both approaches were shown to be highly complementary and converged on a maximal antibacterial efficacy against E. coli, as plate counts showed a decrease of 6 and 1 Log and dead bacteria represented 25% and 2% of the total adhering bacteria for E. coli and S. aureus, respectively. The coating antibacterial potential was then determined over time on E. coli biofilm. Whatever the biofilm age, growth inhibition was observed due to the silver-mediated bacteriostatic effect. The coating bactericidal activity was initially strong. However, differences between coated and bare stainless-steel surfaces tended to collapse above a 2-day contact time. A thorough characterization of the film properties after ageing in biological suspension or saline solution (short and longer-term exposures) revealed an oxidation of both the organosilicon matrix and the silver nanoparticles, accompanied by silver release at the extreme surface. However, a silver reservoir was still present and potentially active in the deep layers of the coating

In 2019, RodianahAlias, et al. **[103]:** Developing a TaO–Ag Nanocomposite on stainless as surface modification for surgical tool application. In this study, the surface of SS 316L was engineered with a thin multi- layer of tantalum oxide (TaO) and silver (Ag) with thickness of 4.7–6.4µm. The thin film multilayered coatings were deposited using physical vapor deposition (PVD) magnetron sputtering. In this study, Ag/AgTa2O5 nano composite thin film is developed to avoid or limit bacterial adhesion on surgical tool surfaces. The as-deposited Ag/AgTa2O5nano composite film were thermally treated to enhance the mechanical properties of the film. The bonding between the amorphous structure and stainless steel 316L substrate was extensively improved hence the adhesion strength increased (by about 152%) up to 2916 ± 147mN after annealing at 400°C. It was found that the optimal coating surface gives relatively homogenous microstructure. Improved Ag segregation, phase transformation, Ag concentration microstructure and a coarsening of the coating structure were observed in the crystallized specimen. The hydrophobicity properties improvement occurred through the annealing of the as-sputtered thin film up to 101.5 ° by about 124%.

2.10.3. Summary of Literature Review

The following statements summarize the important point of the previous literature review.

- Most of the researchers have investigated the influence of a limited number of anodic process parameters on the performance measures of corrosion parts.
- There are a few studies about the anodization of 316L alloys.
- A literature review shows that the primary anodic parameters (time and voltage) have the most influence on the performance requirements when operating.
- Most researchers used magnetron sputtering as a coating process.
- DC magnetron sputtering method can be used to predict the most significant thickness of silver that influence the surface roughness, corrosion rate and bactericidal.

Chapter Three

Experimental Part

Chapter Three

Experimental Work

3.1. Introduction

This chapter deals with the main features of experimental procedures, which were required to achieve the aims of this investigation. This chapter presents the materials used in this work to produce a coating layer by means of the anodizing process, and the DC sputtering plasma process, devices, and tests used in this investigation. This includes, preparation, chemical composition using X-Ray fluoresce (XRF), microstructure investigation using optical microscopy OM, Field Emission Scanning Electron Microscopy FESEM, energy dispersive X-ray spectrometer (EDX), and X-ray diffraction (XRD). In addition, it presents mechanical tests such as micro – Vickers hardness (HV). Finally, it presents in vitro test conditions of electrochemical measurements and anti-bacterial tests. Figure 3.1 shows the summary of the overall experiments used in this investigation to give the reader an overview of everything that was used.

This chapter comprises the materials that were used and preparation of these materials and the experimental procedures. The experimental part of this investigation will contain the following:

- Materials used in this study
- Sample preparation for surface modifications and tests
- Experiments and performance methods

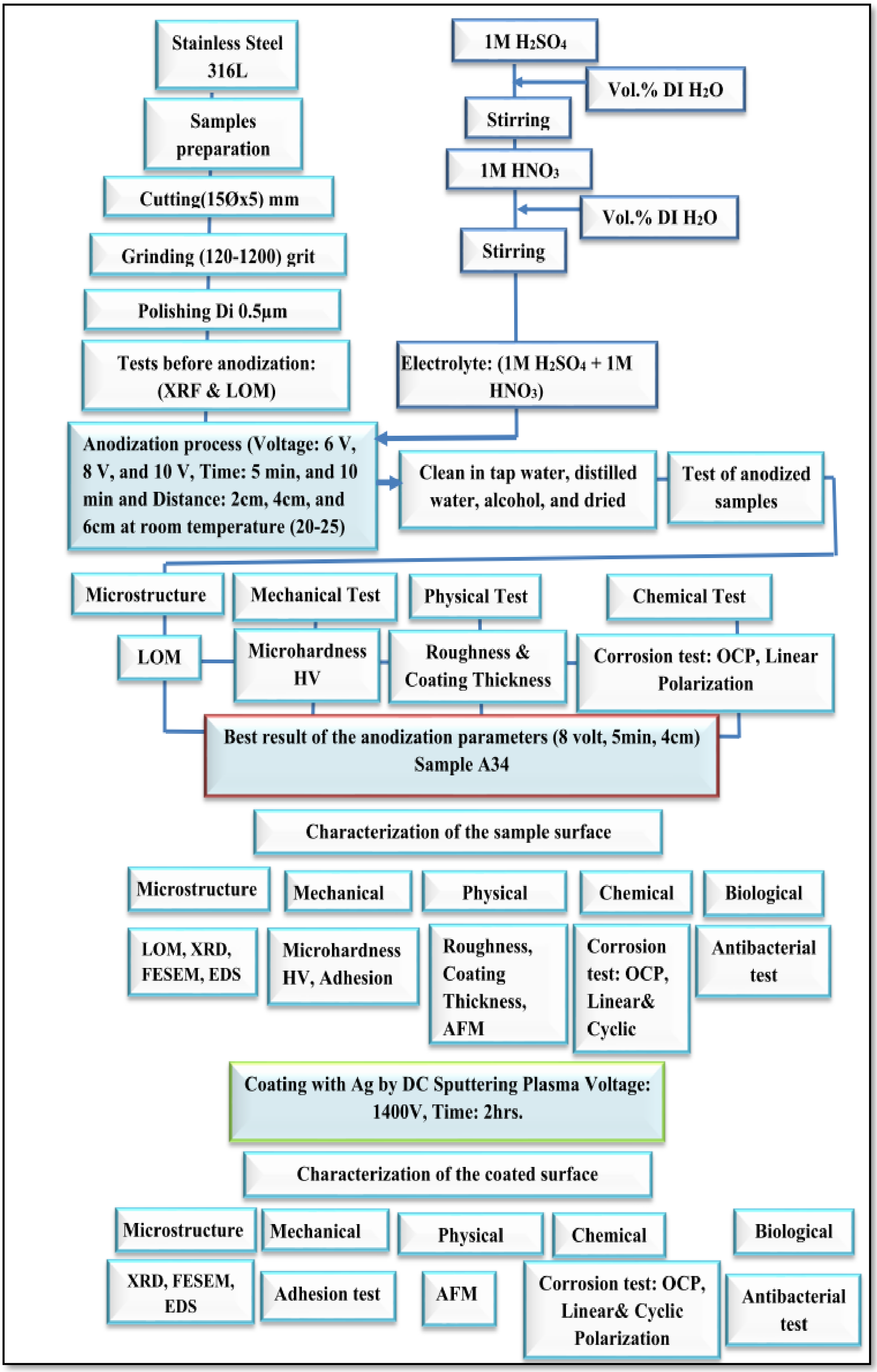

Figure (3.1): Flow Chart of the Procedure Used in this Work.

3.2 Materials Used

3.2.1 Base Alloy

The alloy used in this work was the rod of 316L stainless steel (Figure 3.2) as an anode, which was made in China for stainless steel and high-performance alloys. The analysis of chemical compositions for this alloy is displayed in Table (3.1). This test was performed in the Ministry of Science and Technology, Materials Department / Baghdad - Iraq.

Figure (3.2): 316L Sample.

Table (3.1): Chemical Composition of 316L Alloy used in this Study.

Material	C	Si	Mn	Cr	Ni	Mo	S	P	N	Fe
% Weight	0.027	0.67	1.61	16.18	11.18	2.2	0.01	0.02	0.085	Bal.

A light optical microscope (LOM) has been used to get the microstructure of the etched specimens. The specimens have been etched (the Kroll's solution prepared as an etching solution of 45 ml Glycerol, 15 ml HNO3 and 30 ml HCl) to reveal the grain boundaries in the microstructure. The most common types of features in the microstructure in metallic materials are the boundaries between crystalline grains. The microstructure of 316L stainless steel consists of a solid solution (γ) which has the constitution of nickel and chromium as substantial components dissolved in the matrix as shown in Figure (3.3).

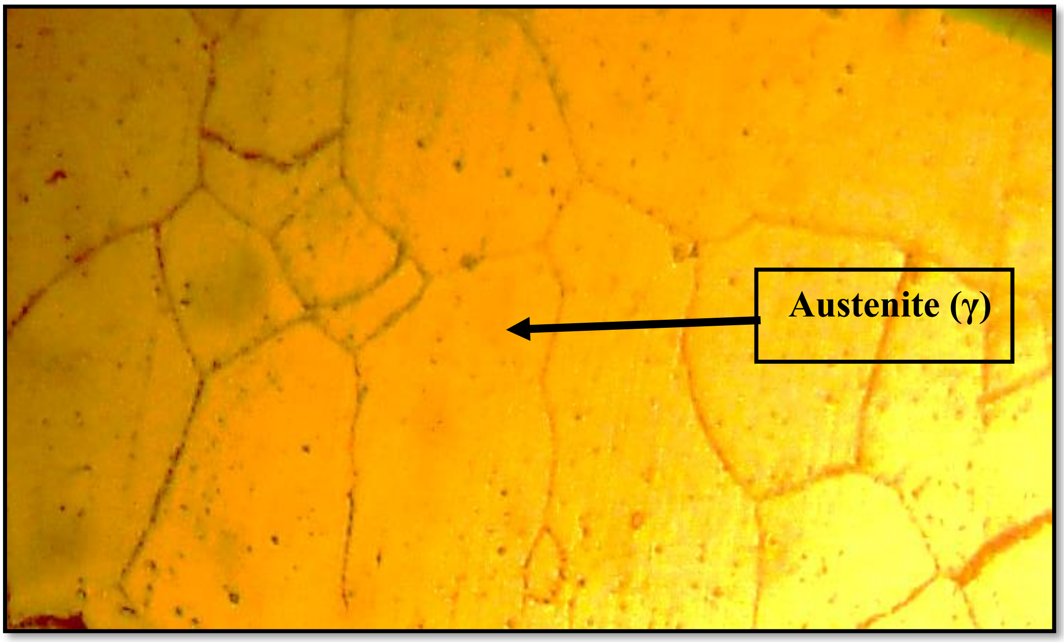

Figure (3.3): Microstructure of the substrate 316L SS (400X).

Figure (3.4) illustrate the XRD pattern for (316L) alloy. The shown patterns are matched to the standard patterns for mentioned alloy.

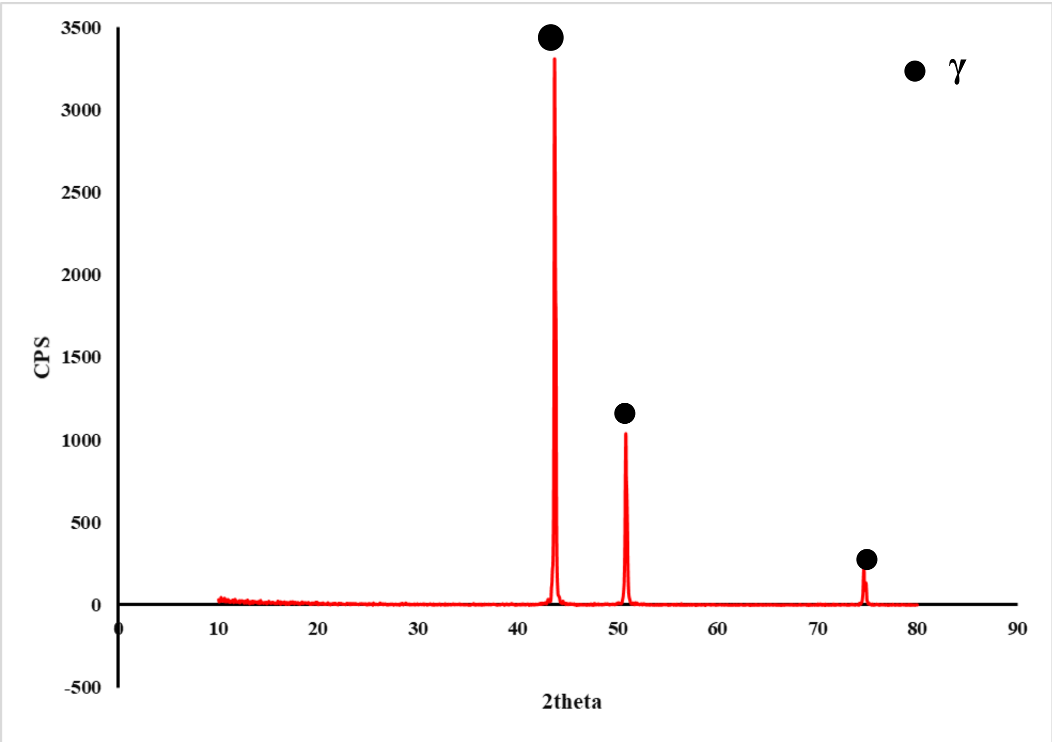

Figure (3.4): XRD Patterns for 316L Stainless Steel alloy.

3.2.2 Cathode Electrode Materials

High purity of silver plate was of dimension (20x10x0.5) mm^3 as shown in Figure (3.5). its available in Iraq market used as a cathode was tested by energy dispersive Xray (EDS) technique joined with the scanning electron microscopic (SEM) device. The purity of silver plate was found more than 97% as shown in Figure (3.6).

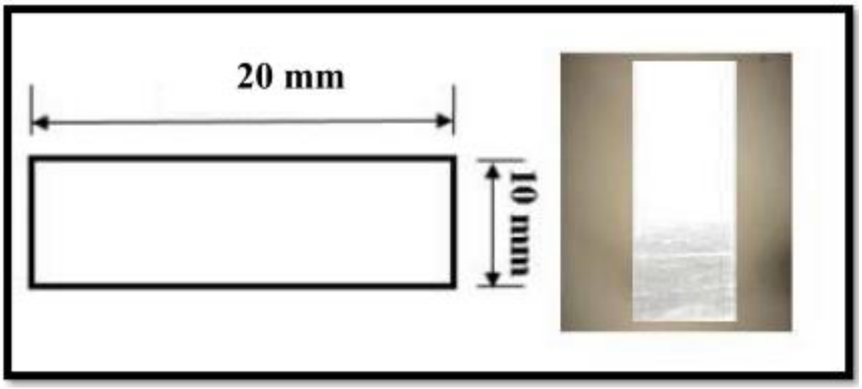

Figure (3.5): Silver Electrode.

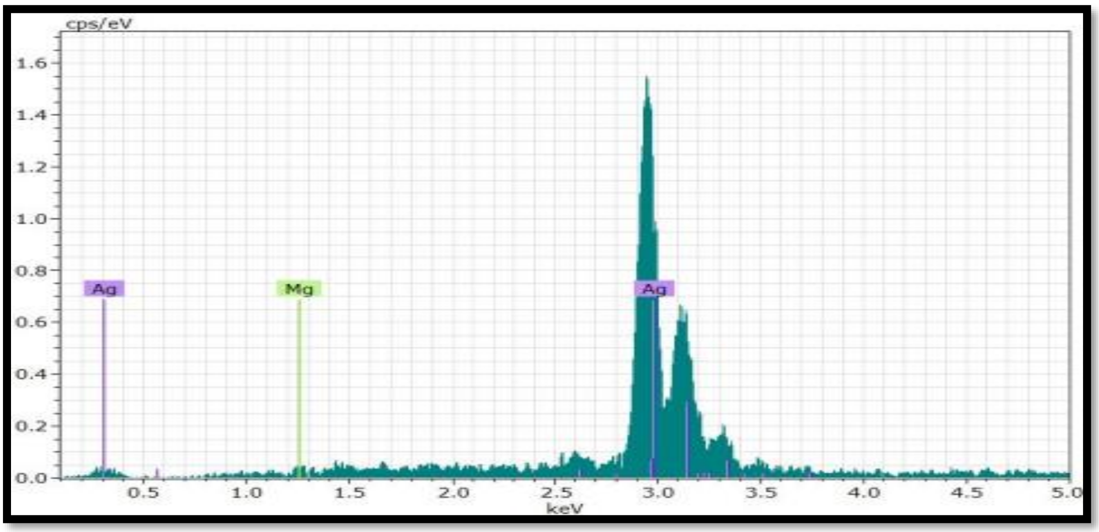

Element	AN	series	[wt.%]	[norm. wt.%]	[norm. at.%]	Error in wt.% (1 Sigma)
Silver	47	L-series	82.15249	99.30903	97.00455	2.937207
Magnesium	12	K-series	0.571602	0.690974	2.995451	0.164164
		Sum:	82.72409	100	100	

Figure (3.6): Energy dispersive spectrum for pure silver.

3.2.3 Electrolyte Materials

Table 3.2 contains the main materials that were used for the Electrolyte.

Table (3.2): The materials used for the Electrolyte.

Material	Formulation	Purity	Origin of Manufacturing
Sulfuric acid	H_2SO_4	98%	**CARLO ERBA**
Nitric acid	HNO_3	70%	**Riedel-de Haen**
Acetone	C_3H_6O	99.0%	**ALPHA**
distilled water	H_2O	-	**-**

3.2.4 Electrolyte Preparation

316L samples were anodically oxidized in an aqueous medium of 1M of H_2SO_4 and 1M of HNO_3 **[99]**. For every experiment, 250 ml of electrolyte was used. To prepare 1M of sulfuric acid we have to add 6 ml of H_2SO_4 and 7 ml of HNO_3.

The electrolyte solution was prepared as follows:

a) 1M of H_2SO_4

The density of 98% sulfuric acid =1.84 g/ml, The molecular weight of H_2SO_4 = 98.07 g/mol

$$M_{\text{H2SO4}} = \frac{\%\,age\ H2SO4 \times \rho \times 1000}{Mole.wt\ of\ H2SO4} = \frac{0.98 \times 1.84 \times 1000}{98.07} = 18.38$$

$$M1V1 = M2V2 \quad \rightarrow \quad V1 = \frac{1 \times 125}{18.38} = 6\ ml$$

b) 1M of HNO_3

The density of 70% Nitric acid =1.413 g/ml, The molecular weight of HNO_3 = 63.01 g/mol.

$$M_{\text{HNO3}} = \frac{\%\,age\ HNO3 \times \rho \times 1000}{Mole.wt\ of\ HNO3} = \frac{0.7 \times 1.413 \times 1000}{63.01} = 15.69$$

$$M1V1 = M2V2 \quad \rightarrow \quad V1 = \frac{1 \times 125}{15.69} = 7\ ml$$

Proper safety measures were taken during the handling of electrolytes, the mixture was magnetically stirred (Figure (3.7)) .

Figure (3.7): Electrolyte solution of (1M H_2SO_4 + 1M HNO_3).

3.3 Samples Preparation

a) The 316L alloy was used as test specimens in this study, these specimens were cut into dimension of (15 diameter * 5 mm thickness) by wire cutting machine (Figure 3.8) at University of Technology/Baghdad. It was prepared up to 20-50 samples for the purpose of conducting coating process.

b) Because of the high sensitivity and accuracy of the anodization process, the specimens used in this process were abraded using silicon carbide (SiC) papers (120–1200 grits) and washed completely with distilled water and, then pure acetone, followed by ultrasonically cleaned with acetone for 20 min, washing specimens distilled water and dried with hot air.

Figure (3.8): Wire Cut Machine.

3.4 Experimental Procedure

3.4.1 First Part: Anodization Process

a) A stainless steel 316L alloy was used as an anode electrode and a plate electrode (silver) as a cathode. The counter electrodes were washed with acetone and then dried.

b) The electrodes were immersed vertically in a 250 ml beaker made of glass containing the electrolyte. The distance between the electrodes in the anodization cell was kept at (20, 40, and 60 mm).

c) The anodization was performed with different deposition times and voltages, (which are explained in Chapter four) using a DC-Power supply (RIGOL DP832) (Figure 3.9).

d) Anodization of 316L alloy at room temperature. After the termination of the anodization process, a jack was used to slowly lower the electrolyte and remove the coated electrode out of electrolyte in order to prevent the detachment. The samples were rinsed with tap water, distil water, ethyl alcohol, and hot air.

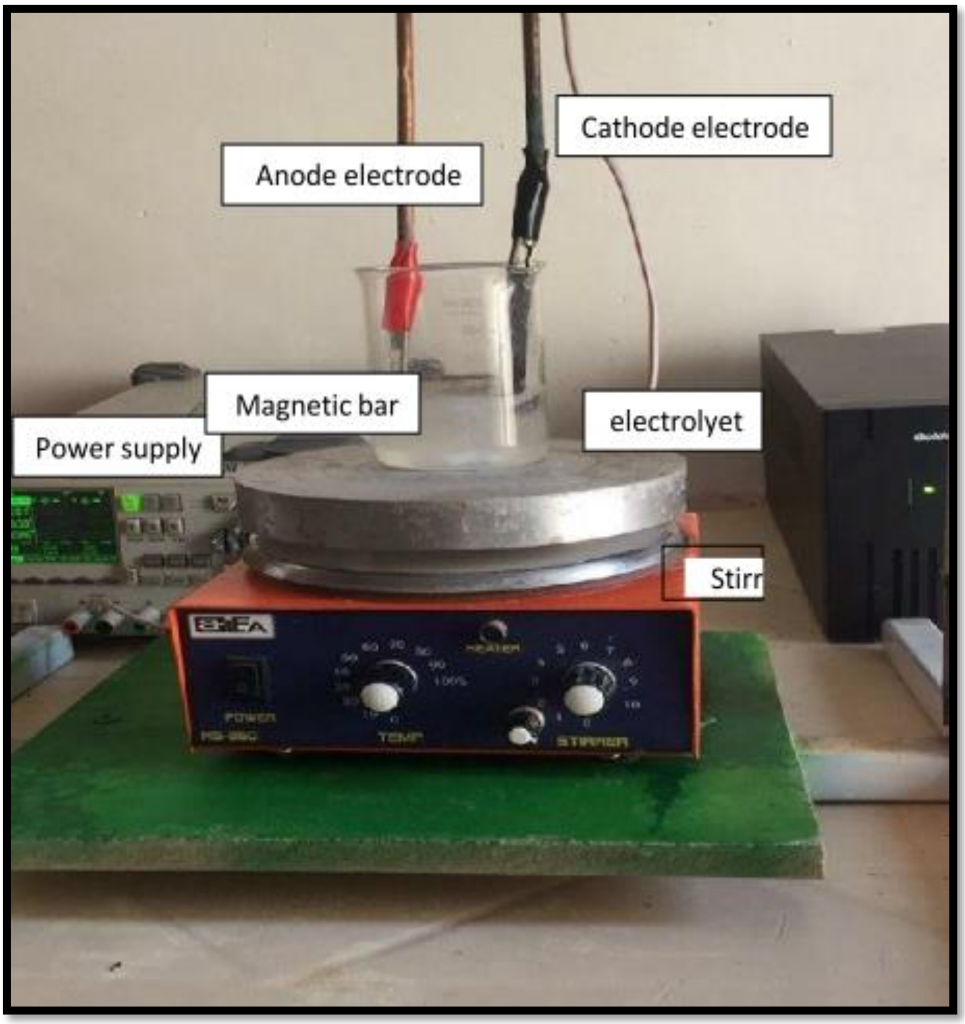

Figure (3.9): An electrochemical cell for anodization process.

The details of different anodization parameters and their levels are given in Table 3.3.

Table 3.3: Major parameters and their levels for anodic oxidation.

No.	Sample code $A_{V,T,D}$*	Voltage (V)	Time (min)	Distance (cm)
1	$A_{6,5,2}$	6	5	2
2	$A_{6,10,2}$	6	10	2
3	$A_{6,5,4}$	6	5	4
4	$A_{6,10,4}$	6	10	4
5	$A_{6,5,6}$	6	5	6

6	**$A_{6,10,6}$**	**6**	**10**	**6**
7	**$A_{8,5,2}$**	**8**	**5**	**2**
8	**$A_{8,10,2}$**	**8**	**10**	**2**
9	**$A_{8,5,4}$**	**8**	**5**	**4**
10	**$A_{8,10,4}$**	**8**	**10**	**4**
11	**$A_{8,5,6}$**	**8**	**5**	**6**
12	**$A_{8,10,6}$**	**8**	**10**	**6**
13	**$A_{10,5,2}$**	**10**	**5**	**2**
14	**$A_{10,10,2}$**	**10**	**10**	**2**
15	**$A_{10,5,4}$**	**10**	**5**	**4**
16	**$A_{10,10,4}$**	**10**	**10**	**4**
17	**$A_{10,5,6}$**	**10**	**5**	**6**
18	**$A_{10,10,6}$**	**10**	**10**	**6**

* ($A_{V,T,D}$): A= anodization sample, V= voltage, T= time, and D= distance

3.5 Test and Characterization.

3.5.1 Light Optical Microscope (LOM)

After the anodization process is completed, visual observation is a very important step for evaluating the layer resulting from the anodization process. The initial evaluation was also considered and checked by (LOM). All specimens that did not result in satisfactory coatings were discarded and work continued on those specimens. the magnification powers were 100 X, 200 X and 400 X. This test was done at specimen's preparation laboratory, the microscope is type (BEL PHOTONICS) as shown in Figure (3.10), located in the Laboratory of thermal transactions in the Laboratories of the Department of Metallurgical - University of Babylon.

Figure (3.10): Light Optical Microscope.

3.5.2. Coating Thickness Measurements

The thickness measuring device (TT260) as shown in Figure (3.11) was used to measure the thickness of oxide thin film, in (College of Material Engineering / University of Babylon).

Figure (3.11): Thickness measuring device.

3.5.3 Surface Roughness

In this work, the surface roughness was measured before and after anodizing. It was measured by surface roughness tester (TR200, SaluTron, made in Germany) shown in Figure (3.12). available at the University of Babylon-Materials Engineering College.

Figure (3.12): (A): Surface roughness tester; (B) and (C): Top and side views to the selected area

3.5.4 Micro Hardness

Microhardness Vickers tester type (Digital Micro Vickers Hardness Tester model TH-714). The utilized loads were (100) g, the holding time was (10) sec, and a standard 136° Vickers diamond pyramid indenter combined with optical microscopy was used to measure the diagonal length of Vickers impression in (college of Material engineering /University of Babylon), show in Figure (3.13). Three readings were reordered for each sample, and the average was calculated. The Vickers micro hardness (HV) in (kg/mm^2) is specified as follows [**104**].

$$HV = 1.854 \times \frac{P}{d^2} \quad \dots\dots\dots\dots\dots.(3-1)$$

Where:

P = applied load kg

d = average length of diagonal mm^2

Figure (3.13): Vickers Hardness Tester.

3.5.5 Electrochemical Test

The electrochemical corrosion tests have been studied for the samples, before and after surface modifications, by polarization tests (potentiodynamic and cyclic). These tests are done in " Tyrode's solution" (chemical composition detailed in Table 3.4). This test is performed by utilizing potentiates/Galvano stats (MLab Bank Elektronik, Germany (Figure 3.14) at the University of Babylon– Department of Metallurgical Engineering. There are three electrodes in the corrosion cell:

1. The electrode of working "316L sample".

2. The counter electrode (platinum rod).

3. The saturated calomel electrode (SCE).

The exposed surface area was (1.767 cm^2) for the electrode working where used for all samples.

Table (3.4): " Tyrode's Solution" Chemical Ingredients.

Component	Concentration(g/L)
NaCl	**8**
KCl	**0.2**
$CaCl_2$	**0.2**
$MgCl_2$	**0.1**
NaH_2PO_4	**0.05**
$NaHCO_3$	**1**
Glucose	**1**
Ph	**6.5**

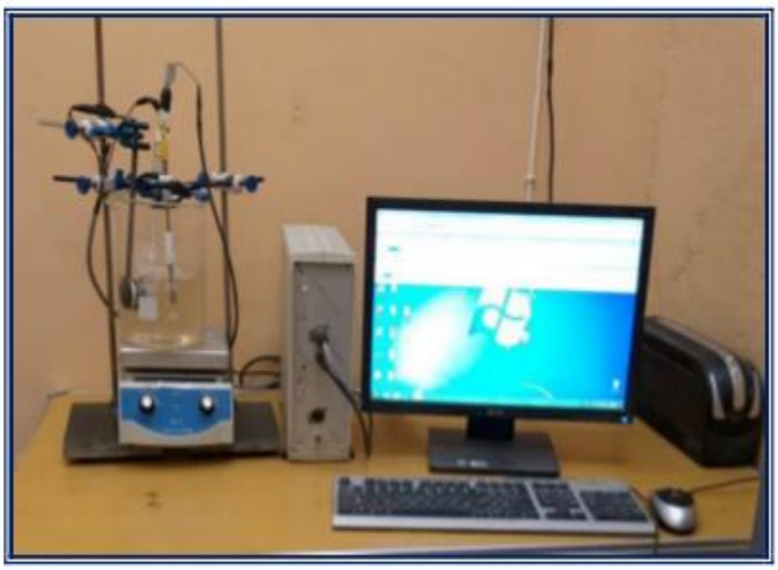

Figure (3.14): The electrochemical Corrosion Test System.

The corrosion rate is calculated using the equation below: **[105]**.

$$CR\ (mpy) = \frac{0.13 i_{corr}\ (E.W.)}{A.\rho} \quad \ldots\ldots\ldots\ldots\ldots\ldots\ldots (3.2)$$

E. W. = equivalent weights (g/ eq)

A = areas (cm^2)

ρ = density's (g/ cm^3)

0.13 = metric and time conversion factor.

$i_{corr.}$ = density of current (μA / cm^2).

3.5.6 Potentiodynamic Polarization

The corrosion behavior of 316L stainless steel was studied here both before and after the surface changes were made by using an electrochemical cell (three-electrode Polarization experiments were carried out using a potentiate of the type "Winking M Lab 200." The potentiodynamic polarization curves were drawn, and Tafel plots were used to quantify both the potential of corrosion (E_{corr}) and the current density of corrosion (I_{corr}) using both anodal and cathodic polarization branches. The experiments were performed at room temperature in " Tyrode's solution."

3.5.7. Cyclic Potentiodynamic Polarization

The cyclic potentiodynamic polarization method gives a reasonable, rapid technique for qualitatively predicting the propensity of an alloy or metal to suffer localized corrosion in the form of pitting. The test was performed in the same system used in the potentiodynamic polarization shown in (Figure 3.14) and the same conditions and test parameters.

3.6. Second Part: Best Anodic Sample Coated by Deposition of Silver by DC Sputtering Technique

3. 6. 1 Manufacture Target (Ag)

The target (Ag) metal has been a diameter (5 cm) and a thickness of (3 mm) was manufactured from a 25 g from micro powder of silver, as a binding material, it has been combined with polyvinyl alcohol (PVA). Then, the mixture powder has been mold in (50mm) diameters for silver by compressing molds, and pressed at pressure (150MPa) utilizing compacted device, to get target hand able. The mould has been pre-lubricated to reduce friction and to release the compact models easily. Next, the target has been dried utilizing the dry box at 100°C for 3 hrs for dehumidify and PVA liberating. The target then cleaned and polished was carried out for sputtering. Figure (3.15) shows the target before sputtering.

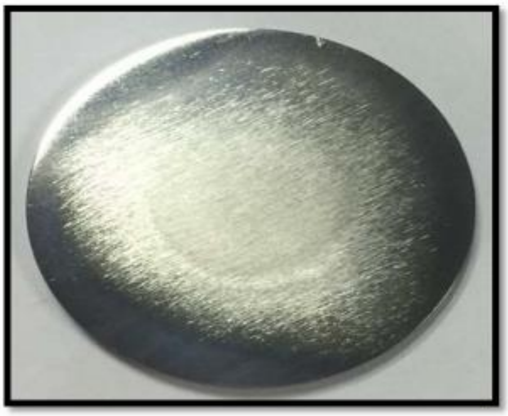

Figure (3.15): Silver target before sputtering.

3. 6.2. DC Sputtering Plasma System

Figure (3.16) shows a photograph of the experimental set up of plasma system which consists of:

(1) plasma chamber: a cylindrical stainless steel vacuumed chamber with length (50 cm) and diameter (50 cm).

(2) chiller.

(3) vacuum pumps system (Rotary and turbo pumps).

(4) gases regulator.

(5) 4 kV, power supply on middle H.V DC.

(6) multimeters for discharge voltage and current measurements.

(7) argon gas cylinder.

(8) oxygen gas cylinder.

(9) anode electrode.

(10) cathode electrode.

Figure (3.16): Image of DC Sputtering plasma system set-up.

The plasma source is made up of a silver cathode (target) and anode (anodized 316L). The cathode is located opposite the anode and gives an electrical field to the gas discharge. The schematics of the plasma chamber shown in Figure (3.17), an insulator disk (ceramic) and a quartz tube with a diameter of 14.5 cm protect the cathode electrodes' bottom change although the target electrode has a surface area of 7.5 cm2 and the target substrate distance was 3 cm with an angle of 90°, tubing and fittings for gas storage cylinders (Argon and Oxygen) deposition time is 2 hr. The background pressure was used to clean the chamber to less than 1.0×10-3 torr by rotary pumps. Working pressure of 6 x 10-2 torr was kept with the O2 /Ar oxygen equally flowing (0:10). Operating voltage in this work is 1400V, and electrical current 20 mA.

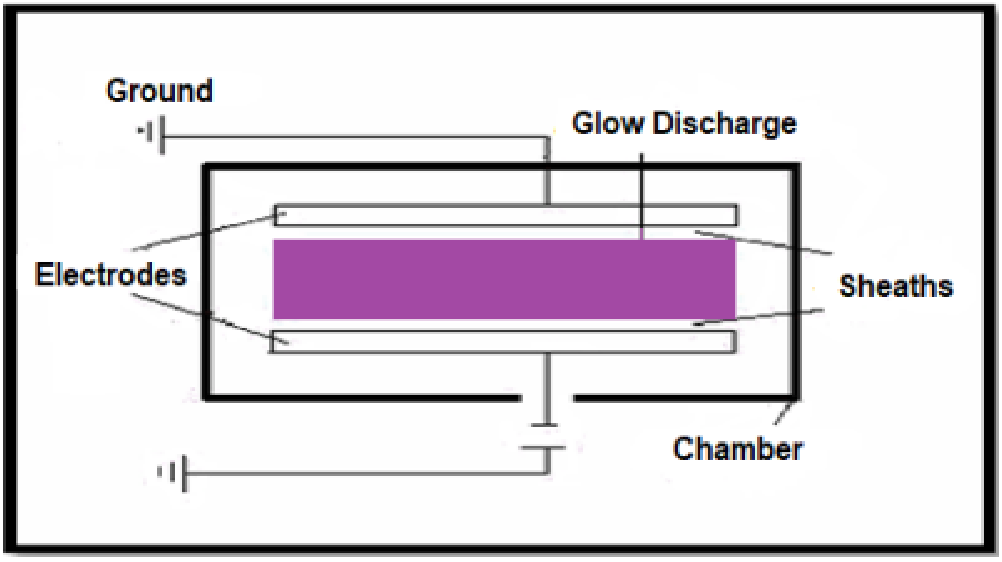

Figure (3.17): Schematic of the plasma chamber.

3. 6.3. Vacuum System

The vacuum system consists of turbo pump assisted by a mechanical rotary pump. Pumping system of the mechanical rotary pump (Blazer of 60 m3/ h) and turbo pump (Varian, V-1000HT). To install the plasma chamber, (Edward CP25-K with controller 1102) and Pirani gauges (LH-

Thermo vac with COMBITRON CM350) were required to monitor actual pressure and measure partial pressures in the plasma chamber. Plasma sputtering, which is worked out in the Ministry of Science and Technology, Baghdad-Iraq.

3. 6.4. Deposition of Thin Films Silver

Before starting the preparation of samples, the following steps were taken:

1- Clean the inside of the system (chamber) with alcohol and acetone.
2- Putting the target in front of the cathode.
3- Putting the anodized substrate in place on the thermal platform and fixing them.
4- Close the system door and start the vacuum operation inside the system space until the pressure inside the system reaches less than 1.0×10-3 torr, and this is the initial pressure.
5- The sputtering chamber was evacuated to a base pressure of 6×10-2 torr and was backfilled with pure argon up to the sputtering pressure of 1.0×10-3 torr and the flowing gas was O2: Ar (0:10).
6- The target and substrate distance were 3 cm with an angle of 90° and the potential was 1400 volt.
7- The deposition time was 2 hours. These operating conditions were the same for all deposited samples.

3. 6.5. Annealing Process of Thin Films

Silver thin films were annealed at 400 °C for one hour in furnace type OTF-1200X, the temperature rise was at a rate of 2 °C/min. Then the samples were left to cool. The process of annealing was carried out with vacuum in order to avoid or minimize sample oxidation or contamination. Figure (3.18) displays a schematic illustration of the annealing process.

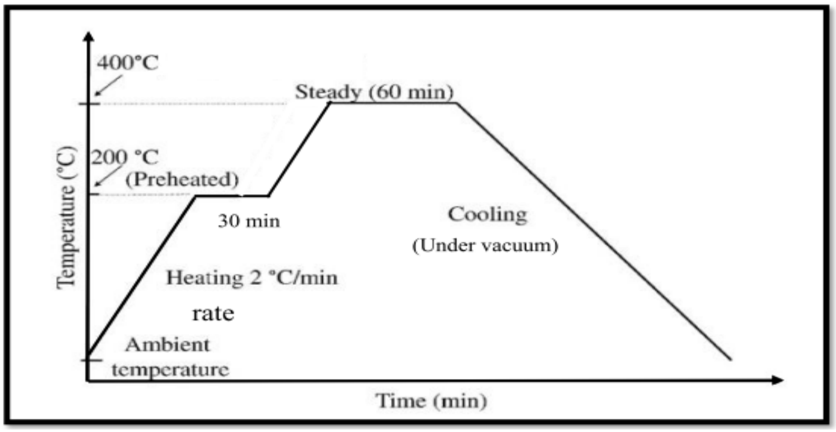

Figure (3.18): Temperature vs. time graph profile of the annealing process for the coated samples.

3.7 Characterizations of Samples

3.7.1 Scanning Electron Microscopy/Energy Dispersive Spectroscopy (FSEM/EDS)

Field emission scanning electron microscopy (FESEM) provides topographical and elemental information at magnifications of (10x - 300,000x) with virtually unlimited depth of field. Compared with convention scanning electron microscopy (SEM), field emission SEM (FESEM) produces clearer, less electrostatically distorted images with spatial resolution down to 11/2 nanometers which is three to six times better. Energy dispersive spectroscopy (EDS) connected to the FESEM machine was also used. The FESEM test was done at University of Tehran (Amirabad) Iran as shown in Figure (3.19).

Figure (3.19): Field Emission Scanning Electron Microscopy (FESEM) system.

3.7.2 X-Ray Diffraction

X-ray diffraction (XRD) techniques is used method to define the presence phases in anodized 316L alloy and after the DC sputtering plasma of silver. The "SHIMADZU Lab X XRD-6000", Japan X-Ray machine used in this thesis (Figure 3.20). The tests were accomplished at the University of Tehran (Amirabad) Iran. X-ray with a nickel filter and generator copper Kα radiation (λ = 1.5406). The scanning speed of the diffract meter was adjusted to 60 per min with the diffraction angle range $2\theta^{o}$ was (10^{o}-100^{o}). The resulting peaks are then compared to standard peaks for each phase that will appear in the 316L stainless steel alloy and phases that will appear as a result of surface modifications.

Figure (3.20): X-ray diffraction SHIMADZU Lab X XRD-6000.

3.7.3. Atomic Force Microscopy

The surface image feature and nano roughness of the deposition layer is observed with the atomic force microscope (AFM). AFM is a beneficial tool used to detect the high-resolution topographies of coated films. This technique is very effective for characterizing the material in the nano scale. This test performed in the University of Babylon–Faculty of Materials Engineering by using AFM Figure (3.21) (SPM AA3000, Angstrom Advanced Inc., USA).

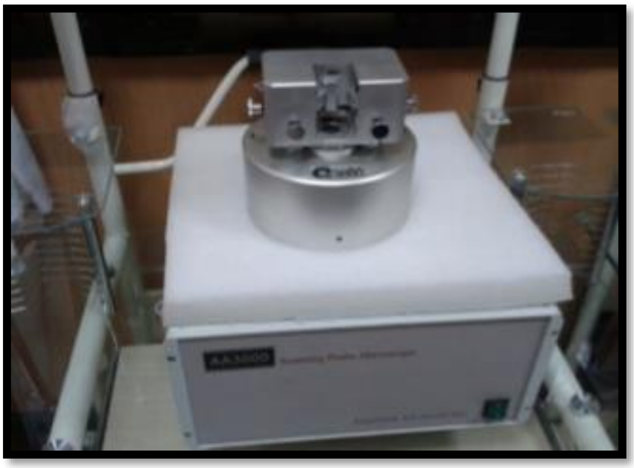

Figure (3.21): Atomic force microscopy system.

3.7.4. Antibacterial Test

The risk of initial microbial colonization and bacterial attack exists on the surface of biomaterial. The activity of antibacterial of the surface layer of modified 316L was investigated to evaluate whether the coated layer is antibacterial or not. The activity of antibacterial is studied by using the inhibition zone method. An antibacterial kinetic test with bacterial strains of "E. coli" (Escherichia coli, American type culture, "ATCC 5922", gram negative bacteria, is prepared at College of Girls science / University of Babylon. The E. coli grown on a (N. agar) “nutrient agar” and placed in the incubator for 24 hrs, then the bacteria spread on a petri dish and incubated at 37 ◦ C for 24 hrs as seen in Figure (3.22), after that, the samples are placed in three different regions on the petri dish and the inhibition zones are observed.

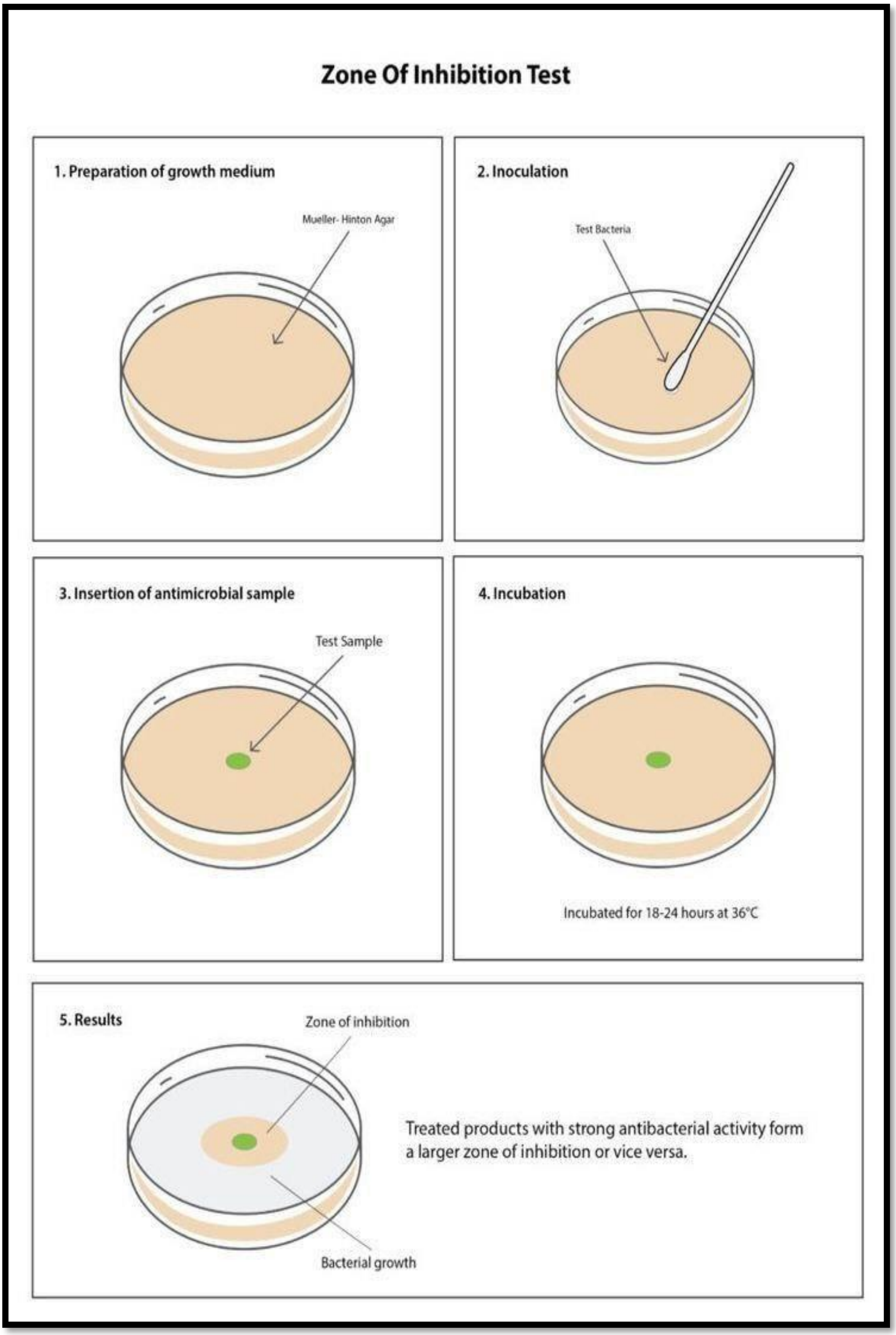

Figure (3.22): Anti-bacterial test.

3.7.5. Adhesion Test

The adhesion test was performed using the Rockwell-C adhesion test, which uses a standard Rockwell hardness tester fitted with a Rockwell (type - C) diamond cone and a load of (150 kg) at 2 sec. Adhesion types as (HF1-HF6) ratio to the cracking level and plating delamination about the indented in Figure (3.23). Adequate adhesion is denoted by the indented classifications ("HF1" and "HF2") [**106**]. Rockwell hardness test was performed on anodized 316L SS substrate and sputtered samples at the University of Tehran (Amirabad) Iran.

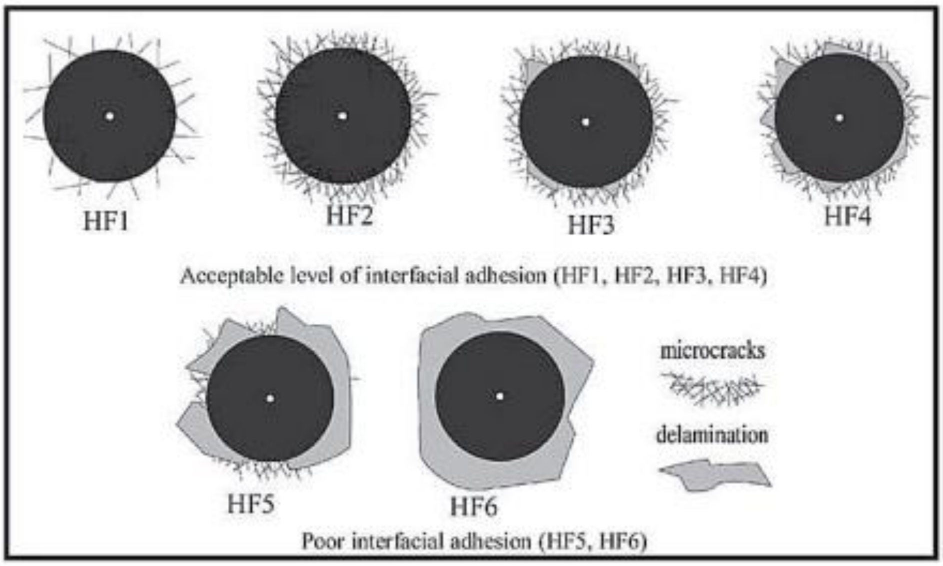

Figure (3.23): The adhesion test planner for Rockwell-C [106]

Chapter Four

Results and Discussion

Chapter Four

Experimental Results and Analysis

4.1 Introduction

This chapter offers the results that have been inferred from the practical part, mechanical, physical, electrochemical, and biological tests followed by their discussion. The results are presented and discussed to demonstrate the effect of surface modifications type and its parameters (such as treatment time, the distance between electrodes, and applied voltage) on the mechanical and surface properties, antibacterial activity, adhesion strength, in addition, corrosion resistance of deposited scale was studied in vitro by "Tyrode’s solution" at room temperature.

4.2. Surface Characterization Techniques after Surface Modifications

Part I: Anodization Technique

4.2.1 Result of Microstructure

In this work, porous structures in different diameters and morphologies have been obtained by tailoring the major anodization parameters of applied potential, time and distance.

A porous structure is anticipated as a result of a significant increase in local temperatures accomplished at the electrolyte/surface interface along with the dynamic release of oxygen and/or water vapor [**107**].

The samples have been anodized to reveal the porous in the microstructure are shown in the following Figures (4.1) to (4.9) shows the microstructure images that have been taken by using optical microscope for anodized alloys ($A_{6,5,2}$, $A_{6,10,2}$, $A_{6,5,4}$, $_{6,10,4}$, $A_{6,5,6}$, $A_{6,10,6}$, $A_{8,5,2}$, $A_{8,10,2}$, $A_{8,5,4}$, $A_{8,10,4}$,$A_{8,5,6}$,$A_{8,10,6}$,$A_{10,5,2}$, $A_{10,10,2}$, $A_{10,5,4}$, $A_{10,10,4}$, $A_{10,5,6}$ and A_{66}) after anodization process with magnification of (400x).The microstructure showed pores in different size and insures the formation of the chromium oxide (Cr_2O_3), which produce a significant improvement in the mechanical properties such as; microhardness [**108**].

a) At an applied voltage of 6 V and distance 2cm.

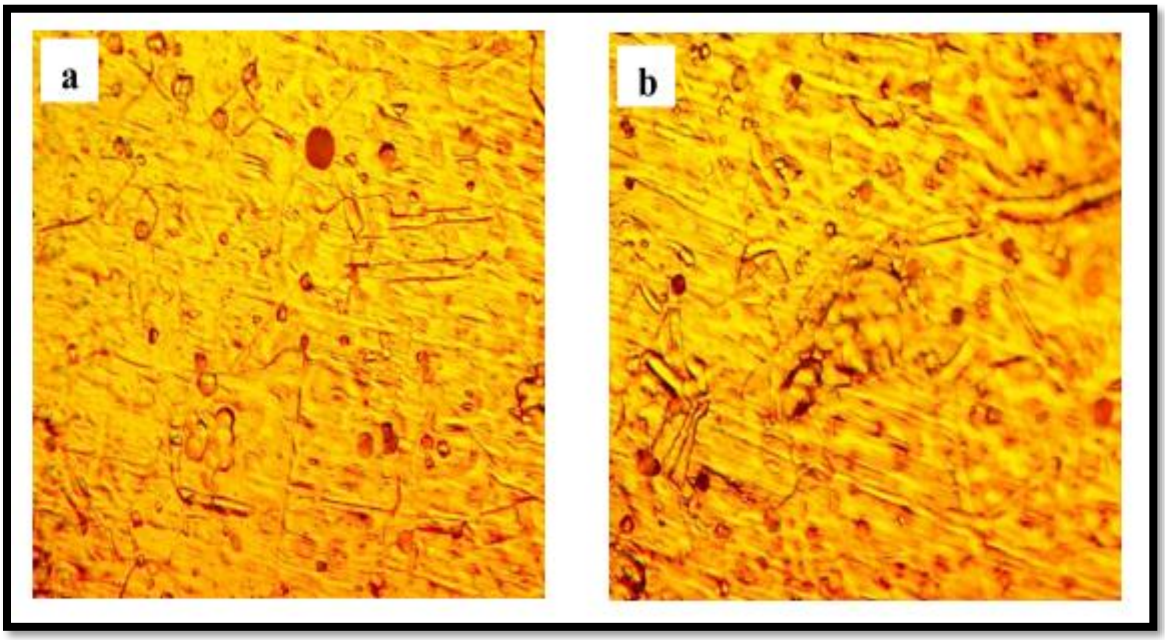

Figure (4.1): Optical Images of ($A_{6,5,2}$ & $A_{6,10,2}$) at Different Conditions of Time: (a) 5 min; and (b) 10 min. (400X).

b) At an applied voltage of 6 V and distance 4 cm.

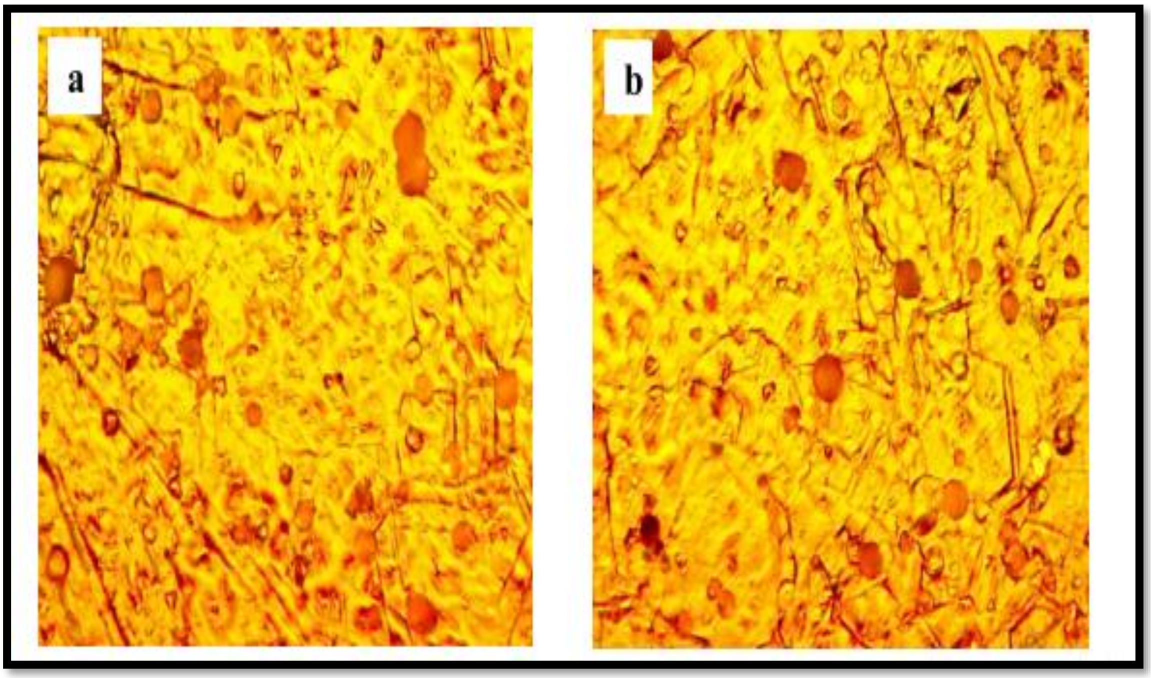

Figure (4.2): Optical Images of ($A_{6,5,4}$&$A_{6,10,4}$) at Different Conditions of Time: (a) 5 min; and (b) 10 min. (400X).

c) At an applied voltage of 6 V and distance 6 cm.

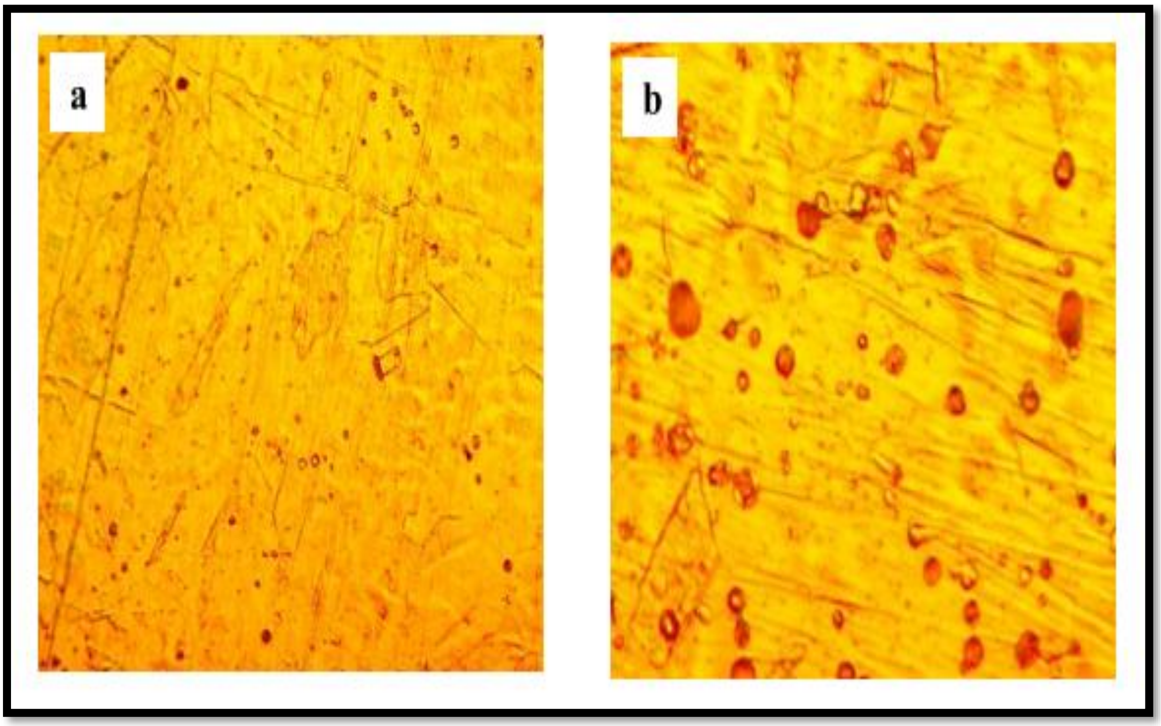

Figure (4.3): optical images of ($A_{6,5,6}$&$A_{6,10,6}$) at different conditions of time: (a) 5 min; and (b) 10 min. (400X).

d) At an applied voltage of 8 V and distance 2 cm.

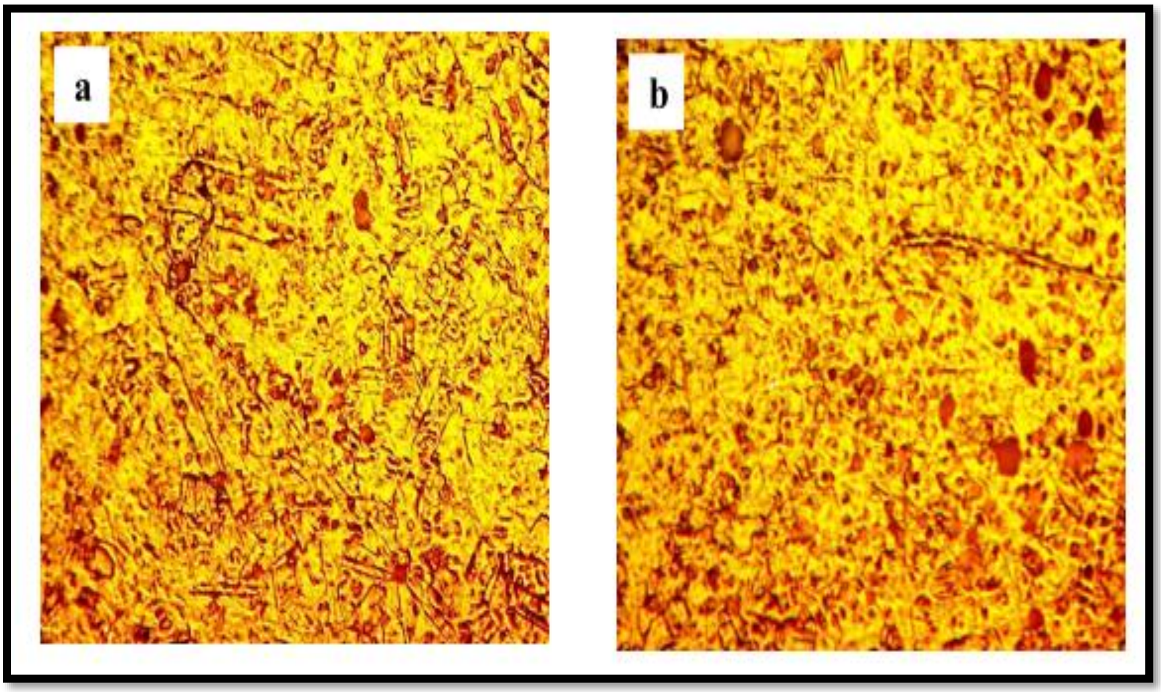

Figure (4.4): optical images of ($A_{8,5,2}$&$A_{8,10,2}$) at different conditions of time: (a) 5 min; and (b) 10 min. (400X).

e) At an applied voltage of 8 V and distance 4 cm.

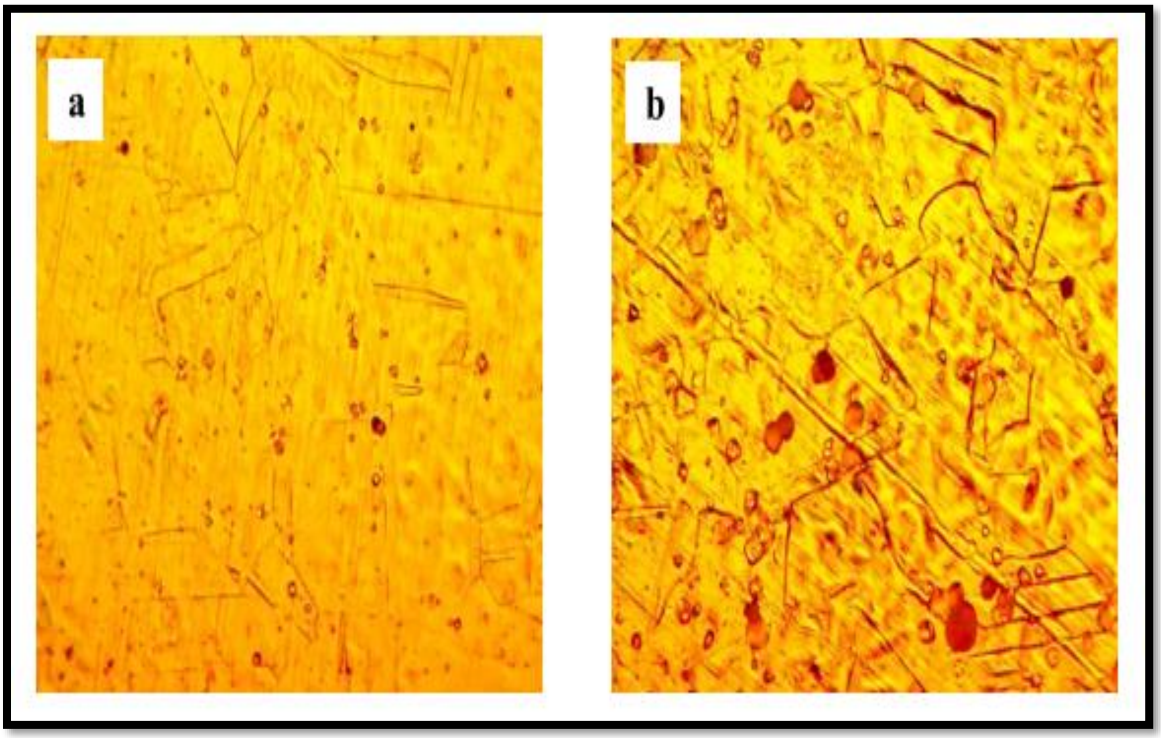

Figure (4.5): optical images of ($A_{8,5,4}$&$A_{8,10,4}$) at different conditions of time: (a) 5 min; and (b) 10 min. (400X).

f) At an applied voltage of 8 V and distance 6 cm.

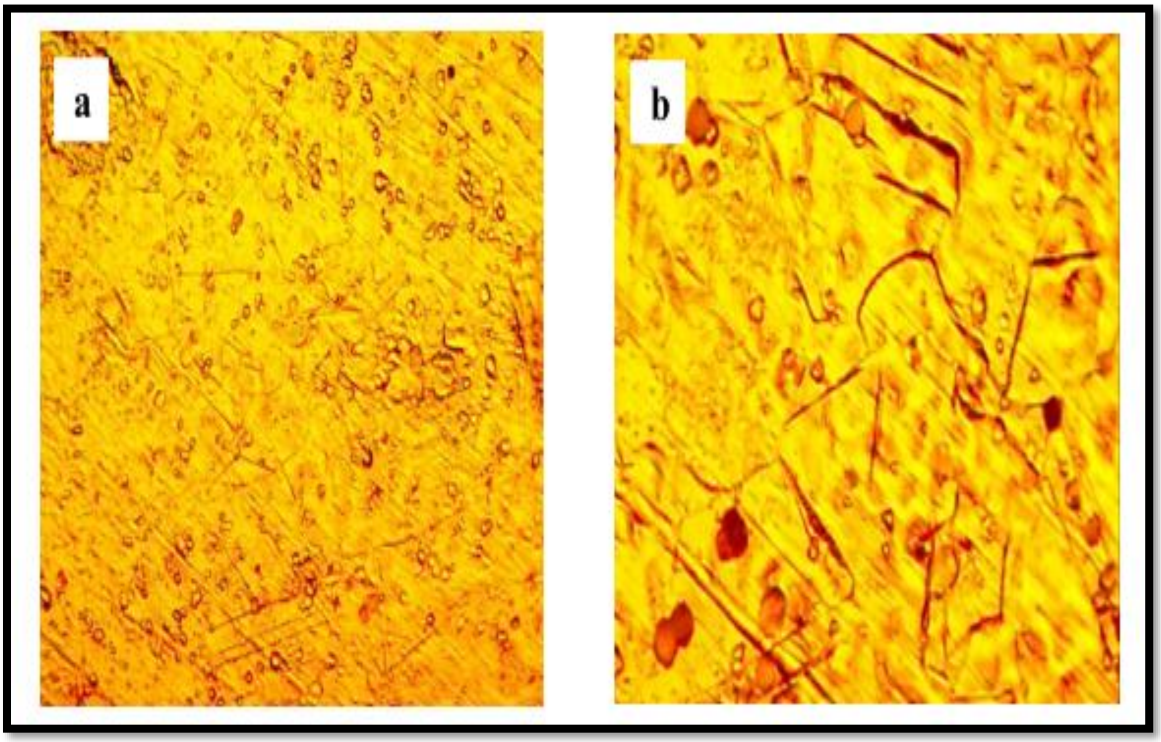

Figure (4.6): optical images of ($A_{8,5,6}$&$A_{8,10,6}$) at different conditions of time: (a) 5 min; and (b) 10 min. (400X).

g) At an applied voltage of 10 V and distance 2 cm.

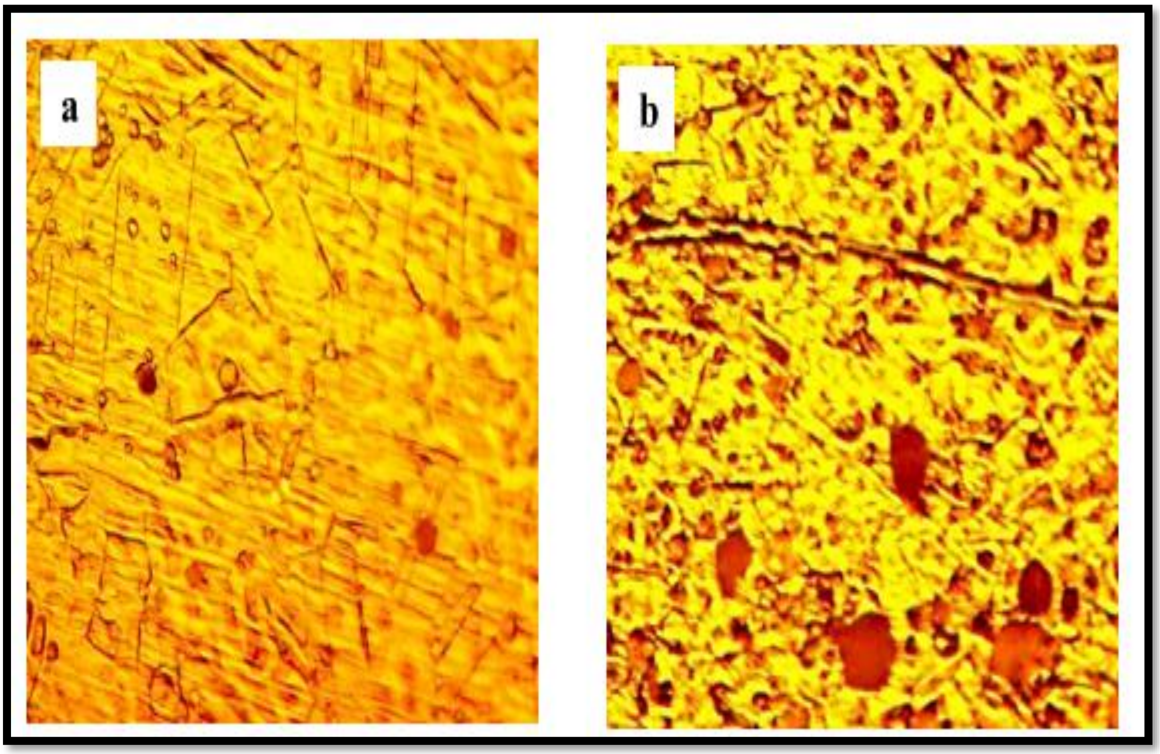

Figure (4.7): optical images of ($A_{10,5,2}$&$A_{10,10,2}$) at different conditions of time: (a) 5 min; and (b) 10 min. (400X).

h) At an applied voltage of 10 V and distance 4 cm.

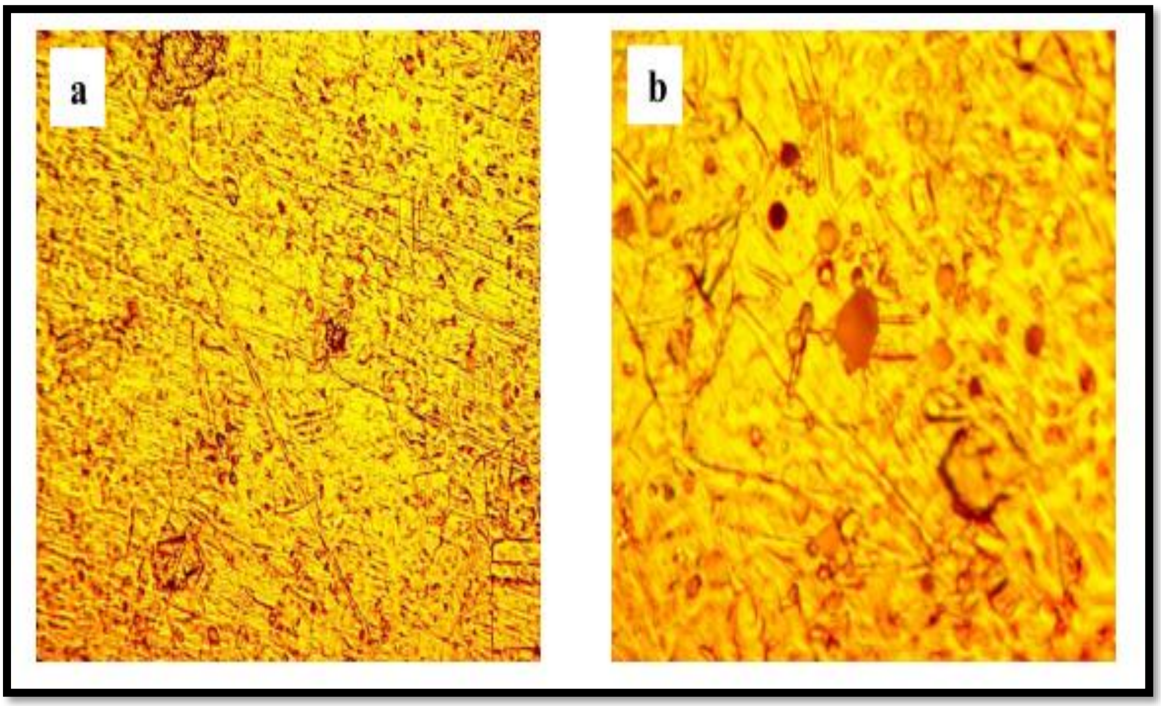

Figure (4.8): optical images of ($A_{10,5,4}$&$A_{10,10,4}$) at different conditions of time: (a) 5 min; and (b) 10 min. (400X).

i) At an applied voltage of 10 V and distance 6 cm.

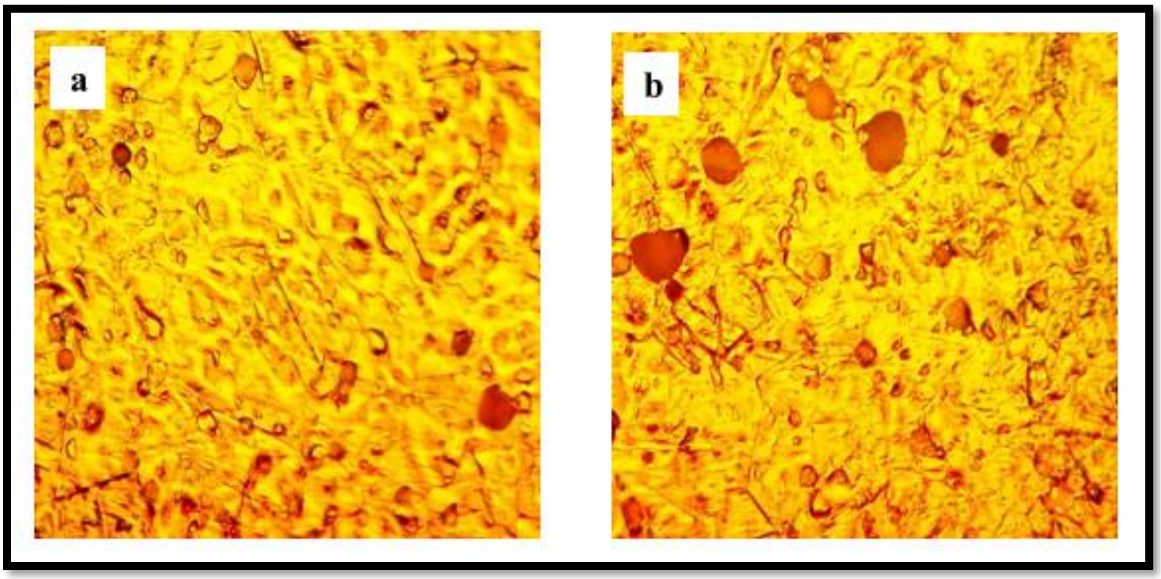

Figure (4.9): optical images of ($A_{10,5,6}$&$A_{10,10,6}$) at different conditions of time: (a) 5 min; and (b) 10 min. (400X).

4.2.2. Results of Coating Thickness Measurements

Table (4.1) represents the results of the coating thickness of oxide coating on (316L) substrate. It is evident from these figures that the parameters of the anodization process like the applied voltage, time, and distance have an obvious influence on the thickness of formed oxide as it increases with increasing these parameters. Among all treated samples, $A_{8,5,4}$ and $A_{8,10,4}$ have the highest thickness values compared to other anodized samples.

Table (4.1): Results of Coating Thickness Measurements

N0.	Sample code	Voltage (V)	Time (min)	Distance (cm)	Coating thickness (µm)
	Base				
1	$A_{6,5,2}$	6	5	2	66.5
2	$A_{6,10,2}$	6	10	2	68.4
3	$A_{6,5,4}$	6	5	4	66.1
4	$A_{6,10,4}$	6	10	4	65.6
5	$A_{6,5,6}$	6	5	6	62.3
6	$A_{6,10,6}$	6	10	6	62.3

7	$A_{8,5,2}$	8	5	2	68.7
8	$A_{8,10,2}$	8	10	2	68.5
9	$A_{8,5,4}$	8	5	4	69.1
10	$A_{8,10,4}$	8	10	4	64.6
11	$A_{8,5,6}$	8	5	6	63.2
12	$A_{8,10,6}$	8	10	6	63.3
13	$A_{10,5,2}$	10	5	2	68.4
14	$A_{10,10,2}$	10	10	2	68.6
15	$A_{10,5,4}$	10	5	4	69
16	$A_{10,10,4}$	10	10	4	65.9
17	$A_{10,5,6}$	10	5	6	62.5
18	$A_{10,10,6}$	10	10	6	63.3

4.2.3. Results of Surface Roughness Measurements

Table (4.2) show the main effect of the three controllable parameters on Ra. It is understandable that two of the variables (voltage and time) have more influence impacts on Ra. Ra increases with applied voltage increasing, in other words, the increase in (I_{input}) causes the increase in Ra, and the charge strikes the surface of the sample more intensely, some pores were observed in the scale, which showed an increase in Ra.

From the result in the table (4.2) notice the highest surface roughness value for the sample $A_{10,10,6}$ due to the use of high voltage and time, and the lowest surface roughness value for the sample $A_{8,5,4}$ due to the homogenous pore distribution.

Table (4.2): Results of Surface Roughness Measurements.

N0.	Sample code	Voltage (V)	Time (min)	Distance (cm)	Ra. µm
	Base				
1	$A_{6,5,2}$	6	5	2	0.124
2	$A_{6,10,2}$	6	10	2	0.213
3	$A_{6,5,4}$	6	5	4	0.146
4	$A_{6,10,4}$	6	10	4	0.102
5	$A_{6,5,6}$	6	5	6	0.107

6	**$A_{6,10,6}$**	**6**	**10**	**6**	**0.105**
7	**$A_{8,5,2}$**	**8**	**5**	**2**	**0.309**
8	**$A_{8,10,2}$**	**8**	**10**	**2**	**0.461**
9	**$A_{8,5,4}$**	**8**	**5**	**4**	**0.090**
10	**$A_{8,10,4}$**	**8**	**10**	**4**	**0.208**
11	**$A_{8,5,6}$**	**8**	**5**	**6**	**0.274**
12	**$A_{8,10,6}$**	**8**	**10**	**6**	**0.208**
13	**$A_{10,5,2}$**	**10**	**5**	**2**	**0.419**
14	**$A_{10,10,2}$**	**10**	**10**	**2**	**0.405**
15	**$A_{10,5,4}$**	**10**	**5**	**4**	**0.526**
16	**$A_{10,10,4}$**	**10**	**10**	**4**	**0.812**
17	**$A_{10,5,6}$**	**10**	**5**	**6**	**0.634**
18	**$A_{10,10,6}$**	**10**	**10**	**6**	**1.497**

4.2.4. Results Vickers Micro Hardness Test

Table (4.3) represents the Vickers hardness. The test of hardness was done by taking the average of 5 readings. Hardness tests have been performed on all anodized specimen and these values will be compared, that there is a significant increase in hardness. The value of the hardness is increase, due to the existence of the oxide scale. Experiments showed that the specimen $A_{8,5,4}$ has the highest hardness (457HV), while the specimen $A_{10,10,4}$ has the lowest (85 HV), Voltage factor influences the hardness values more than anodizing time and distance. At 8V, 5min and 4cm high hardness condition is achieved when the porosity is uniformly distributed. At time of 5 min to 10min the hardness increases with increasing of voltage from 6V to 8V. At time 10 min, the hardness decreases with increasing of voltage from 8V to 10V.

Table (4.3): Results Vickers Micro Hardness Test.

N0.	Sample code	Voltage (V)	Time (min)	Distance (cm)	HV
	Base				210
1	**$A_{6,5,2}$**	6	5	2	323
2	**$A_{6,10,2}$**	6	10	2	335

3	**$A_{6,5,4}$**	6	5	4	324
4	**$A_{6,10,4}$**	6	10	4	379
5	**$A_{6,5,6}$**	6	5	6	291
6	**$A_{6,10,6}$**	6	10	6	373
7	**$A_{8,5,2}$**	8	5	2	425
8	**$A_{8,10,2}$**	8	10	2	317
9	**$A_{8,5,4}$**	8	5	4	457
10	**$A_{8,10,4}$**	8	10	4	368
11	**$A_{8,5,6}$**	8	5	6	399
12	**$A_{8,10,6}$**	8	10	6	355
13	**$A_{10,5,2}$**	10	5	2	372
14	**$A_{10,10,2}$**	10	10	2	359
15	**$A_{10,5,4}$**	10	5	4	134
16	**$A_{10,10,4}$**	10	10	4	85
17	**$A_{10,5,6}$**	10	5	6	314
18	**$A_{10,10,6}$**	10	10	6	351

4.2.5. Corrosion Behavior

Investigation of corrosion behavior of anodizing samples were obtained by potentiodynamic polarization test. At first, the sample is immersed in Tyrode's physiological solution for 30 min and the open circuit potential (OCP) has been recorded after this period, where a steady state potential is attained. The corrosion behavior has been studied for different anodizing parameter.

The anodization at 8 V has the lowest corrosion rate than the anodized sample at (6 and 10) V as a result of the low layer thickness compared with the other samples. The anodization with lower potential result in incomplete oxide scale that produces a nonhomogeneous layer. Moreover, the presence of porosity in the microstructure that allows the penetration of the corrosive fluid into the substrate and corrodes it.

4.2.5.1 linear Polarization Tests

Figures (4.10 – 4.18) shows the potentiodynamic polarization curves for base 316L SS substrate and anodized samples in the Tyrode's solution at room temperture for different time. The corrosion current (i_{corr}) and corrosion potentials (E_{corr}) are derived from the potentiodynamic curves by employing Tafel extrapolation and they are listed in tables (4.4- 4.6). In addition, the corrosion rates (CR) were also included in this table and it was estimated by the Eq (3.2).

It can be seen from the results obtained in tables, the unmodified substrate has corrosion current (i_{corr} = 0.44 μA), as a result of metal ions dissolving on the unmodified substrate's surface, it has the lowest corrosion resistance.

After anodization, it can be observed that the corrosion current of anodized samples decreases for ($A_{8,5,2}$, $A_{8,10,2}$, $A_{10,5,2}$, $A_{6,10,4}$, $A_{8,5,4}$, $A_{8,10,4}$, $A_{10,5,4}$, $A_{8,5,6}$), this mean that the anodization provide a protective layer on the substrate surface that would reduce the corrosion rate.

The anodization at 10 V has the lowest corrosion resistance than the anodization at (6 and 8) V as a result of the non-uniform oxide thickness compared with the other samples. Moreover, the presence of porosity in the microstructure that allows the penetration of the corrosive fluid into the substrate and corrodes it.

On the other hand, when anodization at 8 V, 4cm and 5 min, a lowest corrosion current (i_{corr} = 0.112 μA) was obtained and this result has the highest corrosion resistance than the anodization at 10 V. This is attributed to dense structure of this oxide layer. In addition, the anodization at higher potential led to produce a turbulence in the electrolyte that result in rough and poor surface quality.

As stated in table 4.5 that summarizes the electrochemical parameters values extracted from Figure 4.14, the anodized sample after 5min shows an increase in the E_{corr} and decrease i_{corr} values, which are observed to be (-66.8 mV and 0.112 µA) respectively. When looking at these values it is clear that the anodized sample after 5 min at 8V, 4 cm demonstrates a more prominent move towards the positive region and is consequently more corrosion resistance than anodized sample after 5 min **[99]**.

This means a high oxide protection layer on the $A_{8,5,4}$ 316L substrate is obtained because of uniform, dense and compact layer structure of this sample. The improvement in the corrosion resistance for $A_{8,5,4}$ at ideal anodization condition (8V, 4cm and 5min) was 75%. These results indicate that $A_{8,5,4}$ has less toxicity and consequently the tool life is expected to be higher.

a) At an applied voltage of 6 V and distance 2cm.

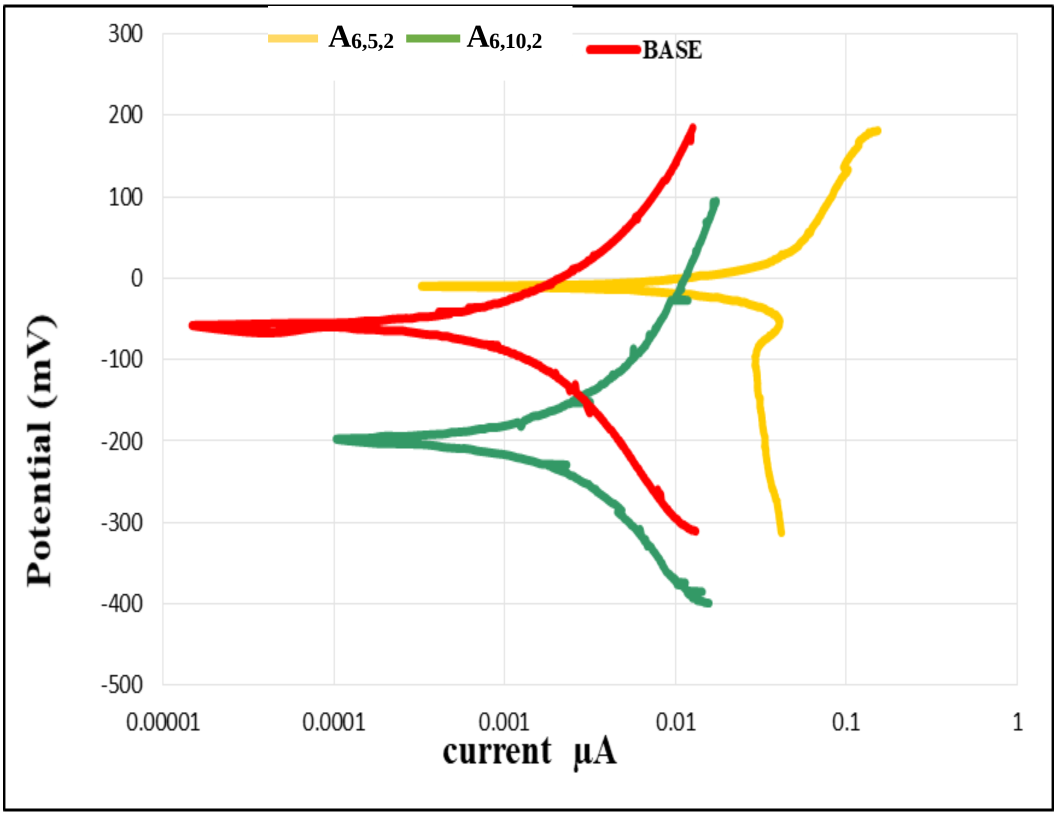

Figure (4.10): Potentiodynamic Polarization for anodized 316l Alloy in Tyrode's solution $A_{6,5,2}$ and $A_{6,10,2}$.

b) At an applied voltage of 6 V and distance 4cm.

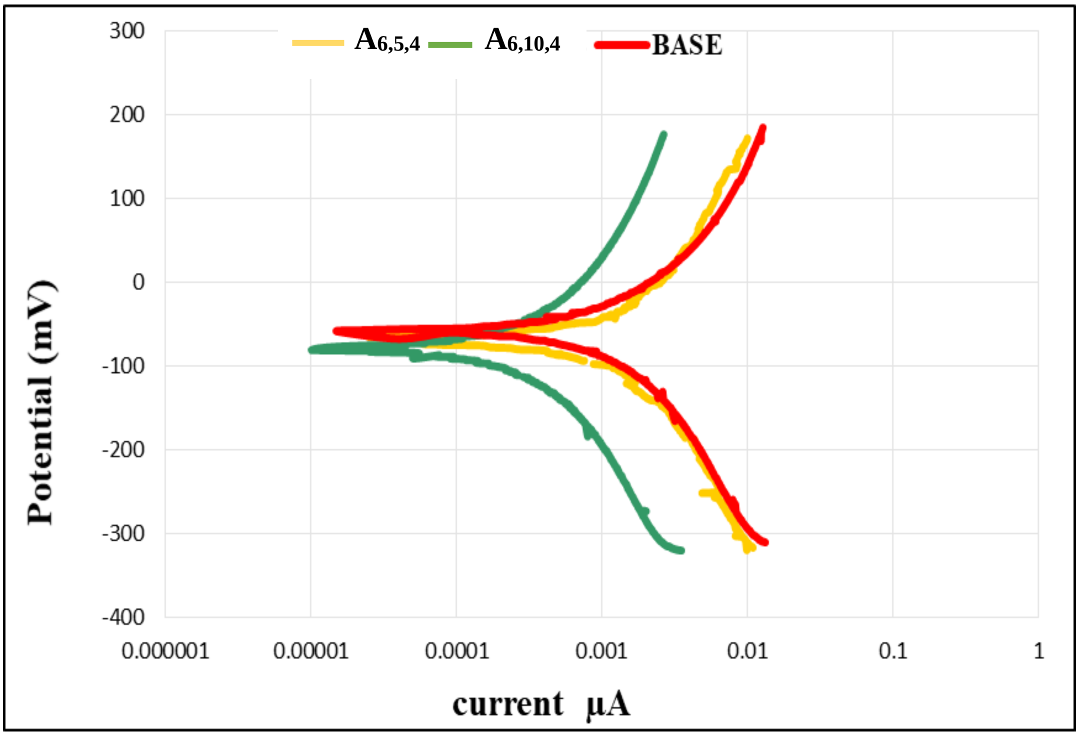

Figure (4.11): Potentiodynamic Polarization for anodized 316l Alloy in Tyrode's solution $A_{6,5,4}$ and $A_{6,10,4}$.

c) At an applied voltage of 6 V and distance 6 cm.

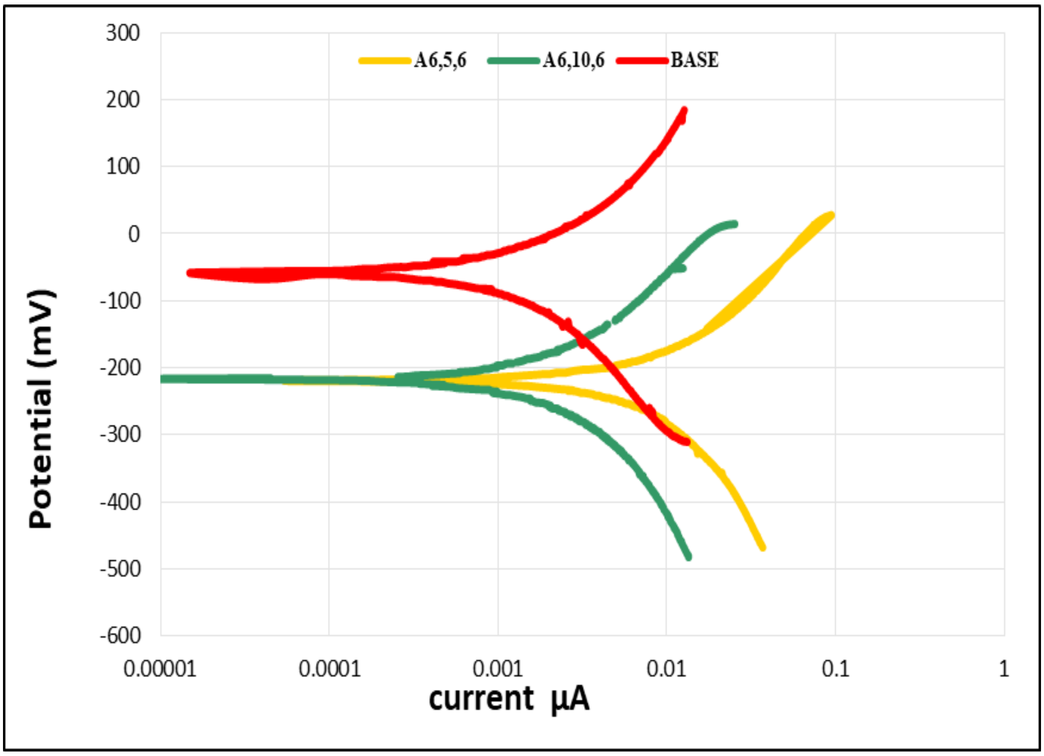

Figure (4.12): Potentiodynamic Polarization for anodized 316l Alloy in Tyrode's solution $A_{6,5,6}$ and $A_{6,10,6}$.

d) At an applied voltage of 8 V and distance 2cm.

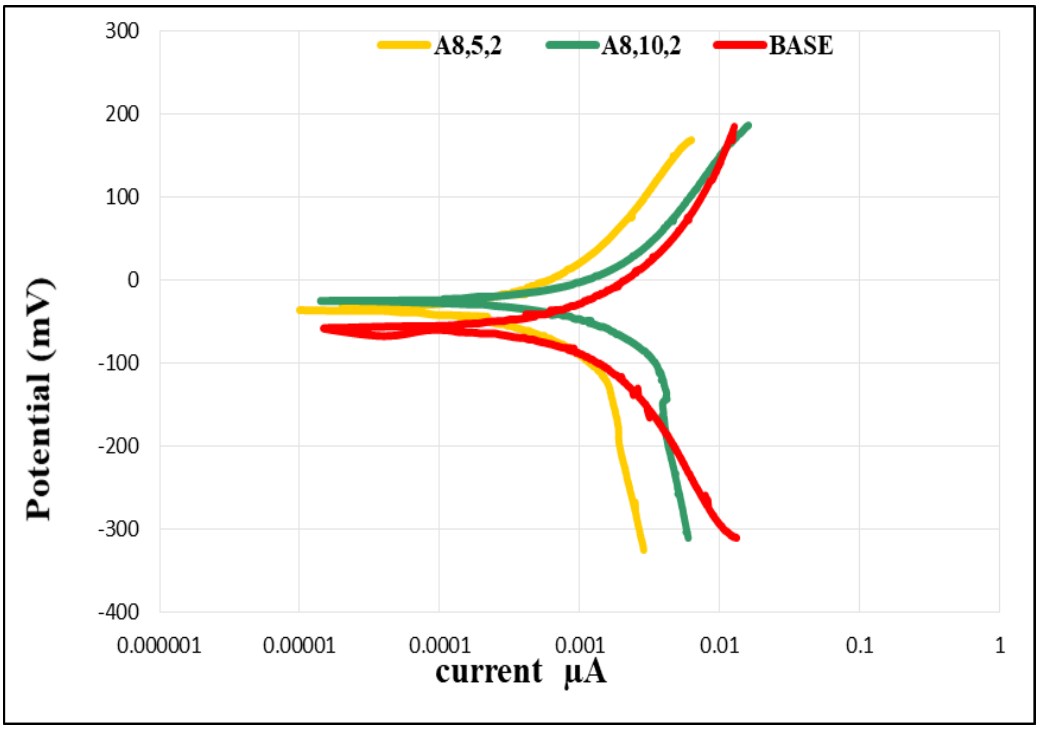

Figure (4.13): Potentiodynamic Polarization for anodized 316l Alloy in Tyrode's solution $A_{8,5,2}$ and $A_{8,10,2}$.

e) At an applied voltage of 8 V and distance 4cm.

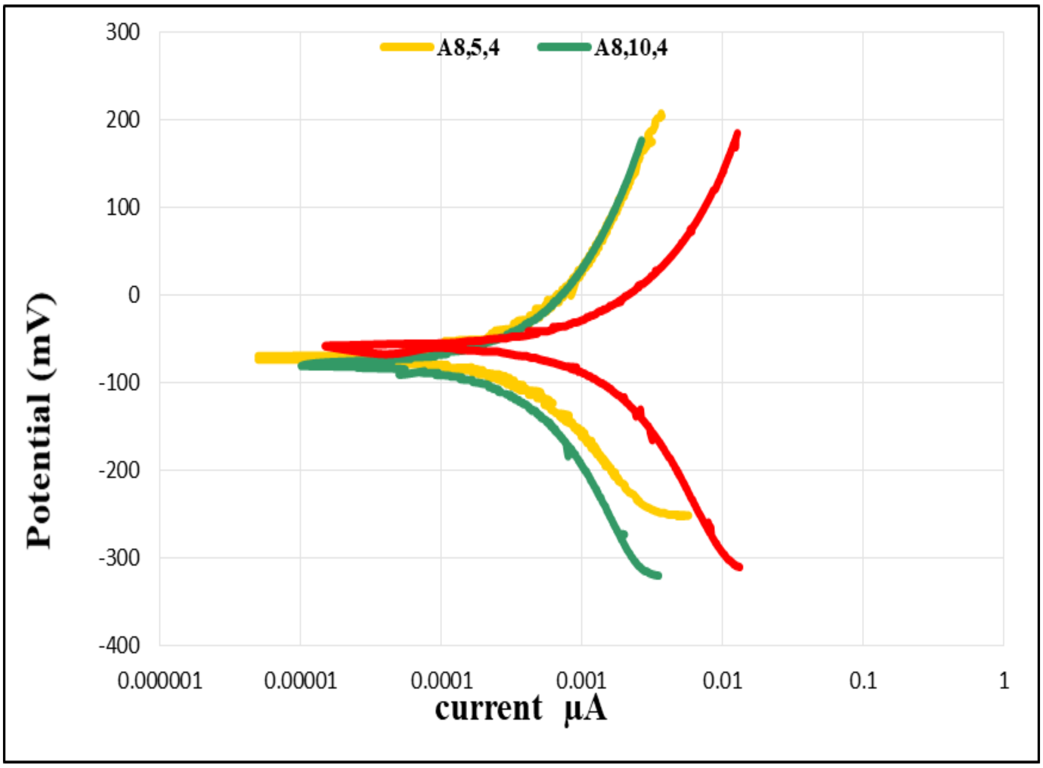

Figure (4.14): Potentiodynamic Polarization for anodized 316l Alloy in Tyrode's solution $A_{8,5,4}$ and $A_{8,10,4}$

f) At an applied voltage of 8 V and distance 6cm.

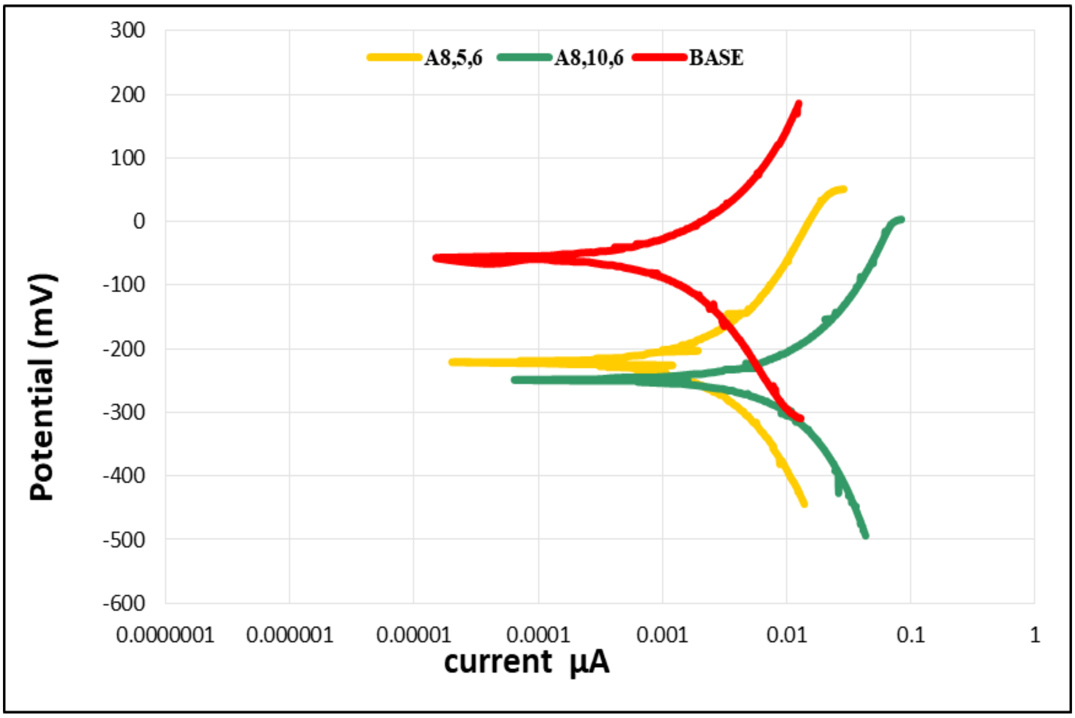

Figure (4.15): Potentiodynamic Polarization for anodized 316l Alloy in Tyrode's solution $A_{8,5,6}$ and $A_{8,10,6}$.

g) At an applied voltage of 10 V and distance 2cm.

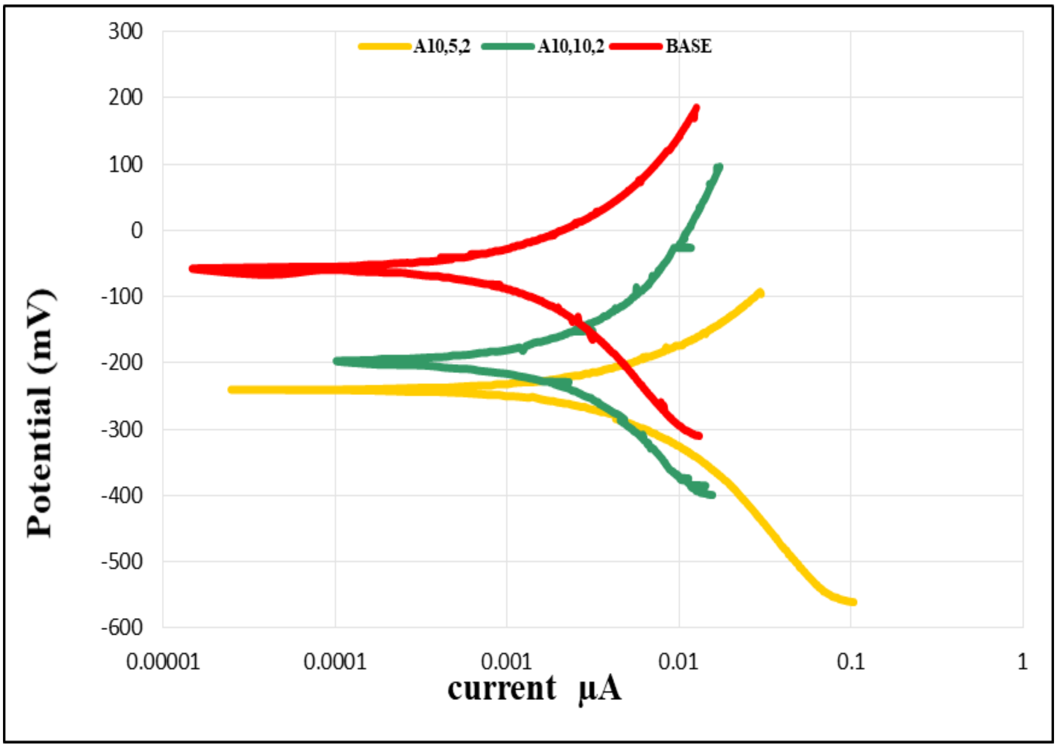

Figure (4.16): Potentiodynamic Polarization for anodized 316l Alloy in Tyrode's solution $A_{10,5,2}$ and $A_{10,10,2}$.

h) At an applied voltage of 10 V and distance 4cm.

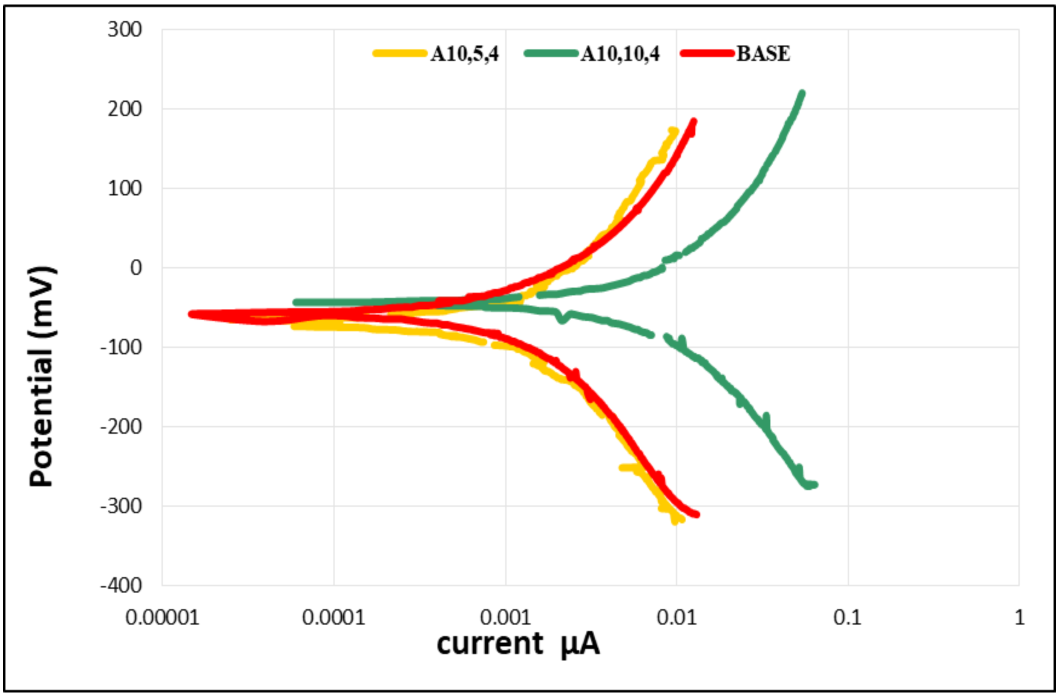

Figure (4.17): Potentiodynamic Polarization for anodized 316l Alloy in Tyrode's solution $A_{10,5,4}$ and $A_{10,10,4}$.

i) At an applied voltage of 10 V and distance 6cm.

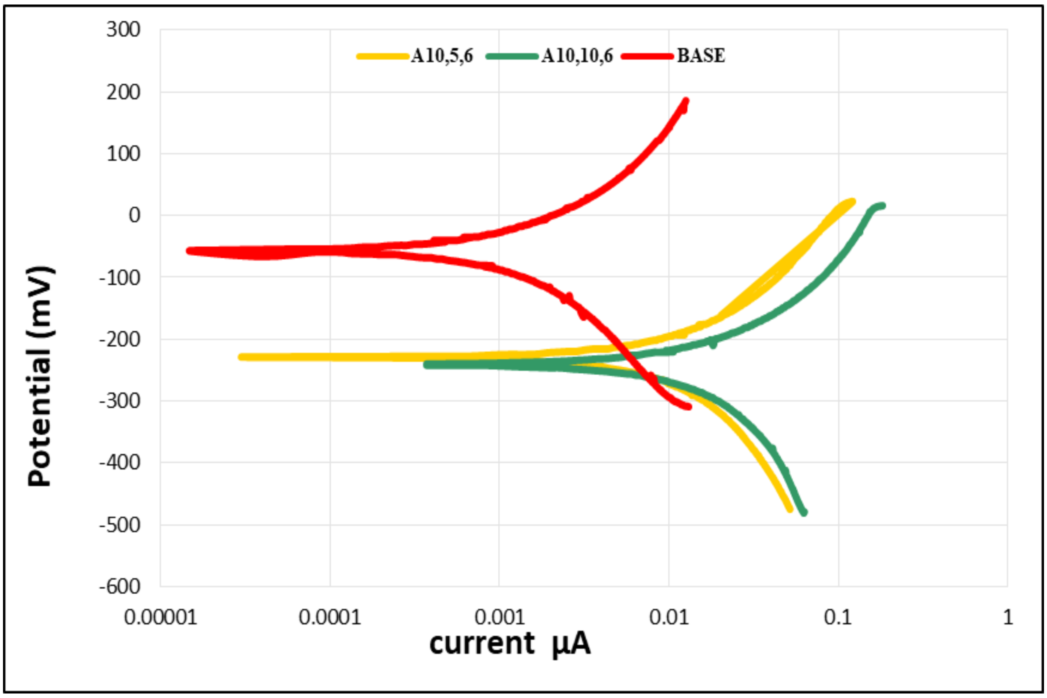

Figure (4.18): Potentiodynamic Polarization for anodized 316l Alloy in Tyrode's solution $A_{10,5,6}$ and $A_{10,10,6}$.

Table (4.4): Electrochemical parameters of the anodized samples for 316L SS at different parameters at 2cm.

Sample code	Conditions	$i_{corr.}$ µA	$E_{corr.}$ mV	CR (mpy)	Improvement Percentage%
Base	**Untreated**	0.44	-56.7	0.1033	-
$A_{6,5,2}$	**6volt, 5min**	22	-7.1	5.1654	-
$A_{6,10,2}$	**6volt, 10min**	0. 645	-197.4	0.490	-
$A_{8,5,2}$	**8volt, 5min**	0.183	-37.1	0.0429	58
$A_{8,10,2}$	**8volt, 10min**	0.28	-27.1	0.0657	36
$A_{10,5,2}$	**10volt, 5min**	0.43	-72.2	0.1009	2
$A_{10,10,2}$	**10 volts,10min**	0.51	-58.5	0.1197	-

Table (4.5): Electrochemical parameters of the anodized samples for 316L SS at different parameters at 4 cm.

Sample code	Conditions		$i_{corr.}$ µA	Ecorr. mV	CR (mpy)	Improvement Percentage%
Base	**Untreated**		**0.44**	**-56.7**	**0.1033**	**-**
$A_{6,5,4}$	**6volt, 5min**		**0.681**	**-84.7**	**0.1598**	**-**
$A_{6,10,4}$	**6volt, 10min**		**0.130**	**-76.2**	**0.0305**	**70**
$A_{8,5,4}$	**8volt, 5min**		**0.112**	**-66.8**	**0.0262**	**75**
$A_{8,10,4}$	**8volt, 10min**		**0.336**	**-91.9**	**0.0788**	**24**
$A_{10,5,4}$	**10volt, 5min**		**0.412**	**-64.7**	**0.0967**	**6**
$A_{10,10,4}$	**10 volt, 10min**		**2.28**	**-44.8**	**0.5353**	**-**

Table (4.6): Electrochemical parameters of the anodized samples for 316L SS at different parameters at 6 cm.

Sample code	Conditions	$i_{corr.}$ µA	Ecorr. mV	CR (mpy)	Improvement Percentage%
Base	Untreated	0.44	-56.7	0.1033	-
$A_{6,5,6}$	6volt, 5min	2.03	-230	0.4766	-
$A_{6,10,6}$	6volt, 10min	2.53	-243.1	0.5940	-
$A_{8,5,6}$	8volt, 5min	0.387	-221	0.0908	12
$A_{8,10,6}$	8volt, 10min	1.6	-248.7	0.3756	-
$A_{10,5,6}$	10volt, 5min	0.955	-218.5	0.2242	-
$A_{10,10,6}$	10volt, 10min	0.664	-216.5	0.1559	-

Note: The obtained results indicated the optimum factors of anodic such as voltages, times, and distances effect on anodic oxide scale $A_{8,5,4}$ (8volt, 5min and 4cm) this agreement with [**99**].

Table (4.7): summary of the result.

N0.	Sample code	Voltage (V)	Time (min)	Distance (cm)	Coating thickness (µm)	Ra. µm	HV	CR (mpy)
	Base						210	0.1033
1	$A_{6,5,2}$	6	5	2	66.5	0.124	323	0.1009
2	$A_{6,10,2}$	6	10	2	68.4	0.213	335	0.0962
3	$A_{6,5,4}$	6	5	4	66.1	0.146	324	0.0967
4	$A_{6,10,4}$	6	10	4	65.6	0.102	379	0.0788
5	$A_{6,5,6}$	6	5	6	62.3	0.107	291	0.2242
6	$A_{6,10,6}$	6	10	6	62.3	0.105	373	0.1559
7	$A_{8,5,2}$	8	5	2	68.7	0.309	425	0.0429
8	$A_{8,10,2}$	8	10	2	68.5	0.461	317	0.0657
9	$A_{8,5,4}$	8	5	4	69.1	0.090	457	0.0262
10	$A_{8,10,4}$	8	10	4	64.6	0.208	368	0.0305
11	$A_{8,5,6}$	8	5	6	63.2	0.274	399	0.0908
12	$A_{8,10,6}$	8	10	6	63.3	0.208	355	0.3756
13	$A_{10,5,2}$	10	5	2	68.4	0.419	372	0.1514
14	$A_{10,10,2}$	10	10	2	68.6	0.405	359	0.3357
15	$A_{10,5,4}$	10	5	4	69	0.526	134	0.1598
16	$A_{10,10,4}$	10	10	4	65.9	0.812	85	0.5353
17	$A_{10,5,6}$	10	5	6	62.5	0.634	314	0.4766
18	$A_{10,10,6}$	10	10	6	63.3	1.497	351	0.5940

4.3 Part II: Characterization of Best Anodized Sample Coated by Silver Deposition by DC Sputtering Plasma Technique

4. 3.1 XRD Analysis

The XRD results for the anodized SS sample Figure. (4.19) show peaks for chromium oxide (Cr_2O_3) and a few substrates (316L SS) of anodized sample at (8 volt, 5min and 4cm) thereby proving the formation of chromium oxide layer on the substrate. The XRD pattern of the anodized sample. From the d-spacing calculation, the diffraction rings can be indexed to be (012), (104), (024), (113) and (116) for Cr_2O_3. Along the XRD test, it is found that Cr_2O_3 is the main phase of after anodization [**99**].

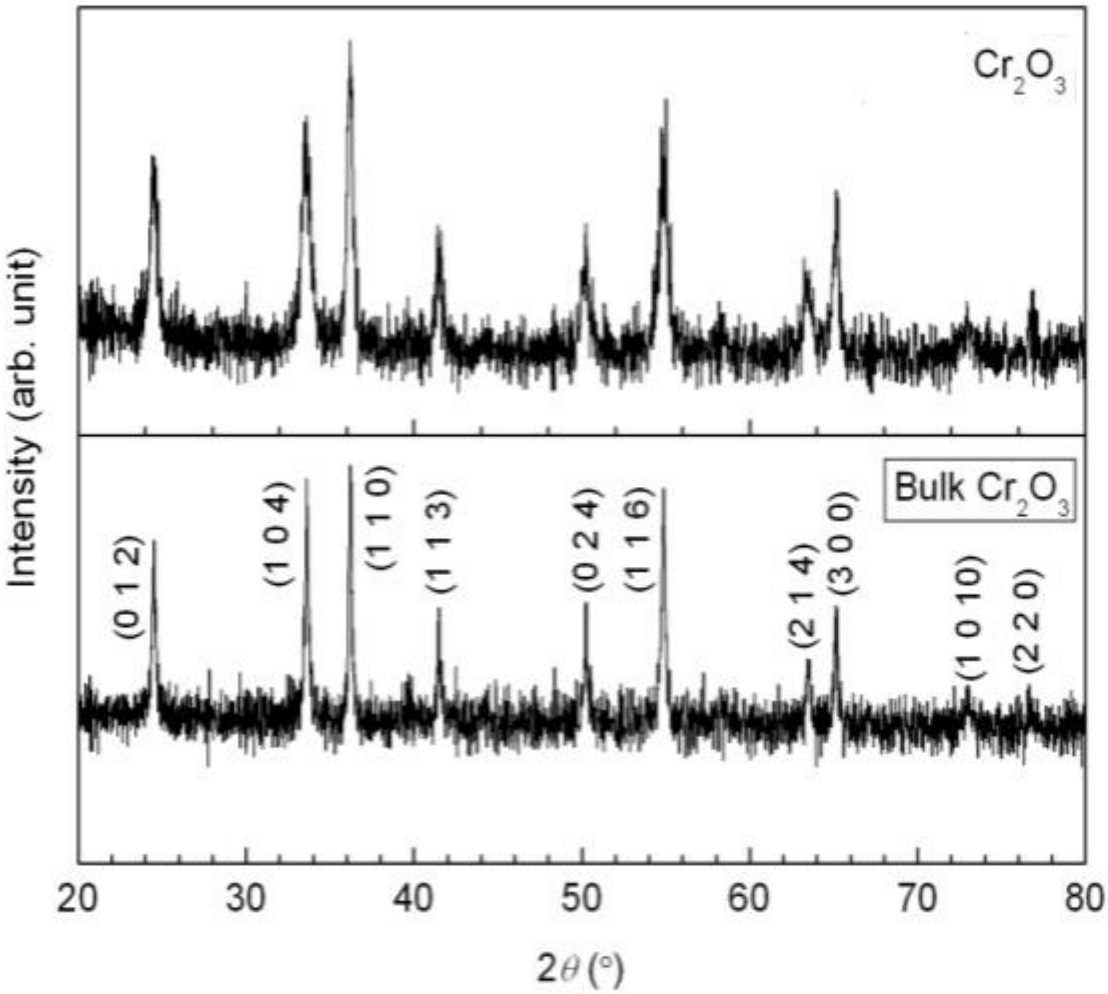

Figure (4.19): XRD profiles of the anodized sample at (8 volt, 5min and 4cm).

Figure 4.20 shows the XRD pattern of the as-sputtered Ag thin scale of the anodized sample. From the d-spacing calculation, the diffraction rings can be indexed to be (111), (200), (220), and (311) for Ag [**103**].

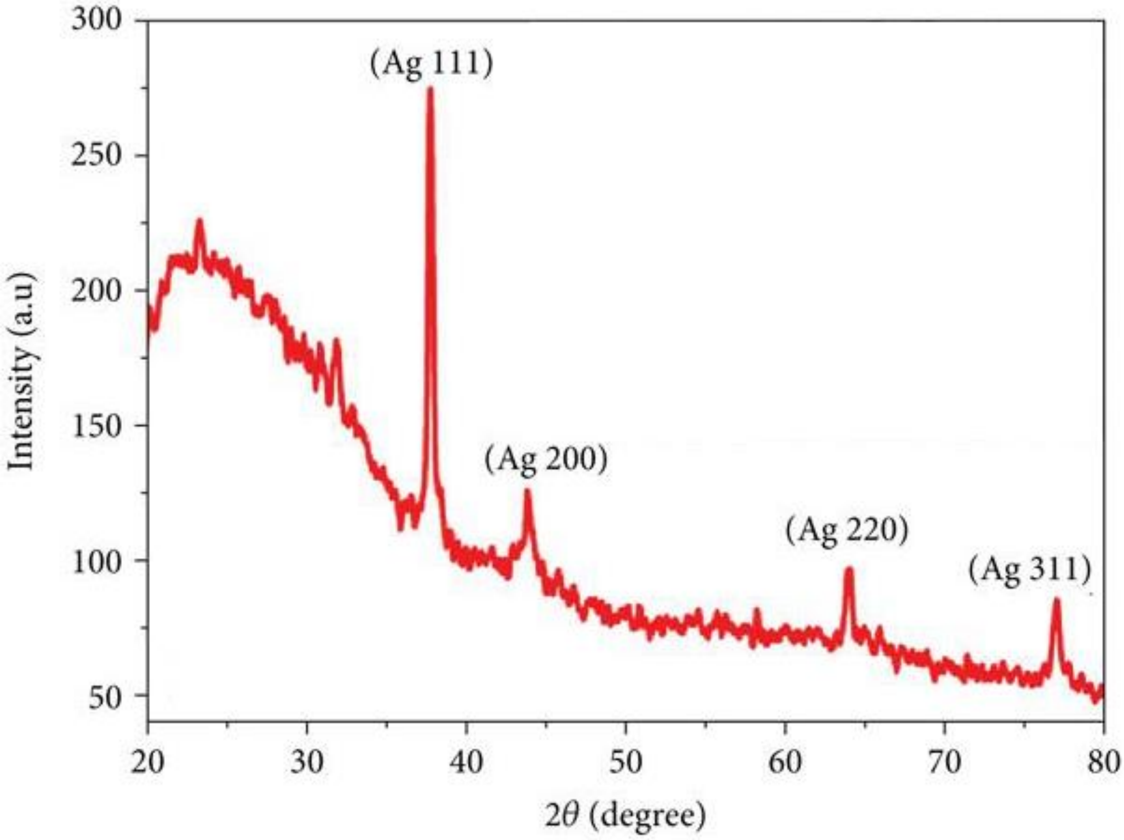

Figure (4.20): XRD profiles of the sputtered sample at 2hr.

4. 3.2 Field Emission Scanning Electron Microscopy FESEM

Figure 4.21 shows the morphological features of the 316L SS surface modified by anodization process at 8 V for 5min time at 4cm distance. The figure reveals the formation of a homogeneously distributed oxide scale with a porous structure. The dual porous structure was related to the anodic voltage.

Figure 4.22 demonstrates the EDS analysis of the 316L SS surface modified by anodization process at 8 V ,5 min. The results confirm the formation of Cr_2O_3 oxide scale in the treated sample due to existence of Cr and O elements as major constituents of Cr_2O_3. It can be observed that the main elements of Fe, O, Si and Cr are presented in the oxide scale. The existence of these elements confirms the formation of Cr_2O_3 on the 316l SS alloy.

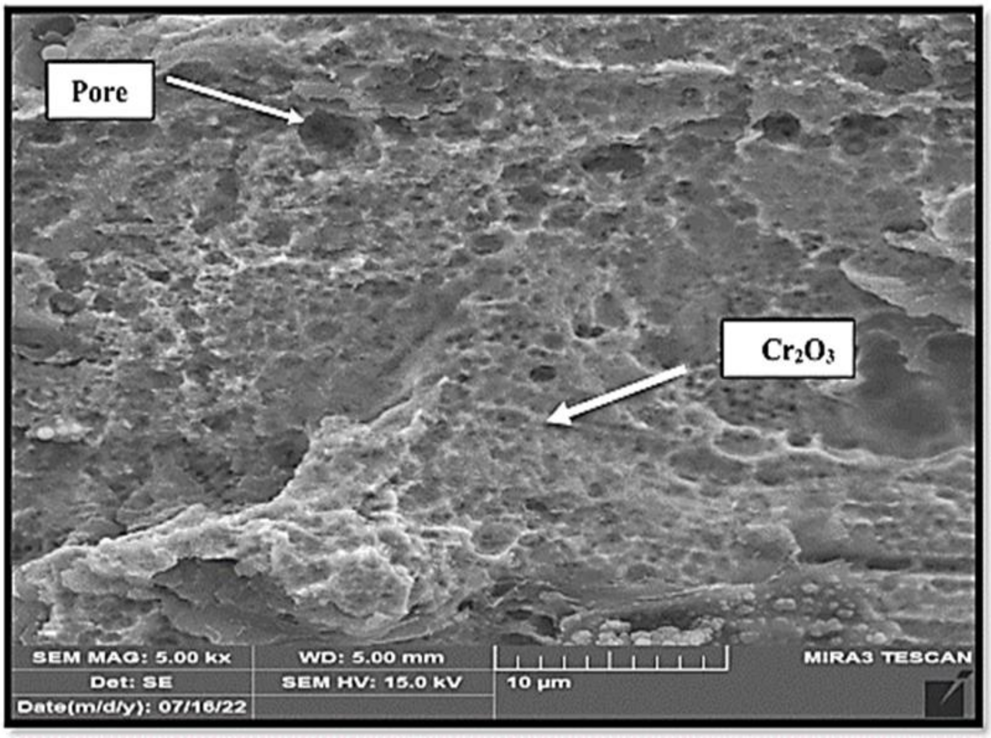

Figure (4.21): FESEM micrographs of the 316L SS anodized at 8 volts for 5 min .

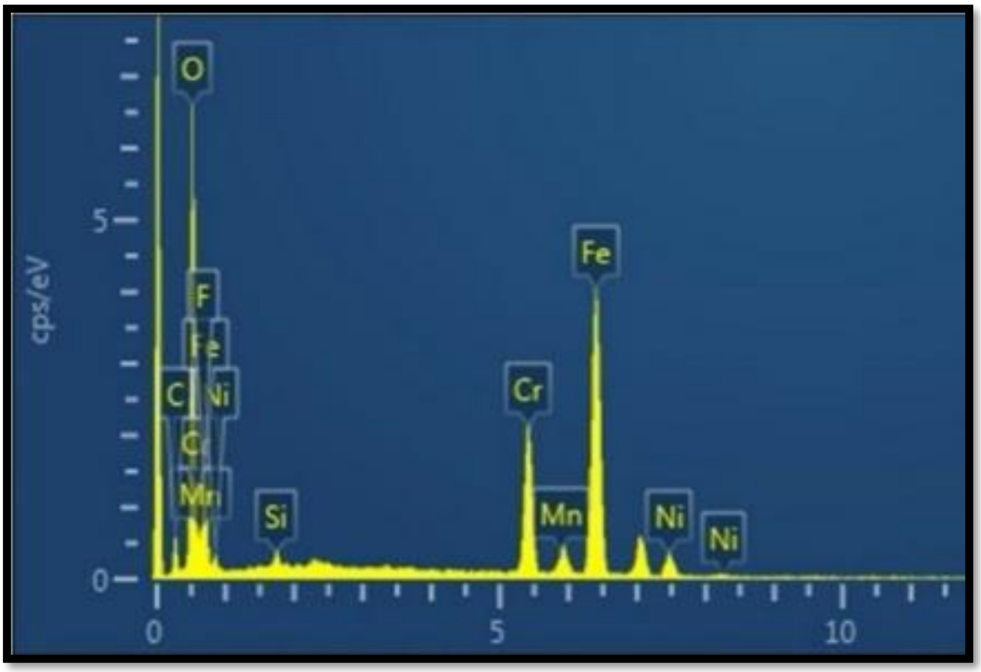

Figure (4.22): EDS analysis for anodized samples at: 8volt, 5min and 4cm.

Figure 4.23 shows as a typical FESEM cross sections morphology of the oxide scales on the anodized steel for 5min at 8volt and 4cm. The anodized films grew to a very uniform thickness across the surface.

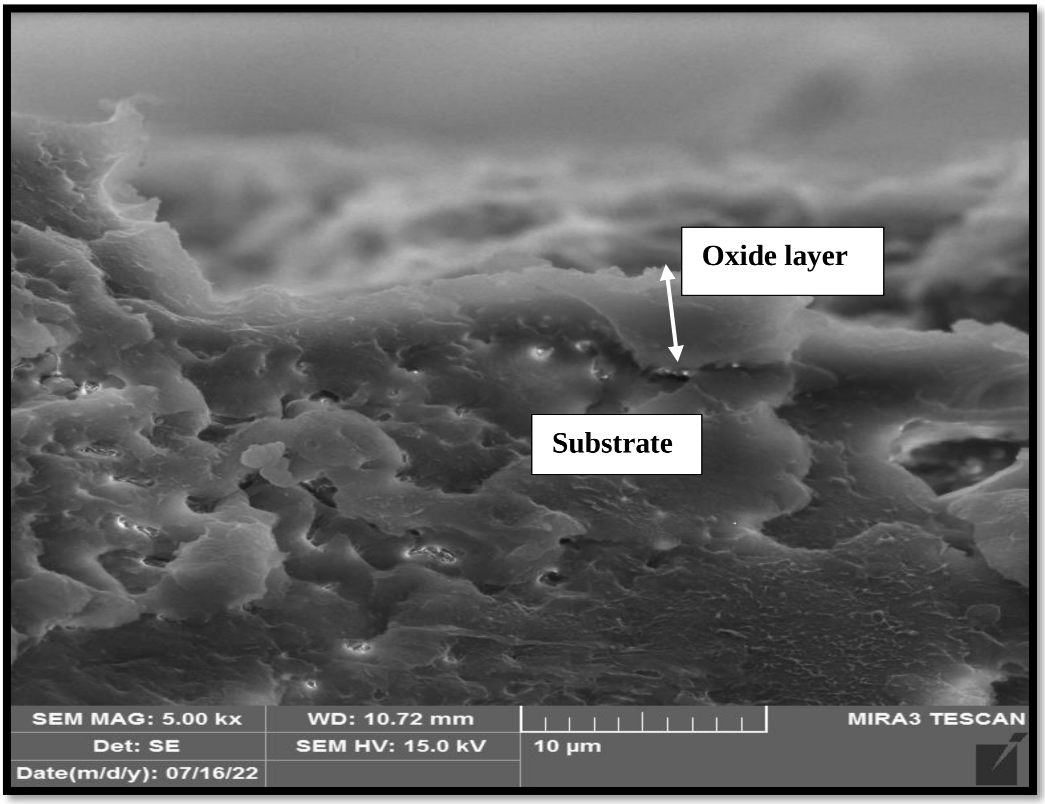

Figure. (4.23): FESEM cross sections morphology of anodized sample.

The morphology and topography of sputtered sample with Ag was observed by FSEM in Figure (4.24). The FSEM surface micrograph shows a smoother surface. It can be observed that the microstructure is densely packed and contain a homogeneous particles distribution and leads to the formation of homogeneous coatings.

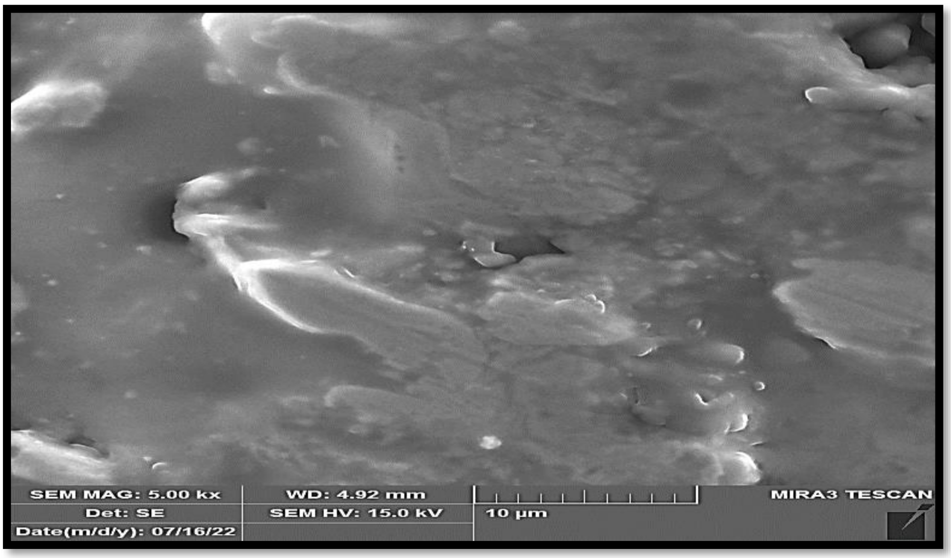

Figure (4.24): FSEM micrographs of silver coating on anodized 316L SS alloy at 2 hrs.

Figure 4.25 illustrate the cross-sectional topography of sputtered sample with Ag at 2 hrs. It can be seen that the sputtered scale has a regular thin scale structure of (89.05 nm) in thickness with higher compact, homogeneity and complete adhesion between the coating and the substrate. It can be concluded that with the increase of sputtering time, thickness of coating scale increases significantly. Interfaces can be seen clearly between sputtered scale and substrate. As well as Figure 4.26 shows mapping of elements that present in sputtered Ag samples which are O, Cr, and Ag that match with EDS analysis.

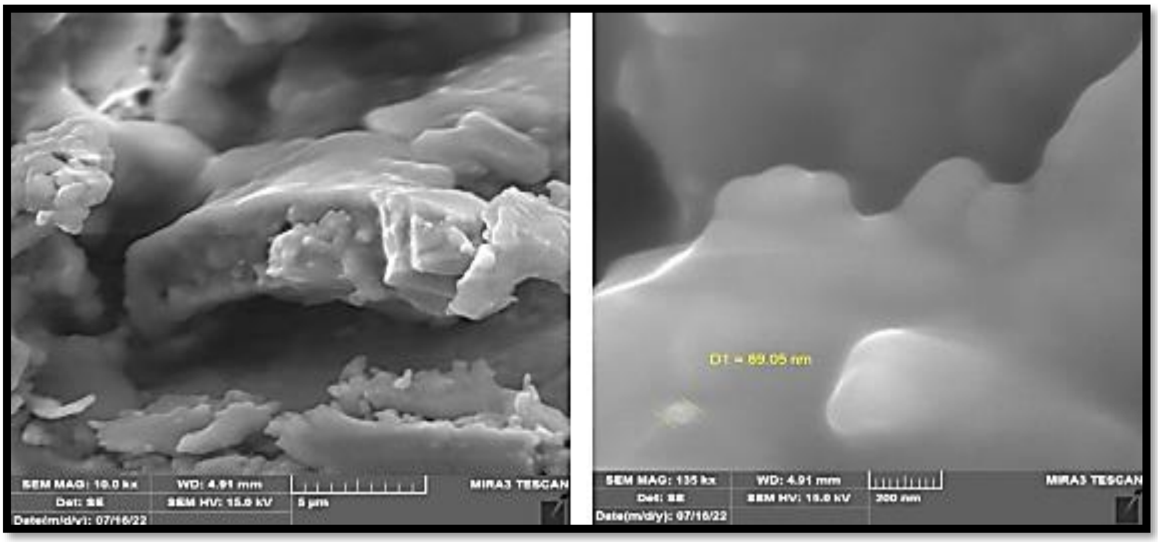

Figure. (4.25): FESEM cross sections morphology of sputtered sample.

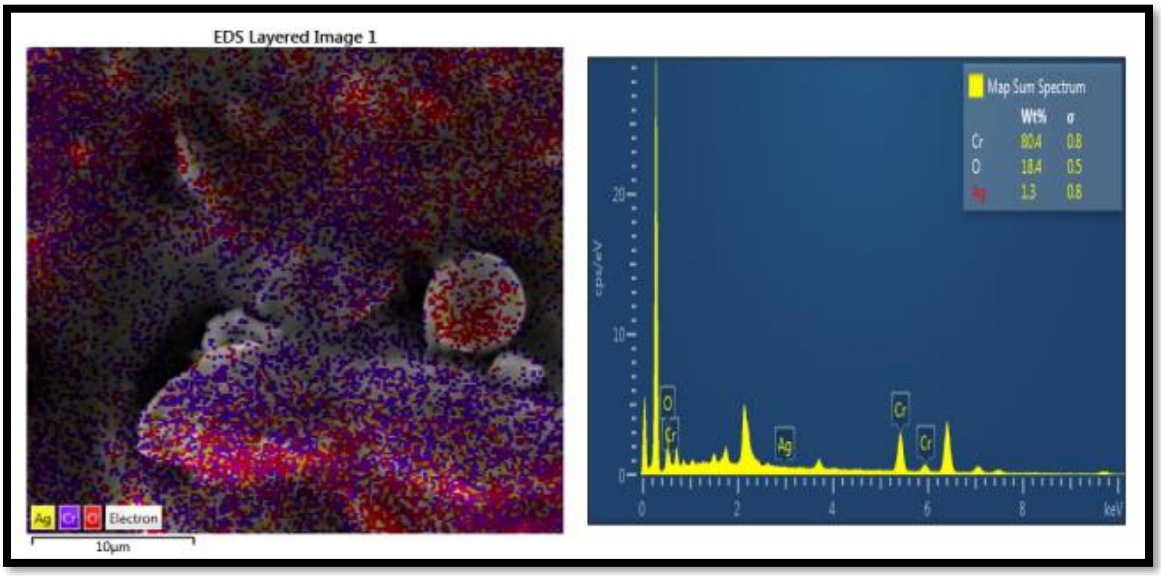

Figure (4.26): EDS analysis for sputtered sample at: 2hr.

4.3.3. Atomic Force Microscopy Analysis

The AFM analysis is done for the anodized alloy and the topography of the anodized sample with 3D performance images were shown in Figure (4.27). The topography shows some spherical packed particles in a dense and homogeneous scale of the anodized sample, as well as the surface roughness, was (11.7) nm. The illustrated topographies indicate that the surface of anodized sample is covered by semispherical Cr_2O_3 particles.

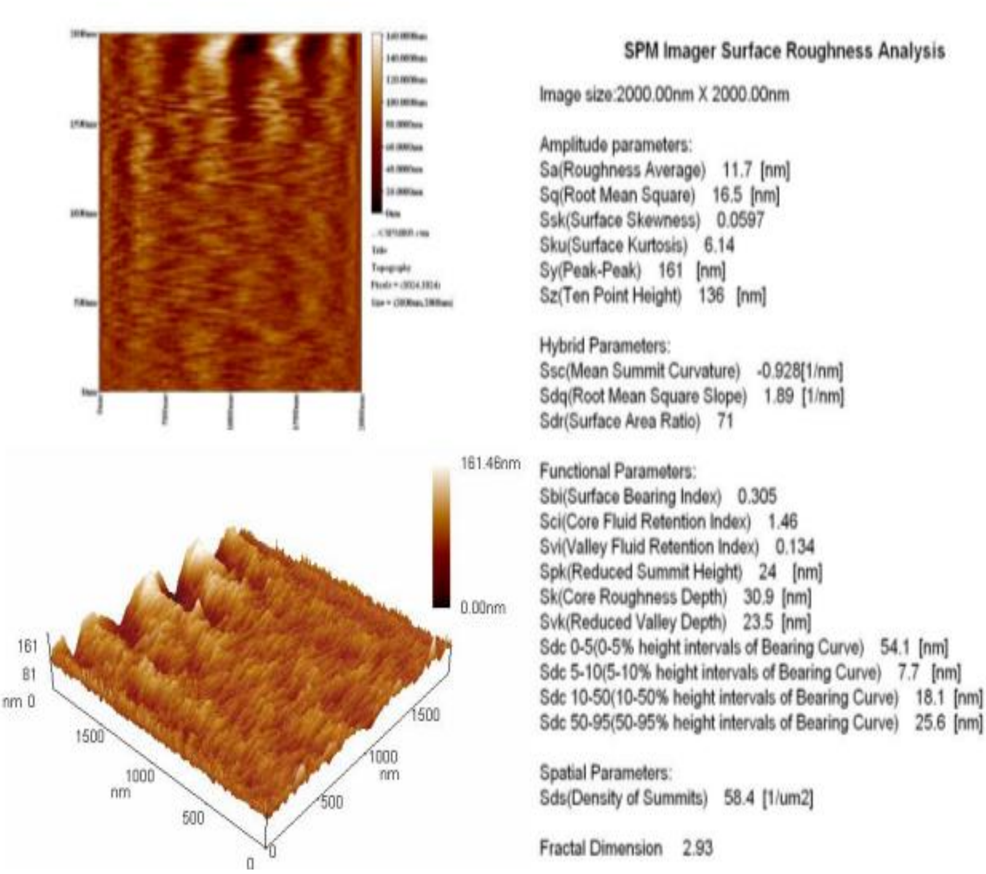

Figure (4.27): The topography of the anodized samples with 3D performance images at: 8 volt, 5min, 4 cm.

The AFM analysis is done for the sputtered sample and the topography of the surface with 3D performance images were shown in Figure (4.28) exhibits low surface roughness with several hills and valleys which is characteristic feature for as-deposited scales. Due to the homogenous sputtering, the roughness of the as deposited sample is very low.

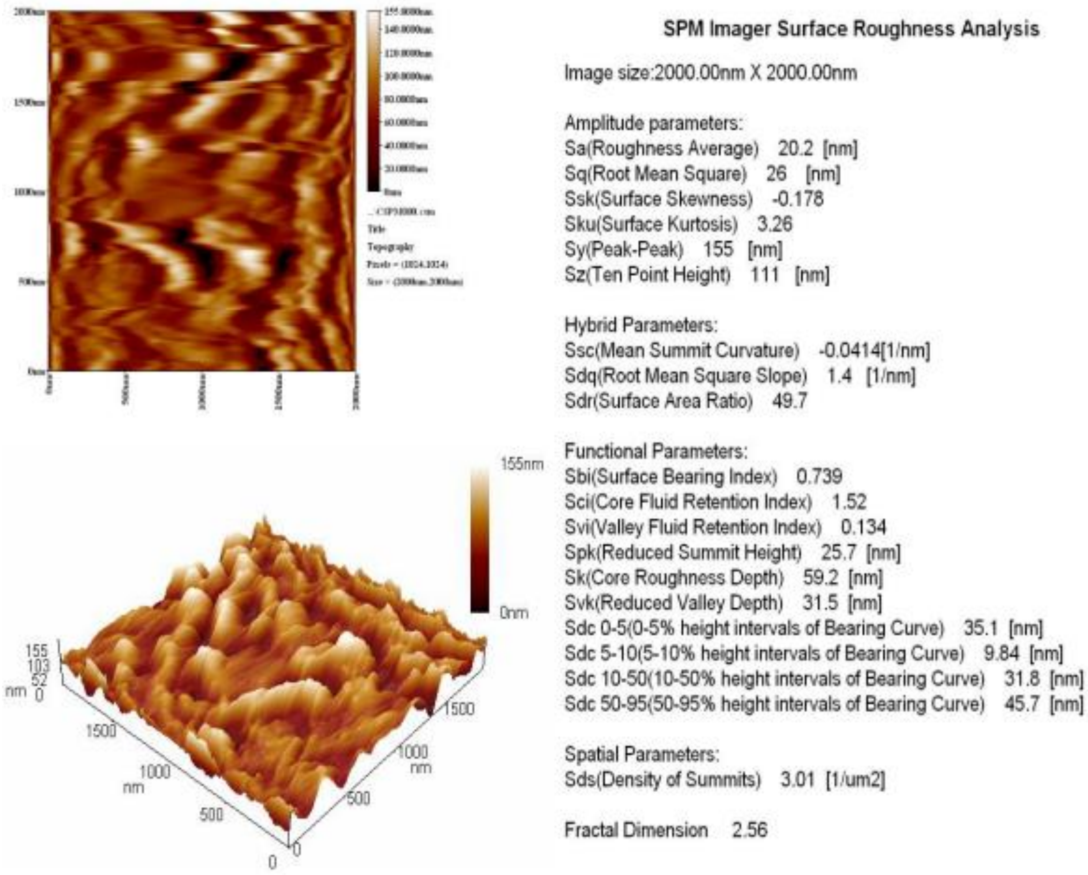

Figure (4.28): The topography of the sputtered sample with 3D performance images.

4.3.4 Adhesion Test

The adhesion quality of chromium oxide coatings was evaluated with Rockwell-C indentation tests, where the imprints were observed by an optical microscope for a sign of any failure or delamination. The results showed that the coatings conformed well to the indentation, indicating that they have an acceptable adhesion without any adhesive delamination

Figure (4.29) shows the optical microscope (OM) images of Rockwell C indentation on the anodized sample. Deep and long cracks were observed around the indentation point in the anodized sample. Furthermore, no delamination was observed around the Rockwell C indentation effect. These results show that the adhesion strength quality of these sample is related to HF1 and HF2 and these failures represent HF2–HF3 type of the adhesion strength quality [**109**].

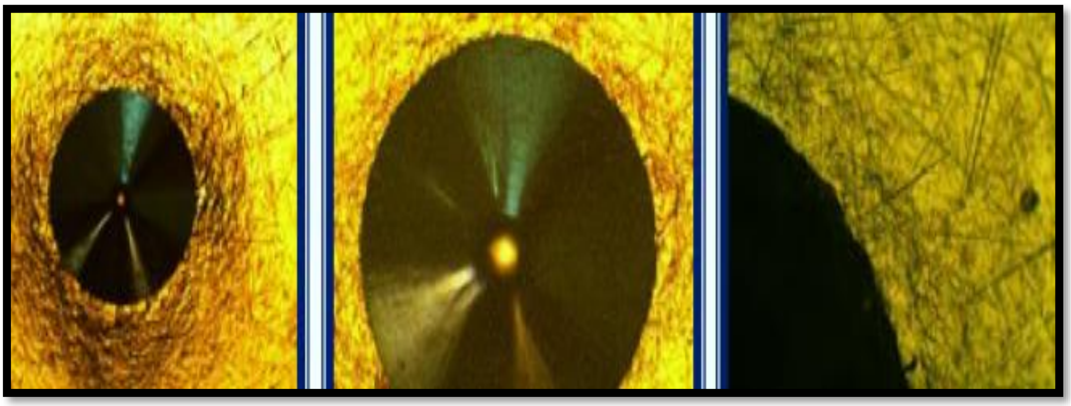

Figure (4.29): Optical photographs of Rockwell type - C effect an indentation for anodized sample at: 8volt, 5min and 4cm.

Figure 4.30 shows the Optical microscope (OM) images of Rockwell C indentation with three different magnifications (5X, 10X, 20X) on the sputtered samples with Ag. Shallow and short cracks are observed around the indentation point in the sputtering samples with Ag at deposition time of 2 hrs. Furthermore, no delamination is observed around the Rockwell C indentation effect. The only cracking on any of these scales is located within the indentation and is minimal. the sample has an HF rating of 1 that implies Ag scale and coating deposited by sputtering in this study exhibit good adhesion regardless of thickness. the scale and coating exhibited good adhesion. The coating also showed very little cracking indicating good adhesion to the substrate.

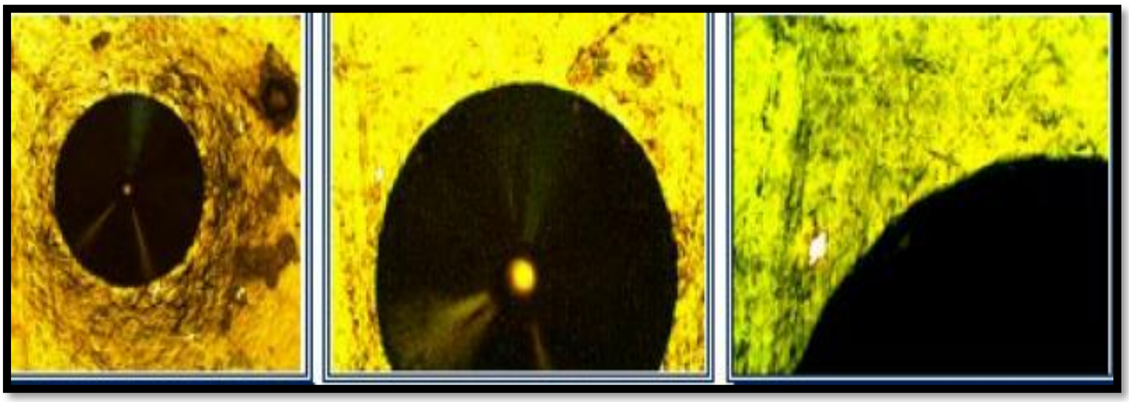

Figure (4.30): Optical photographs of Rockwell type - C effect an indentation for sputtered samples with Ag at: 2 hrs.

4.3.5 Corrosion Behavior

Corrosion behavior of sputtering sample is studied by potentiodynamic and cyclic polarization tests.

4.3.5.1 Potentiodynamic Polarization

Figure 4.31 shows the potentiodynamic polarization curves for base 316L SS alloy, anodized sample $A_{8,5,4}$ and sputtered sample with Ag in the Tyrode's solution at room temperature. The corrosion current (icorr) and corrosion potentials (Ecorr) are derived from the potentiodynamic curves by employing Tafel extrapolation (Table 4.8). Also, the corrosion rates (CR) were also included in this Table. It can be seen from the results obtained in Table 4.8, unmodified sample has corrosion current (i_{corr} = 0.44 µA), the sputtering with time (2 hrs), this time treated sample show better corrosion resistance than the untreated sample. This mean that sputtering with Ag coating layer provide a protective passive layer on the alloy surface that would reduce the corrosion rate. When sputtering at 2 hrs, a lowest corrosion current (icorr = 0.085 µA) is obtained and this result has the highest corrosion resistance. This is attributed to dense structure of this coating layer.

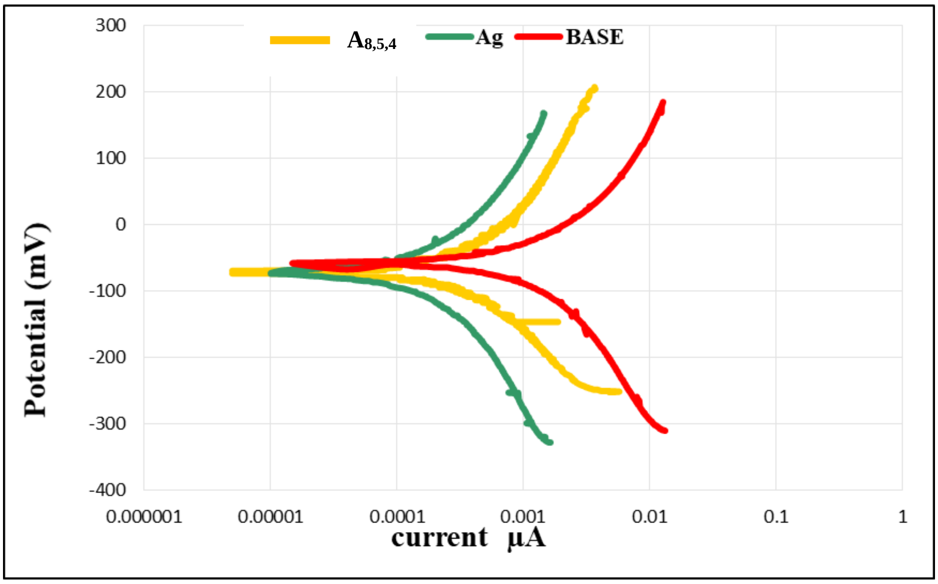

Figure (4.31): Potentiodynamic polarization curves of base 316L and sputtered sample with Ag of anodized sample at (8 V, 5min and 4cm).

Table (4.8): Electrochemical parameters of the sputtered sample with Ag for anodized 316L SS.

Sample code	Conditions	$i_{corr.}$ µA	E_{corr}.m V	CR (mpy)	Improvemen%
Base	Untreated	0.44	-56.7	0.1033	-
A8,5,4	8volt, 5min	0.112	-66.8	0.0262	75
Ag	DC sputtering	0.085	-72.9	0.0199	81

4.3.5.2 Cyclic Polarization

In order to investigate the resistance of the sample to the localized corrosion, the cyclic polarization is carried out. Figures (4.32, and 4.33) illustrates the cyclic polarization curve for anodized sample at 8 volt, 5 min, 4 cm and sputtered sample at 2 hrs. Typically, the reading starts at the open circuit potential and scans upwards until breakdown is attained. Then the direction of scan is inverted after specific amount of localized corrosion is established and the passive scale is damaged. The potential at which stable pit formed is called breakdown potential (Eb) or pitting potential (Ep). Consequently, the Ep imply the potential over which the pits initiated and developed. If the Ep is high, the material has high resistance to the pitting corrosion. During the reverse scan, a negative hysteresis can be observed on the curve as that shown in Figures (4.32, and 4.33). The difference between Ep and Eprot (ΔE) will give an indication to the corrosion resistance of the sample, where the smaller ΔE value means the highest corrosion resistance Table (4.9).

Table (4.9): Values of pitting potential for anodized and sputtered samples with Ag from cyclic polarization.

Sample code	Conditions	Ep (mV)	Eprot. (mV)	ΔE=(Epit-Eprot.) (mV)
Ag	DC sputtering	-150	-90	-60
A34	8volt, 5min, 4cm	-140	-150	10

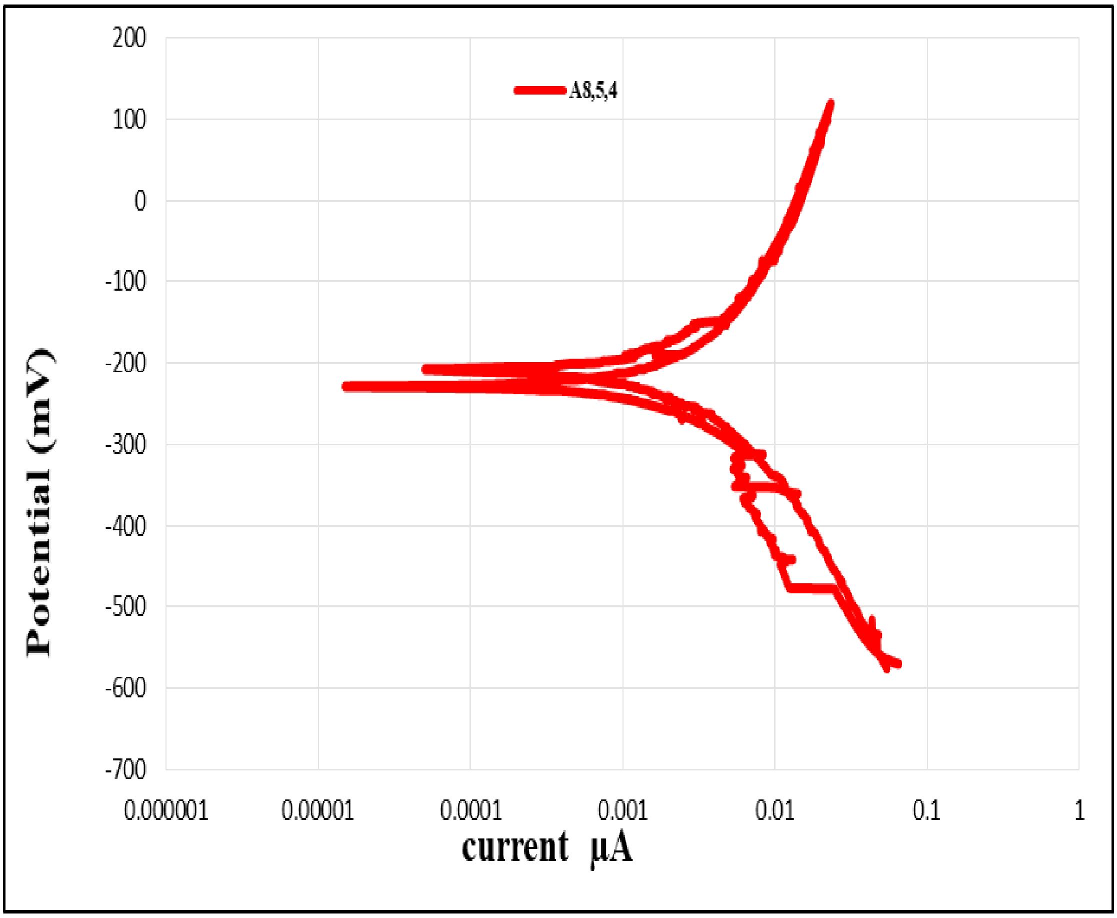

Figure (4.32): Cyclic polarization curves for anodized sample in Tyrode's solution.

The cyclic Potentiodynamic polarization of sputtered samples at 2 hrs. time has been investigated also in the Tyrode's solution at room temperature as illustrated in Figure 4.33. It is cleared that the sputtered sample at 2 hrs had the lowest pitting or break down potential and thus highest pitting and protection potential with an adjacent hysteresis loop where this polarization behavior tends to be resistance to the localized corrosion. In addition, the lowest value of ΔE is obtained and consequently this sample would have the more resistance to pitting corrosion. Coating of Ag increases resistance to pitting corrosion of anodized 316l SS.

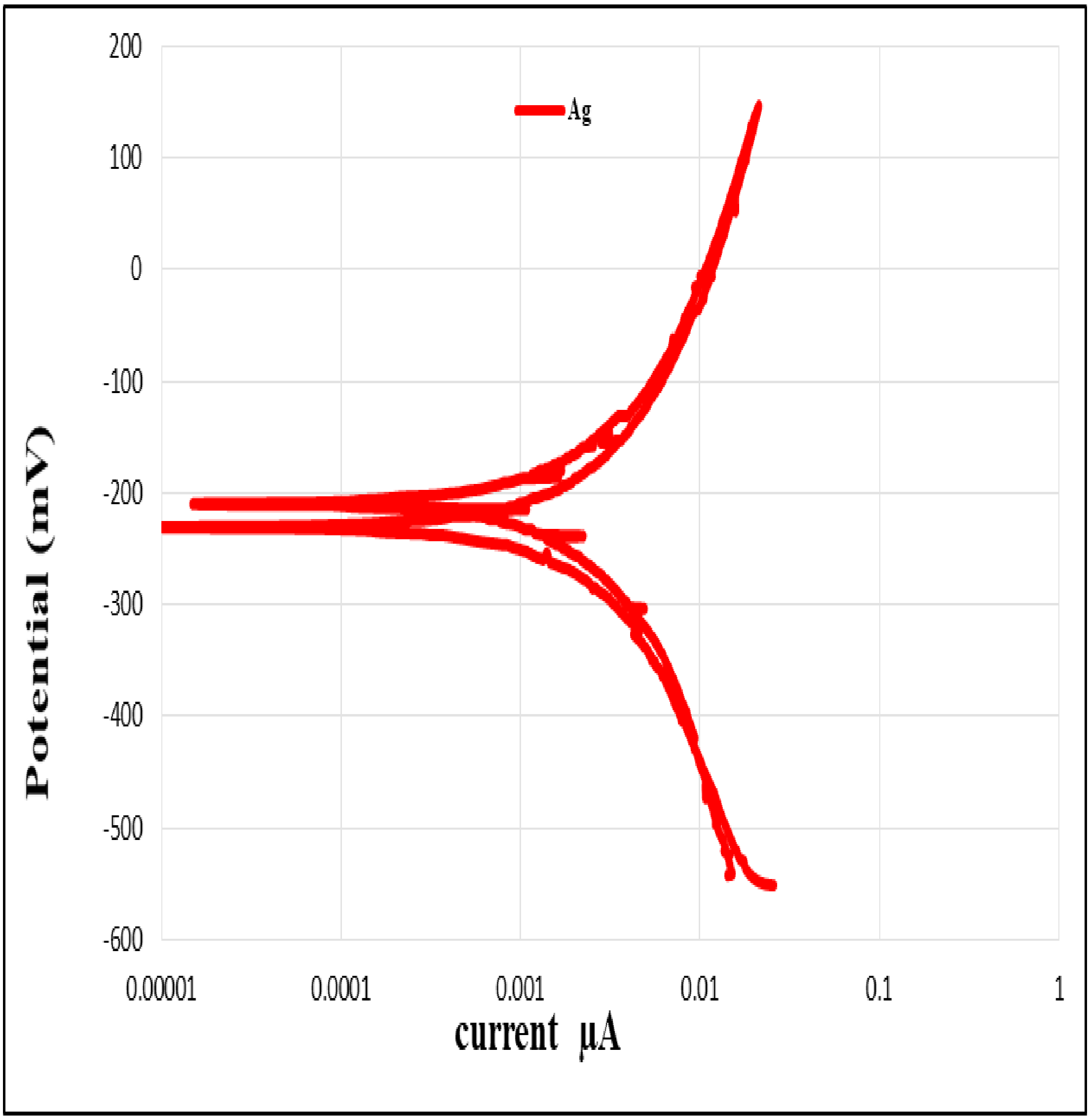

Figure (4.33): Cyclic polarization curves for sputtered sample in Tyrode's solution.

4.3.6. Antibacterial Test

The effect of the antibacterial for 316L, anodized 316L SS alloy and sputtered samples were examined against E. coli culture as shown in (Figure 4.34). The formation of a clear region around the disc is referred to as the bacterial inhibition zone. After 24 hours of incubation, and then the oxide scale exhibited a strong antibacterial effect. Therefore, the presence of Cr_2O_3 was effective in preventing bacterial adhesion on the surface and, in turn, preventing bacteria growth, which would improve the antibacterial activity. For sputtered samples, it has shown the highest antimicrobial activity, this refers to silver coating's active role in killing bacterial strains [**108**].

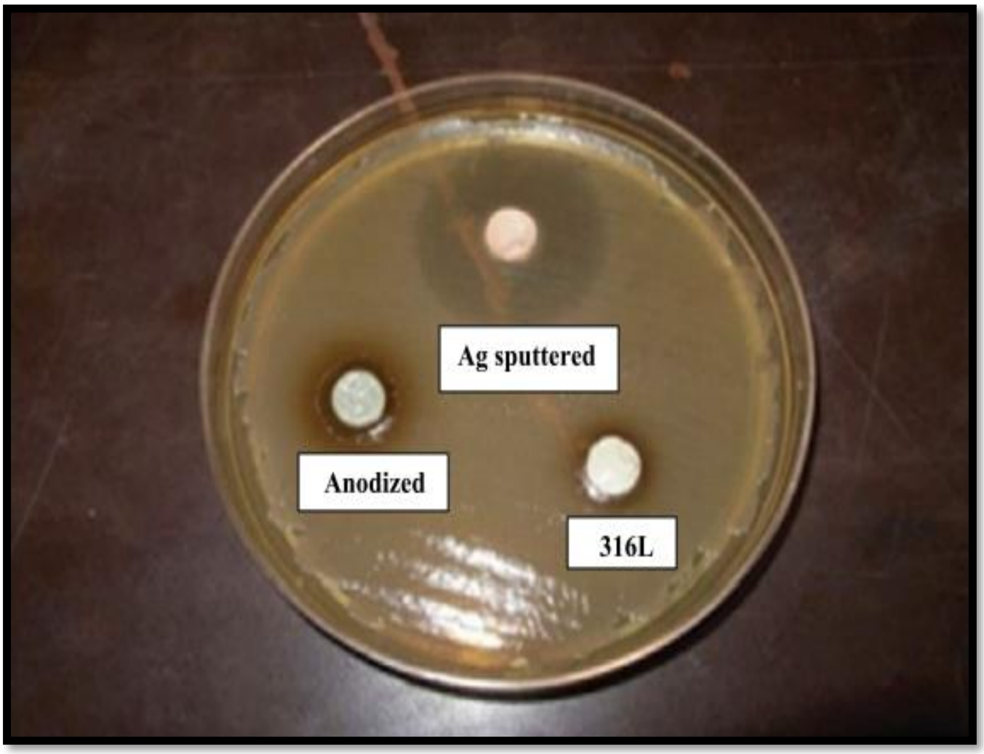

Figure (4.34): Inhibition zones of 316L, anodized 316L and sputtered samples against E. coli bacteria for 24 hr.

Chapter Five

Conclusions and Future work

Chapter Five

Conclusions and Recommendations

5.1. Conclusions

In the present study, the anodization treatment and DC sputtering technique has been used to alter the 316l SS's surface, successfully creating porous Cr2O3 nanostructures on the surfaces of 316l SS substrates by an anodization treatment under different parameters of applied voltage-time and distance and then the porous surface was modified by DC sputtering plasma deposition of silver for biomedical applications. These nanostructures and silver film were characterized concerning morphology, phase composition, surface topography, thickness, adhesion, and corrosion properties. The key findings of this study are as follows:

1. Cr_2O_3 structures with nanopores in different morphologies are obtained by tailoring the major anodization parameters of applied potential, distance, and time.
2. The main anodization parameters of applied voltage, distance, and time have a significant effect on the corrosion resistance of the anodized sample produced throughout the anodization process of 8V, 4Cm, and time of 5 min.
3. XRD analysis reveals the formation of several sharp and strong intense peaks attributed to anatase Cr_2O_3 along with one diffraction peak corresponding to rutile Cr_2O_3 in the anodized 316L substrates at 8V, 4Cm and time of 5 min.
4. The major anodization parameters of applied voltage, distance, and time have a noticeable influence on the thickness of formed Cr_2O_3 as it increases with increasing these parameters. Here, 316L substrates anodized at a voltage of 8V at 4cm for 5 min had the highest thickness compared to other anodized samples.

5. The results confirmed that the protective anodized Cr_2O_3layer formed onto 316L surface at 8 V for 5 min is more stable compared to that formed at 6 and 10 volts, resulting in further prevention from corrosion effect.
6. The morphology of the sputtered Ag layer is homogenous and crack-free when sputtered, with the optimum time at 2 hrs.
7. The potentiodynamic and cyclic polarization results demonstrate that the DC sputtering plasma method on 316L SS at 2 hrs has the highest corrosion resistance, and an improvement in the pitting corrosion resistance when immersed in the Tyrode's solution.
8. Adhesion strength results for modified samples compared with nonmodified samples appear to be good adhesive for the anodized and sputtered deposited layers with Ag on 316L substrate.
9. The results of the antibacterial analysis have confirmed that the DC sputtered coating by Ag reveals good antibacterial activity against gram-negative E. coli. This antibacterial activity increases when surface treatment time increases. That makes these coatings safe and they can be used for surgical instruments applications.

5.2 Recommendations

The analysis of the current work's results suggests numerous future study directions. Several of them have been listed below:

1. Using other anodization parameters, such as electrolyte pH, and electrolyte temperature, or using an organic electrolyte, for developing the surface properties of 316L.
2. Studying the influence of the anodization process achieved at the same parameters of this study on the wear, fatigue, and fritting corrosion characteristics of 316L tools.
3. The effect of using alternating techniques, such as the spray process, instead of DC sputtered coating on anodized 316L SS can be studied.
4. Study deposition of another coating biomaterial instead of Ag such as ZnO, TiO_2, and Al_2O_3.

References

References

1. Park, J., & Lakes, R. S. (2007). *Biomaterials: An Introduction*. Springer Science & Business Media.

2. Park, J. B., & Bronzino, J. D. (Eds.). (2002). Biomaterials: Principles and Applications.

3. Bose, S., & Bandyopadhyay, A. (2013). Introduction to Biomaterials. In *Characterization of Biomaterials* (pp. 1-9). Academic Press.

4. Puleo, D. A., & Huh, W. W. (1995). Acute Toxicity of Metal Ions in Cultures of Osteogenic Cells Derived from Bone Marrow Stromal Cells. *Journal of Applied Biomaterials*, *6*(2), 109-116.

5. W. Khan, E. Muntimadugu, M. Jaffe, and A. J. Domb, (2014). "Implantable Medical Devices.," Focal Controlled Drug Delivery, pp. 33–59.

6. Selvaduray, G., & Trigwell, S. (2005, November). Effect of Surface Treatment on the Surface Characteristics of AISI 316L Stainless Steel. In *Proceedings of the Conference of Materials and Processes for Medical Devices, Boston, MA, USA* (pp. 14-18).

7. Kubie, L. S., & Shults, G. M. (1925). Studies on The Relationship of The Chemical Constituents of Blood and Cerebrospinal Fluid. *The Journal of experimental medicine*, *42*(4), 565.

8. Duan, H., Du, K., Yan, C., & Wang, F. (2006). Electrochemical Corrosion Behavior of Composite Coatings of Sealed MAO Film on Magnesium Alloy AZ91D. *Electrochimica Acta*, *51*(14), 2898-2908.

9. Buddy, D., Ratner, Allan, S., Hoffman, Frederick, J., Schoen, Jack and E. Lemons (2000), "Biomaterial's science An Introduction to Materials in Medicine", University of Siena, Elsevier Academic Press, 2nd Edition.

10. Barbucci, R. (Ed.). (2002). *Integrated Biomaterials Science*. Springer Science & Business Media.

11. Mattox, D. M. (2010). *Handbook of Physical Vapor Deposition (PVD) processing*. William Andrew.

12. Frey, H., & Khan, H. R. (Eds.). (2015). *Handbook of Thin Film Technology* (pp. 1-379). Berlin: Springer.

13. Talha, M., Behera, C. K., & Sinha, O. P. (2013). A review on Nickel-Free Nitrogen-containing Austenitic Stainless Steels for Biomedical Applications. *Materials Science and Engineering: C*, *33*(7), 3563-3575.

14. McGannon, P. E. T. E. R., & Rubenstien, J. (2007). HP Metal Blades. Cataract & Refractive Surgery Today, 85-92.

15. Subramani, R., Elangomannan, S., Louis, K., Kannan, S., & Gopi, D. (2016). Fabrication of Minerals Substituted Porous hydroxyapatite/poly (3, 4-methylenedioxy pyrrole-co-3, 4-ethylene dioxythiophene) Bilayer Coatings on Surgical Grade Stainless Steel and Its Antibacterial and Biological Activities for Orthopedic Applications. *ACS applied materials & interfaces*, *8*(19), 12404-12421.

16. Jaganathan, S. K., Supriyanto, E., Murugesan, S., Balaji, A., & Asokan, M. K. (2014). Biomaterials in Cardiovascular Research: Applications and Clinical Implications. *BioMed research international*.

17. Jackson, M. J., & Ahmed, W. (Eds.). (2007). *Surface Engineered Surgical Tools and Medical Devices*. Boston, MA: Springer US.

18. Duan, K., & Wang, R. (2006). Surface Modifications of Bone Implants Through Wet Chemistry. *Journal of materials chemistry*, *16*(24), 2309-2321.

19. Geyao, L., Yang, D., Wanglin, C., & Chengyong, W. (2020). Development and Application of Physical Vapor Deposited Coatings for Medical Devices: A review. *Procedia CIRP*, *89*, 250-262.

20. McDonnell, G. E., & Sheard, D. (2012). *A practical Guide to Decontamination in Healthcare*. John Wiley & Sons.

21. Nicholson, P. (2015). Getting A handle on Instrument Loan Sets and Reusable Medical Devices. *ACORN: The Journal of Perioperative Nursing in Australia*, *28*(4), 41-42.

22. Xu, Y. (2017). *Safety Evaluation of Surgical Instruments* (Doctoral dissertation, University of Dundee).

23. Rutala, W. A., & Weber, D. J. (2013). Disinfection and Sterilization: An overview. *American journal of infection control*, *41*(5), S2-S5.

24. Zaccagnini, M., & Pechacek, J. M. (2019). *The doctor of Nursing Practice Essentials: A new Model for Advanced Practice Nursing*. Jones & Bartlett Learning.

25. Instruments, S. (1991). Metallic materials—Part 1: Stainless Steel. BSI. p. 12.

26. Cissé, S., Laffont, L., Tanguy, B., Lafont, M. C., & Andrieu, E. (2012). Effect of Surface Preparation on The corrosion of Austenitic Stainless Steel 304L in High Temperature Steam and Simulated PWR Primary Water. *Corrosion Science*, *56*, 209-216.

27. Luo Q Y (2010). Development of Biomedical Materials and Industrialization of Interventional Medical Devices. New Material Industry; 25-27.

28. Subramanian, B., Ananthakumar, R., Kobayashi, A., & Jayachandran, M. (2012). Surface Modification of 316L Stainless Steel with Magnetron Sputtered TiN/VN Nanoscale Multilayers for Bio Implant Applications. *Journal of Materials Science: Materials in Medicine*, *23*, 329-338.

29. Cobb, H. M. (2010). *The history of Stainless Steel*. ASM International.

30. Bakterij, A. J. M. T. (2014). An overview of The influence of Stainless-Steel Surface Properties on Bacterial Adhesion. *Mater. Tehnol*, *48*, 609-617.

31. Zaffora, A., Di Franco, F., & Santamaria, M. (2021). Corrosion of Stainless Steel in Food and Pharmaceutical Industry. *Current Opinion in Electrochemistry*, *29*, 100760.

32. Moerman, F., & Partington, E. (2014). Materials of Construction for Food Processing Equipment and Services: Requirements, Strengths, and Weaknesses. *J. Hyg. Eng*, *6*, 10-37.

33. Olsson, C. O., & Landolt, D. (2003). Passive Films on Stainless Steels—Chemistry, Structure and Growth. *Electrochimica acta*, *48*(9), 1093-1104.

34. Clayton, C. R., & Olefjord, I. N. G. E. M. A. R. (2002). The passivity of Austenitic Stainless Steels. Corrosion mechanism in theory and practice, Marcel Dekker, NY.

35. Schmuki, P. (2002). From Bacon to Barriers: A review on The passivity of Metals and Alloys. *Journal of Solid State Electrochemistry*, *6*, 145-164.

36. Pound, B. G. (2014). Passive Films on Metallic Biomaterials under Simulated Physiological Conditions. *Journal of Biomedical Materials Research Part A*, *102*(5), 1595-1604.

37. Hanawa, T., Hiromoto, S., Yamamoto, A., Kuroda, D., & Asami, K. (2002). XPS Characterization of The surface Oxide Film of 316L

Stainless Steel Samples that were Located in Quasi-biological Environments. *Materials transactions*, *43*(12), 3088-3092.

38. Herting, G. (2008). *Bioaccessibility of Stainless Steels: Importance of Bulk and Surface Features* (Doctoral dissertation, KTH).

39. Niinomi, M. (2008). Metallic Biomaterials. *Journal of Artificial Organs*, *11*, 105-110.

40. Steels, H. S. L. A. (2005). ASM handbook, volume 1, Properties and Selection: Irons, Steels, and High-performance Alloys Section: Carbon and Low-alloy Steels.

41. Oyj, O. (2013). *Handbook of Stainless Steel*. Outokumpu Oyj.

42. McGuire, M. F. (2008). *Stainless Steel for Design Engineers*. Asm International.

43. Manninen, T., & Säynäjäkangas, J. (2012, December). Mechanical Properties of Ferritic Stainless Steels at Elevated Temperature. In *Proceedings of the Fourth International Experts Seminar on Stainless Steel in Structures*.

44. Shettlemore, M. G., & Bundy, K. J. (2001). Examination of In vivo Influences on Bioluminescent Microbial Assessment of Corrosion Product Toxicity. *Biomaterials*, *22*(16), 2215-2228.

45. Karimi, S., Nickchi, T., & Alfantazi, A. M. (2012). Long-term Corrosion Investigation of AISI 316L, Co–28Cr–6Mo, and Ti–6Al–4V Alloys in Simulated Body Solutions. *Applied Surface Science*, *258*(16), 6087-6096.

46. McGuire, M. F. (2008). *Stainless steels for Design Engineers*. Asm International.

47. Charles, J., Mithieux, J. D., Krautschick, J., Suutala, N., Simón, J. A., Van Hecke, B., & Pauly, T. (2009). A new European 200 Series Standard to Substitute 304 Austenitic. *Metallurgical Research & Technology*, *106*(2), 90-98.

48. Francis, R., & Byrne, G. (2021). Duplex Stainless-Steel Alloys for the 21st Century. *Metals*, *11*(5), 836.

49. Ratner, B. D. (2013). Correlation, Materials Properties, Statistics and Biomaterials Science. In *Biomaterials Science* (pp. 1354-1361). Academic Press.

50. Niinomi, M., Nakai, M., & Hieda, J. (2012). Development of New Metallic Alloys for Biomedical Applications. *Acta biomaterialia*, *8*(11), 3888-3903.

51. Wang, H., Zhang, Z. H., Hu, Z. Y., Song, Q., Yin, S. P., Kang, Z., & Li, S. L. (2018). Improvement of Interfacial Interaction and Mechanical Properties in Copper Matrix Composites Reinforced with

Copper Coated Carbon Nanotubes. *Materials Science and Engineering: A*, *715*, 163-173.

52. Zhang, Y., Zhai, D., Xu, M., Yao, Q., Zhu, H., Chang, J., & Wu, C. (2017). 3D-printed Bio Ceramic Scaffolds with Antibacterial and Osteogenic Activity. *Bio fabrication*, *9*(2), 025037.

53. Parsapour, A., Khorasani, S. N., & Fathi, M. H. (2012). Effect of Surface Treatment and Metallic Coating on Corrosion Behavior and Biocompatibility of Surgical 316L Stainless Steel Implant. *Journal of Materials Science & Technology*, *28*(2), 125-131.

56. Nouri, A., & Wen, C. (2015). Introduction to Surface Coating and Modification for Metallic Biomaterials. *Surface Coating and Modification of Metallic Biomaterials*, 3-60.

57. Amani, H., Arzaghi, H., Bayandori, M., Dezfuli, A. S., Pazoki-Toroudi, H., Shafiee, A., & Moradi, L. (2019). Controlling Cell Behavior Through The design of Biomaterial Surfaces: A focus on Surface Modification Techniques. *Advanced materials interfaces*, *6*(13), 1900572.

58. Singh, H., Singh, S., & Prakash, C. (2019). Current Trends in Biomaterials and Bio-manufacturing. *Biomanufacturing*, 1-34.

59. Revie, R. W. (2008). *Corrosion and Corrosion Control: An introduction to Corrosion Science and Engineering*. John Wiley & Sons.

60. Chen, P. C. (2014). *Fabrication of Metal/oxide Nanostructures by Anodization Processes for Biosensor, Drug Delivery, and Supercapacitor Applications*. Texas A&M University.

61. Ahmad, Z. (2006). *Principles of Corrosion Engineering and Corrosion Control*. Elsevier.

62. Van Gils, S., Mast, P., Stijns, E., & Terryn, H. (2004). *Colour Properties of Barrier Anodic Oxide Films on Aluminum and Titanium Studied with Total Reflectance and Spectroscopic Ellipsometry*. *Surface and Coatings Technology*, *185*(2-3), 303-310.

63. Callister Jr, W. D., & Rethwisch, D. G. (2020). *Callister's Materials Science and Engineering*. John Wiley & Sons.

64. Karambakhsh, A., Afshar, A., & Malekinejad, P. (2012). Corrosion Resistance and Color Properties of Anodized Ti-6Al-4V. *Journal of materials engineering and performance*, *21*, 121-127.

65. Saji, V. S. (2020). Superhydrophobic Surfaces and Coatings by Electrochemical Anodic Oxidation and Plasma Electrolytic Oxidation. *Advances in Colloid and Interface Science*, *283*, 102245.

66. Franetovic, V., & Schroth, J. G. (2007, January). Improved Hot Aluminum Forming Tribology by Anodization. In *International Joint Tribology Conference* (Vol. 48108, pp. 753-755).

67. Hamlekhan, A. (2014). *Fabrication of Drug-eluting Ti Implants for Dental/orthopedic Applications*. Michigan Technological University.

68. Chen, C. C., Chen, J. H., Chao, C. G., & Say, W. C. (2005). Electrochemical Characteristics of Surface of Titanium Formed by Electrolytic Polishing and Anodizing. *Journal of materials science*, *40*, 4053-4059.

69. Behrisch, R., & Eckstein, W. (Eds.). (2007). *Sputtering by Particle Bombardment: Experiments and Computer Calculations from Threshold to MeV Energies* (Vol. 110). Springer Science & Business Media.

70. Foster, J. E., Kovach, Y. E., Lai, J., & Garcia, M. C. (2020). Self-organization in 1 atm DC Glows with Liquid Anodes: Current Understanding and Potential Applications. *Plasma Sources Science and Technology*, *29*(3), 034004.

71. Jilani, A., Abdel-Wahab, M. S., & Hammad, A. H. (2017). Advance Deposition Techniques for Thin Film and Coating. *Modern Technologies for Creating the Thin-film Systems and Coatings*, *2*(3), 137-149.

72. Lieberman, M. A., & Lichtenberg, A. J. (2005). *Principles of Plasma Discharges and Materials Processing*. John Wiley & Sons.

73. Hebbar Kannur, K., Yaqub, T. B., Pupier, C., Héau, C., & Cavaleiro, A. (2020). Mechanical Properties and Vacuum Tribological Performance of Mo–S–N Sputtered Coatings. *ACS Applied Materials & Interfaces*, *12*(38), 43299-43310.

74. Seshan, K., & Schepis, D. (Eds.). (2018). *Handbook of Thin Film Deposition*. William Andrew.

75. Axelevitch, A., Gorenstein, B., & Golan, G. (2012). Investigation of Optical Transmission in Thin Metal Films. *Physics Procedia*, *32*, 1-13.

76. Chiad, B. T., Al-Zubaydi, T. L., Khalaf, M. K., & Khudiar, A. I. (2009). Construction and Characterization of A low Pressure Plasma Reactor using DC Glow Discharge. *Journal of Optoelectronics and Biomedical Materials*, *1*(3), 255-262.

77. Gudmundsson, J. T., & Hecimovic, A. (2017). Foundations of DC Plasma Sources. *Plasma Sources Science and Technology*, *26*(12), 123001.

78. Gudmundsson, J. T. (2020). Physics and Technology of Magnetron Sputtering Discharges. *Plasma Sources Science and Technology*, *29*(11), 113001.

79. Boenig, H. (2019). *Plasma Science and Technology*. Cornell University Press.

80. Abdelrahman, M. M. (2015). Study of Plasma and Ion Beam Sputtering Processes. *Journal of Physical Science and Application*, *5*(2), 128-142.

81. Abd Al Kareem, S. M., & Yaseen, W. I. (2020, March). Study Optical Properties of Copper and Silver for Astronomical Solar Filters Prepared by DC Sputtering Plasma. In *IOP Conference Series: Materials Science and Engineering* (Vol. 757, No. 1, p. 012054). IOP Publishing.

82. Chen, F., Zhou, Y., Zhu, Y., Zhu, R., Guan, P., Fan, J., ... & Chu, D. (2021). Recent Progress in Artificial Synaptic Devices: Materials, Processing and Applications. *Journal of Materials Chemistry C*, *9*(27), 8372-8394.

83. Liu, G., Wang, X., Chen, Z., Cheng, H. M., & Lu, G. Q. M. (2009). The role of Crystal Phase in Determining Photocatalytic Activity of Nitrogen Doped TiO2. *Journal of Colloid and Interface Science*, *329*(2), 331-338.

84. Medvedovski, E., & Dudziak, T. (2019). Protective Coatings for High-temperature Steam Oxidation in Coal-fired Power Plants. *Surface and Coatings Technology*, *369*, 127-141.

85. Geetha, M., Singh, A. K., Asokamani, R., & Gogia, A. K. (2009). Ti Based Biomaterials, The ultimate Choice for Orthopaedic Implants–A review. *Progress in materials science*, *54*(3), 397-425.

86. Singh, M., Singh, S., Prasad, S., & Gambhir, I. S. (2008). Nanotechnology in Medicine and Antibacterial Effect of Silver Nanoparticles. *Digest Journal of Nanomaterials and Biostructures*, *3*(3), 115-122.

87. White, R. J. (2001). An historical Overview of The use of Silver in Wound Management. *British Journal of Community Nursing*, *6*(Sup1), 3-8.

88. Chen, X., & Schluesener, H. J. (2008). Nanosilver: A nanoproduct in Medical Application. *Toxicology letters*, *176*(1), 1-12.

89. Chopra, I. (2007). The increasing use of Silver-based Products As Antimicrobial Agents: A useful Development or A cause for Concern. *Journal of antimicrobial Chemotherapy*, *59*(4), 587-590.

90. Roy, M., Bandyopadhyay, A., & Bose, S. (2013). *Characterization of Biomaterials: Chapter 7.2. Mechanical Properties of Bioceramic Coatings on Medical Implants*. Elsevier Inc. Chapters.

91. DeVasConCellos, P., Bose, S., Beyenal, H., Bandyopadhyay, A., & Zirkle, L. G. (2012). Antimicrobial Particulate Silver Coatings on Stainless Steel Implants for Fracture Management. *Materials Science and Engineering: C*, *32*(5), 1112-1120.

92. Spear, M. (2010). Silver: An age-old Treatment Modality in Modern Times. *Plastic and Aesthetic Nursing*, *30*(2), 90-93.

93. Klasen, H. J. (2000). Historical Review of The use of Silver in The treatment of Burns. I. Early uses. *Burns*, *26*(2), 117-130.

94. Srinivasan, S., Kumar, P. T., Nair, S. V., Nair, S. V., Chennazhi, K. P., & Jayakumar, R. (2013). Antibacterial and Bioactive α-and β-chitin Hydrogel/nano bioactive Glass Ceramic/nano silver Composite Scaffolds for Periodontal Regeneration. *Journal of biomedical nanotechnology*, *9*(11), 1803-1816.

95. Marsich, E., Travan, A., Donati, I., Turco, G., Kulkova, J., Moritz, N., ... & Paoletti, S. (2013). Biological Responses of Silver-coated Thermosets: An in vitro and In vivo Study. *Acta biomaterialia*, *9*(2), 5088-5099.

96. Yang, F., Both, S. K., Yang, X., Walboomers, X. F., & Jansen, J. A. (2009). Development of An electrospun Nano-apatite/PCL Composite

Membrane for GTR/GBR Application. *Acta biomaterialia*, *5*(9), 3295-3304.

97. Herron, M., Agarwal, A., Kierski, P. R., Calderon, D. F., Teixeira, L. B., Schurr, M. J., ... & Abbott, N. L. (2014). Reduction in Wound Bioburden using A silver-loaded Dissolvable Microfilm Construct. *Advanced healthcare materials*, *3*(6), 916-928.

98. Ni, S., Sun, L., Ercan, B., Liu, L., Ziemer, K., & Webster, T. J. (2014). A mechanism for The enhanced Attachment and Proliferation of Fibroblasts on Anodized 316L Stainless Steel with Nano-pit Arrays. *Journal of Biomedical Materials Research Part B: Applied Biomaterials*, *102*(6), 1297-1303.

99. Hassan, N., & Abdel Ghany, N. A. (2017). Corrosion of Biomaterials: Anodic Treatment and Evaluation of 316L Stainless Steel in Simulated Body Fluid. *Corrosion Engineering, Science and Technology*, *52*(4), 267-275.

100. Hsu, H. J., Wu, C. Y., Huang, B. H., Tsai, C. H., Saito, T., Ou, K. L., ... & Peng, P. W. (2020). Surface Characteristics and Cell Adhesion Behaviors of the Anodized Biomedical Stainless Steel. *Applied Sciences*, *10*(18), 6275.

101. Cho, Y. C., Hung, W. C., Lan, W. C., Saito, T., Huang, B. H., Lee, C. H., ... & Ou, K. L. (2021). Anodized Biomedical Stainless-Steel Mini-implant for Rapid Recovery in A rabbit Model. *Metals*, *11*(10), 1575.

102. Turalıoğlu, K., Taftalı, M., Tekdir, H., Çomaklı, O., Yazıcı, M., Yetim, T., & Yetim, A. F. (2021). The tribological and Corrosion Properties of Anodized Ti6Al4V/316L Bimetallic Structures Manufactured by Additive Manufacturing. *Surface and Coatings Technology*, *405*, 126635.

103. Allion-Maurer, A., Saulou-Berion, C., Briandet, R., Zanna, S., Lebleu, N., Marcus, P., ... & Mercier-Bonin, M. (2015). Plasma-

Deposited Nanocomposite Polymer-Silver Coating Against Escherichia coli and Staphylococcus aureus: Antibacterial properties and ageing. *Surface and Coatings Technology*, *281*, 1-10.

104. Alias, R., Mahmoodian, R., & Abd Shukor, M. H. (2019). Development and Characterization of A multilayer Silver/silver-tantalum Oxide Thin Film Coating on Stainless Steel for Biomedical Applications. *International Journal of Adhesion and Adhesives*, *92*, 89-98.

105. ASTM G44-99, 'Standard Practice for Exposure of Metals and Alloys by Alternate Immersion in Neutral 3.5 % Sodium Chloride Solution, January 2000.

106. ASTM G102, "Standard Practice for from Electrochemical Measurements," ASTM, vol. 89, no. Reapproved 2015, pp. 1–7, 2015.

107. Broitman, E., & Hultman, L. (2012, June). Adhesion Improvement of Carbon-based Coatings Through A high Ionization Deposition Technique. In *Journal of Physics: Conference Series* (Vol. 370, No. 1, p. 012009). IOP Publishing.

108. Kuromoto, N. K., Simão, R. A., & Soares, G. A. (2007). Titanium Oxide Films Produced on Commercially Pure Titanium by Anodic Oxidation with Different Voltages. *Materials Characterization*, *58*(2), 114-121.

109. Chen, S., Li, Y., & Cheng, Y. F. (2017). Nanopatterning of Steel by One-step Anodization for Anti-adhesion of Bacteria. *Scientific reports*, *7*(1), 5326.

الخلاصة

تصنع اكثر الاجهزة الطبية من المواد المعدنية ، من نوع الفولاذ المقاوم للصدأ الأوستنيتي وسبائك التيتانيوم ، والتي تمتاز بمقاومة جيدة للتآكل ، وخصائص ميكانيكية مناسبة ، وتوافق حيوي جيد. بشكل عام بسبب الاجراءات غير المناسبة من قبل الطاقم الطبي اثناء عمليات التطهير والتعقيم او استخدام مواد ملوثة او مواد كيميائية مركزة، لذلك غالبا ما يكون عمر الأجهزة الطبية محدوداً.

من أجل تجاوز هذه المحددات ، تم في هذه الرسالة ، إجراء تحسينات سطحية مختلفة على سبيكة (316 L SS)، ثم تمت دراسة تأثير نوع التحسين السطحي ومتغيراته على الخصائص الميكانيكية ، وخصائص السطح ، والنشاط المضاد للبكتيريا وقوة الالتصاق ومقاومة التآكل للطبقة السطحية المتكونة نتيجة لهذه التحسينات وتحديد القيم المثلى لتلك المتغيرات.

تم استخدام طريقتين لتحسين السطح لسبائك الفولاذ المقاوم للصدأ (316 L SS) بظروف مختلفة لكل طريقة: تقنية الأنودة بجهد (6 ، 8 ، 10) فولت ومسافة (2 ، 4 ، 6) سم بأوقات (5 ،10) دقائق؛ بعد ذلك تم اخذ العينة الافضل بعد اجراء الفحوصات المختلفة والتي كانت A34، بعد ذلك تم ترسيب طبقة من الفضة بطريقة الترسيب الفيزيائي وبأستخدام تقنية البلازما المتطايرة DC بجهد (1400 فولت) فولت وتيار (20) مللي أمبير لمدة (2) ساعة.

تمت دراسة الخواص الميكانيكية للطبقة السطحية المتكونة باستخدام اختبار صلادة فيكرز الدقيقة ، بينما تمت دراسة خصائص السطح بالمجهر الإلكتروني (FESEM) ومجهر القوة الذرية (AFM) ، بالإضافة إلى فحص التركيب الكيميائي للتوزيع العناصر الموجودة على سطح الطبقة المترسبة باستخدام التحليل الطيفي المشتت للطاقة (EDS). أما الأطوار المتكونة نتيجة التحسينات السطحية للطبقة المترسبة فقد تم تحليلها بواسطة حيود الأشعة السينية (XRD).

بعد ذلك ، تم اختبار مقاومة الطبقة المترسبة للبكتيريا الضارة ، الإشريكية القولونية ، ومقاومتها للالتصاق. أخيرًا ، تمت دراسة سلوك العينات المحسنة السطحية في السائل الذي يحاكي جسم الإنسان (Tyrode's solution) باستخدام جهد الدائرة المفتوحة واختبار الاستقطاب الكهروكيميائي الديناميكي والدوري.

أظهرت النتائج أن قيمة الصلابة العالية للعينة المؤكسدة بلغت (475) HV. كشفت نتائج (XRD) و (FE-SEM) عن تكوين أطوار جديدة في الطبقة السطحية (Cr_2O_3) ، مما يدل على أن ظروف تعديل السطح كانت جيدة جدًا ، بينما أظهرت نتائج (AFM) زيادة في قيم خشونة السطح لعينات السطح المعدلة مع زيادة زمن المعالجة.

أظهرت نتائج الاختبار المضاد للنشاط البكتيريا بسلالات الإشريكية القولونية أن الطبقة المترسبة من تحسينات السطحية لها تأثير قوي مضاد للبكتريا لمنع نموها. أما بالنسبة لنتائج اختبار مقاومة الالتصاق، فقد تبين أن الطبقة المترسبة لجميع أنواع الطلاءات السطحية لها قوة التصاق مقبولة.

أظهرت نتائج منحنيات الاستقطاب زيادة في مقاومة التآكل للعينات المحسنة سطحياً مقارنة بالعينات غير المطلية. أوضحت النتائج أن أفضل حالة للأنودة كانت عند الوقت (5) دقائق و (8) فولت و (4) سم حيث كان معدل التحسن 75% في محلول (Tyrode's solution) ، بينما كان لترسيب الفضة باستخدام تقنية ترسيب البخار الفيزيائي بتقنية البلازما بالتيار المستمر وبزمن طلاء (2) ساعة حيث كان التحسن للطبقة المترسبة 81%

ستلبي المعالجات والتعديلات السطحية التي تم استخدامها لتحسين سبيكة (316 L SS) من حيث الخواص الميكانيكية ومقاومة التآكل لتحاكي المتطلبات المستقبلية لتطبيق السبيكة اعلاه كمنافس قوي وبديل للتطبيقات الطبية الحيوية وخصوصاً في مجال الأدوات الجراحية.

وزارة التعليـم العالي والبحث العلمــي
جـــامــعـــة بـــابــــــل
كـــليـــة هـنــدسة الـــمـــواد
قـــسم هـنـــدسة الـــمـــعادن

تقنيات مختلفة لتحسين سطح الفولاذ المقاوم للصدأ (316L) للعدد الجراحية

رسالة
مقدمة الى قسم هندسة المعادن في كلية هندسة المواد/جامعة بابل
وهي جزء من متطلبات نيل درجة الماجستير في هندسة المواد/ المعادن

من قبل
ندى طالب جابر طعيمة
بكالوريوس هندسة مواد (2012)
دبلوم عال هندسة معادن (2019)

باشراف

أ. د. علي هوبي حليم | **أ.م.د. نبأ ستار راضي**

2023م | 1444هـــ